Electronic Supplementary Material (ESI) for Dalton Transactions.
This journal is © The Royal Society of Chemistry 2019

Supporting Information for

Accelerating Ethylene Polymerization Using Secondary Metal Ions in Tetrahydrofuran

Dawei Xiao, Zhongzheng Cai, Loi H. Do*

Department of Chemistry, University of Houston, Houston, Texas, 77004

TABLE OF CONTENTS **Page(s)**

EXPERIMENTAL

Synthesis and Characterization

Preparation of 1b. A 100 mL Schlenk flask was charged with magnesium turnings (1.0 g, 41.7 mmol, 4.0 equiv.) under N_2 in 20 mL of THF. The compound 2-bromo-1,3-dimethoxybenzene (4.5 g, 20.7 mmol, 2.0 equiv.) was added and the mixture was stirred at room temperature for 1 h until the solution turned brown. The resulting Grignard reagent was cannula transferred to a THF solution containing PCl_3 (0.8 mL, 10.4 mmol, 1.0 equiv.) at -78 °C. After the addition was complete, the suspension was stirred at room temperature for another 30 min. This solution was used directly in the next step. The compound 1,2-dibromobenzene (1.1 mL, 9.1 mmol, 1.0 equiv.) was combined with 20 mL of Et_2O/THF (1:1). The solution was cooled to -110 °C using a cold bath containing Et_2O/Acetone/Pentane (85:10:5) and liquid N_2. A solution of 1.6 M *n*-butyllithium (5.8 mL, 9.1 mmol, 1.0 equiv.) was added slowly via syringe, taking care that the solution flowed down from the wall of the flask rather than directly into the reaction mixture. The mixture turned slightly yellow and was stirred for 30 mins at -110 °C. The crude PAr_2Cl solution from step 1 was precooled to -78 °C and then added to the reaction flask via syringe. This final mixture was allowed to continue stirring at -110 °C for 10 mins and then slowly warmed up to -90 °C. Saturated NH_4Cl solution (15 mL) was added to quench the reaction. The reaction mixture was extracted into DCM (3×50 mL). The organic extracts were combined, dried over sodium sulfate, filtered, and then evaporated to dryness. The crude material was purified by silica gel column chromatography (hexanes/DCM, 1:1). A white solid (1.55 g, 3.4 mmol, 37.4%) was collected. ^{1}H NMR ($CDCl_3$, 600 MHz): δ (ppm) = 7.45 (m, 1H), 7.23 (m, 2H), 7.05 (m, 3H), 6.48 (dd, J_{HH} = 8.2 Hz, J_{PH} = 2.7 Hz, 4H), 3.49 (s, 12H), ^{13}C NMR ($CDCl_3$, 150 MHz): δ (ppm) = 162.86 (d, J_{PC} = 8.6 Hz), 140.80 (d, J_{PC} = 10.5 Hz), 132.99, 131.52, 130.38, 129.45 (d, J_{PC} = 36.0 Hz), 127.92, 125.79, 112.86 (d, J_{PC} = 19.5 Hz), 104.42, 55.95. ^{31}P NMR ($CDCl_3$, 162 MHz): δ (ppm) = -42.71. GC-MS calc. for $C_{22}H_{22}BrO_4P$ $[M]^+$ = 460.0, found 460.0.

Preparation of 3b. A 100 mL Schlenk flask was charged with (2-bromophenyl)bis(2,6-dimethoxyphenyl)phosphine (0.92 g, 2.00 mmol, 1.0 equiv.) in 30 mL of THF. The flask was cooled to -78°C, and a solution of 1.6 M *n*-butyllithium (1.3 mL, 2.00 mmol, 1.0 equiv.) was added via syringe, giving a deep yellow solution that was stirred for 20 min. A solution of **2** (0.64 g, 2.00 mmol, 1.0 equiv.) in THF (5 mL) was then added by syringe, which turned the solution pale orange. After stirring for 40 min, the cold bath was removed, and the flask was allowed to warm up to room temperature overnight while stirring. The reaction mixture was then concentrated under reduced pressure to afford a yellow solid. The crude product was purified by silica gel column chromatography (100% ethyl acetate to remove mobile impurities, followed by ethyl acetate/chloroform/ methanol=10:1:1 to elute the product) to yield a colorless oil (0.59 g, 0.88 mmol, 44.2%). ^{1}H NMR ($CDCl_3$, 400 MHz): δ (ppm) = 8.03 (m, 1H), 7.41(m, 1H), 7.24 (m, 2H), 7.18 (t, J_{HH} = 8.4 Hz, 2H), 6.44 (dd, J_{HH} = 8.6 Hz, J_{PH} = 2.8 Hz, 4H), 4.15 (m, 2H), 4.06 (m, 2H), 3.54 (m, 4H), 3.46 (m, 8H), 3.40 (s, 12H), 3.34 (s, 6H). ^{13}C NMR ($CDCl_3$, 100 MHz): δ (ppm) = 162.38 (d, J_{PC} = 8.8 Hz), 144.67 (dd, J_{PC} = 25.3, 12.7 Hz), 134.67 (d, J_{PC} = 15.5 Hz), 133.82 (dd, J_{PC} = 10.7, 8.6 Hz), 131.83 (dd, J_{PC} = 187.8, 36.0 Hz), 130.58 (d, J_{PC} = 2.9 Hz), 129.69, 126.40 (d,

J_{PC} = 14.6 Hz), 115.34 (d, J_{PC} = 23.3 Hz), 104.74, 71.94, 70.34, 70.02 (d, J_{PC} = 6.8 Hz), 64.51 (dd, J_{PC} = 5.8, 2.9 Hz), 59.10, 55.96. ^{31}P NMR ($CDCl_3$, 162 MHz): δ (ppm) = 21.12, -40.64. ESI–MS(+) calc. for $C_{32}H_{44}O_{11}P_2$ $[M+Na]^+$ = 689.2256, found 689.2212.

Preparation of 5b. A 100 mL Schlenk flask was charged with (2-bromophenyl)bis(2,6-dimethoxyphenyl) phosphine (0.8 g, 1.73 mmol, 1.0 equiv.) in 30 mL of THF. The flask was cooled to -78 °C, and a solution of 1.6 M *n*-butyllithium (1.1 mL, 1.73 mmol, 1.0 equiv.) was added via syringe, giving a deep yellow solution. After stirring for 20 min, a solution of chlorodiethylphosphate (0.30 g, 1.73 mmol, 1.0 equiv.) in THF (5 mL) was added by syringe, which turned the solution pale orange. After stirring for 40 min, the cold bath was removed, and the flask was allowed to warm up to room temperature overnight while stirring. The reaction mixture was then concentrated under reduced pressure to afford a white solid. The crude product was purified by silica gel column chromatography (ethyl acetate/hexane= 7:3) to yield a white solid (0.85 g, 1.56 mmol, 53%). ^{1}H NMR ($CDCl_3$, 400 MHz): δ (ppm) = 8.09 (m, 1H), 7.42 (m, 1H), 7.24 (m, 2H), 7.18 (td, J_{HH} = 8.0 Hz, J_{HH} = 1.2 Hz, 2H), 6.44 (dd, J_{HH} = 8.4 Hz, J_{PH} =2.8 Hz, 4H), 4.00 (m, 4H), 3.40 (s, 12H), 1.05 (t, J_{HH} = 7.2 Hz, 6H). ^{13}C NMR ($CDCl_3$, 100 MHz): δ (ppm) = 162.38 (d, J_{PC} = 8.8 Hz), 144.43 (dd, J_{PC} = 25.3, 11.7 Hz), 134.65 (d, J_{PC} = 15.6 Hz), 134.02 (dd, J_{PC} = 11.2, 8.8 Hz), 132.38 (dd, J_{PC} =185.8, 35.0 Hz), 130.52 (d, J_{PC} = 2.9 Hz), 129.56, 126.34 (d, J_{PC} =15.5 Hz), 115.55 (d, J_{PC} =22.4 Hz), 104.72, 61.75 (d, J_{PC} = 3.9 Hz), 55.96, 16.07 (d, J_{PC} = 5.9 Hz). ^{31}P NMR ($CDCl_3$, 162 MHz): δ (ppm) = 20.82, -40.40. ESI–MS(+) calc. for $C_{26}H_{32}O_7P_2$ $[M+K]^+$ = 557.1260, found 557.1225.

POLYMER CHARACTERIZATION

Comonomer Incorporation Calculations: The following equations were used to calculate the approximate percentage of polar monomer incorporation. I_{tot} = total integration of all hydrogen signals.

A. **Poly(ethylene-co-PVE).**[1] The H_b peak at ~3.2 ppm corresponding to the methine –CH(OPr)– hydrogen was used in the calculation.

$$\text{Incorporation of PVE (mol \%)} = \frac{H_b}{H_b + \dfrac{I_{Tot} - 10 \times H_b}{4}} \times 100\%$$

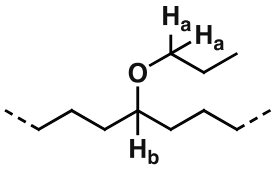

B. **Poly(ethylene-co-ABE)**.[2] The H_a peak at ~3.4 ppm corresponding to the methylene –OCH_2(CH)– hydrogens was used in the calculation.

$$\text{Incorporation of ABE (mol \%)} = \frac{H_a/2}{H_a/2 + \dfrac{I_{Tot} - 14 \times (H_a/2)}{4}} \times 100\%$$

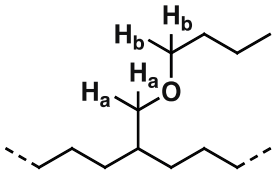

C. **Poly(ethylene-co-MU)**.[3] The H_a peak at ~3.7 ppm corresponding to the methyl CH_3(COO)– hydrogens was used in the calculation.

$$\text{Incorporation of MU (mol \%)} = \frac{H_a/3}{H_a/3 + \dfrac{I_{Tot} - 22 \times (H_a/3)}{4}} \times 100\%$$

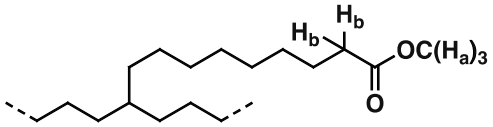

D. **Poly(ethylene-co-AP)**.[3] The H_b peak at ~4.1 ppm corresponding to the methylene –CH_2(O)– hydrogens was used in the calculation.

$$\text{Incorporation of AP (mol \%)} = \frac{H_b/2}{H_b/2 + \dfrac{I_{Tot} - 12 \times (H_b/2)}{4}} \times 100\%$$

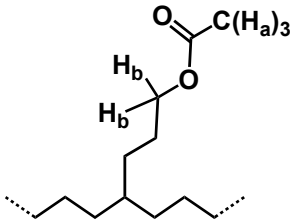

METAL BINDING STUDIES

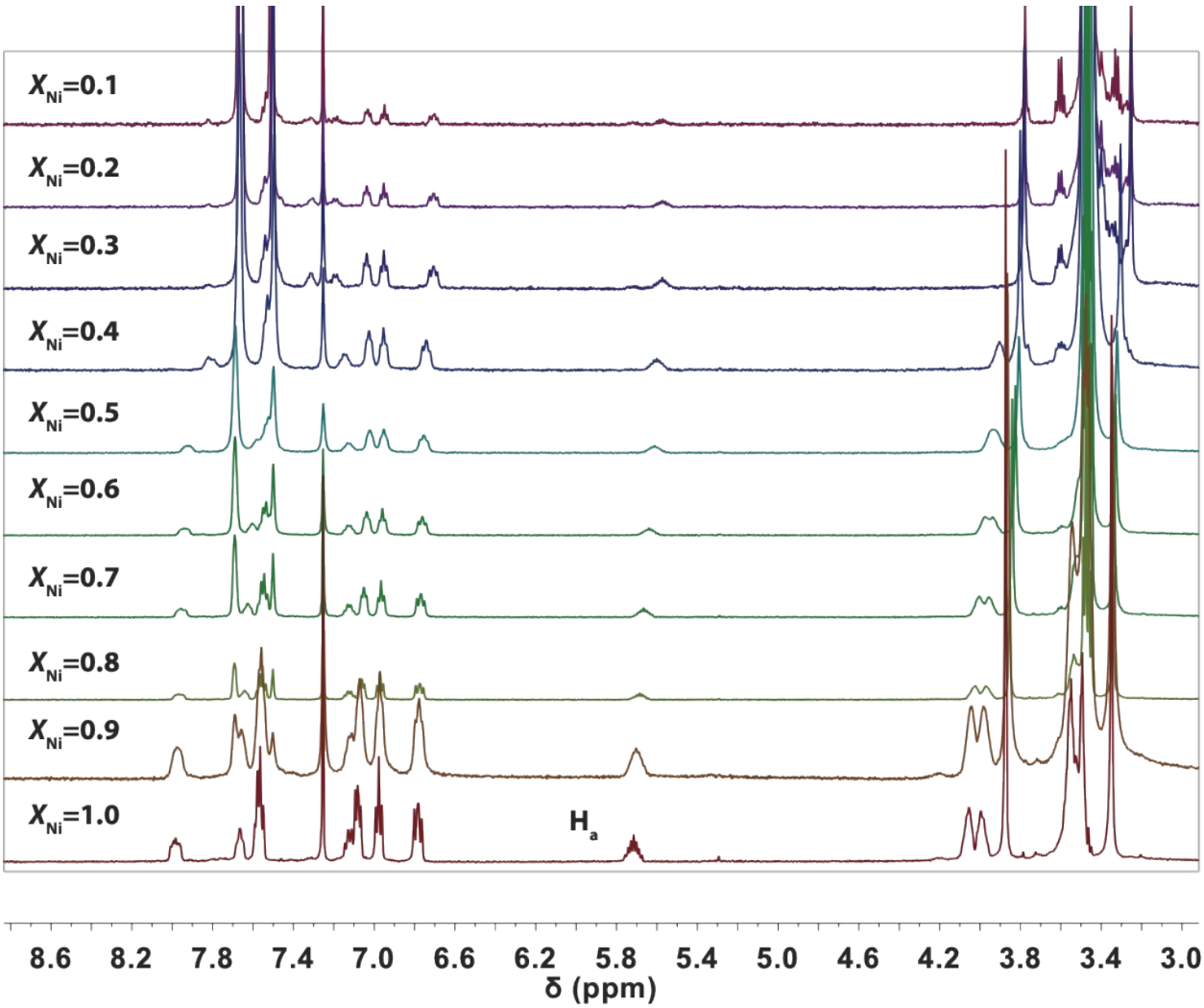

Figure S1. Job plot study: ^{1}H NMR spectra ($CDCl_3$, 500 MHz) of samples containing complex **4a** and $NaBAr^F{}_4$ mixed in different ratios. The mole fraction of **4a** (χ_{Ni}) is defined as [**4a**]/([**4a**]+[Na^+]). The peaks labeled as H_a was assigned to the hydrogen attached to the central carbon of the allyl group in **4a**.

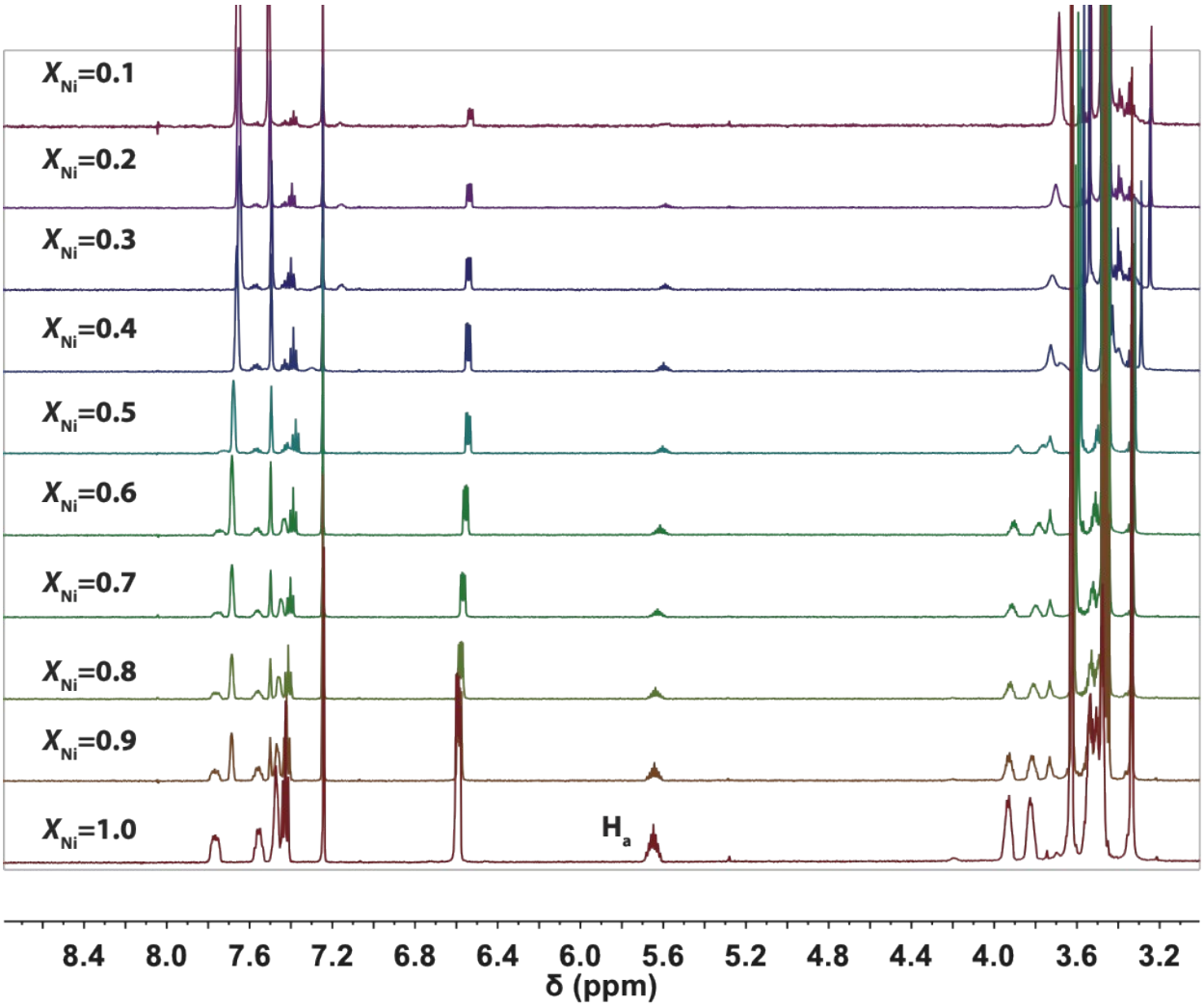

Figure S2. Job plot study: ^{1}H NMR spectra ($CDCl_3$, 500 MHz) of samples containing complex **4b** and $NaBAr^F{}_4$ mixed in different ratios. The mole fraction of **4b** (χ_{Ni}) is defined as [**4b**]/([**4b**]+[Na^+]). The peaks labeled as H_a was assigned to the hydrogen attached to the central carbon of the allyl group in **4b**.

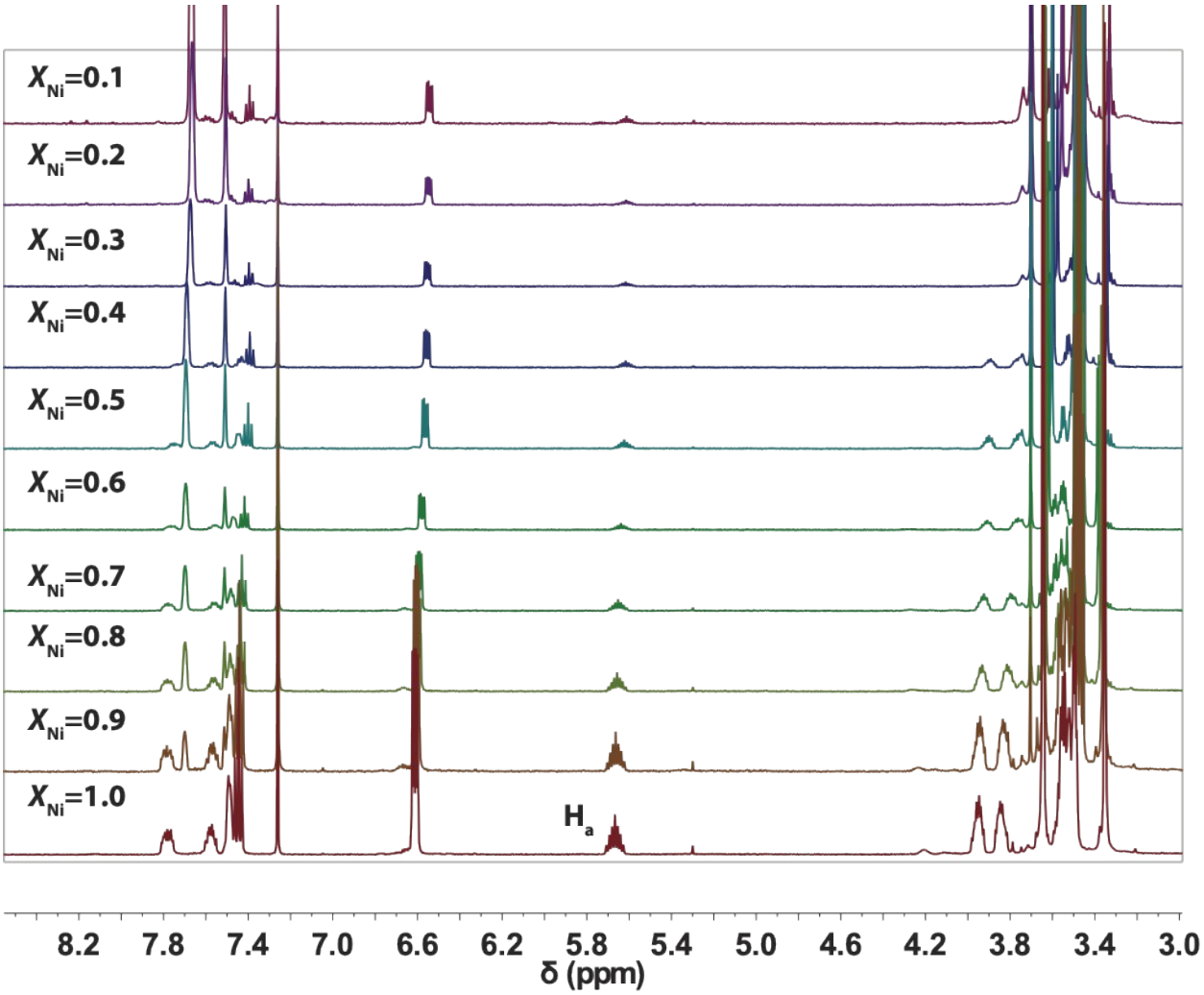

Figure S3. Job plot study: ^{1}H NMR spectra ($CDCl_3$, 500 MHz) of samples containing complex **4b** and $LiBAr^F{}_4$ mixed in different ratios. The mole fraction of **4b** (χ_{Ni}) is defined as [**4b**]/([**4b**]+[Li^+]). The peaks labeled as H_a was assigned to the hydrogen attached to the central carbon of the allyl group in **4b**.

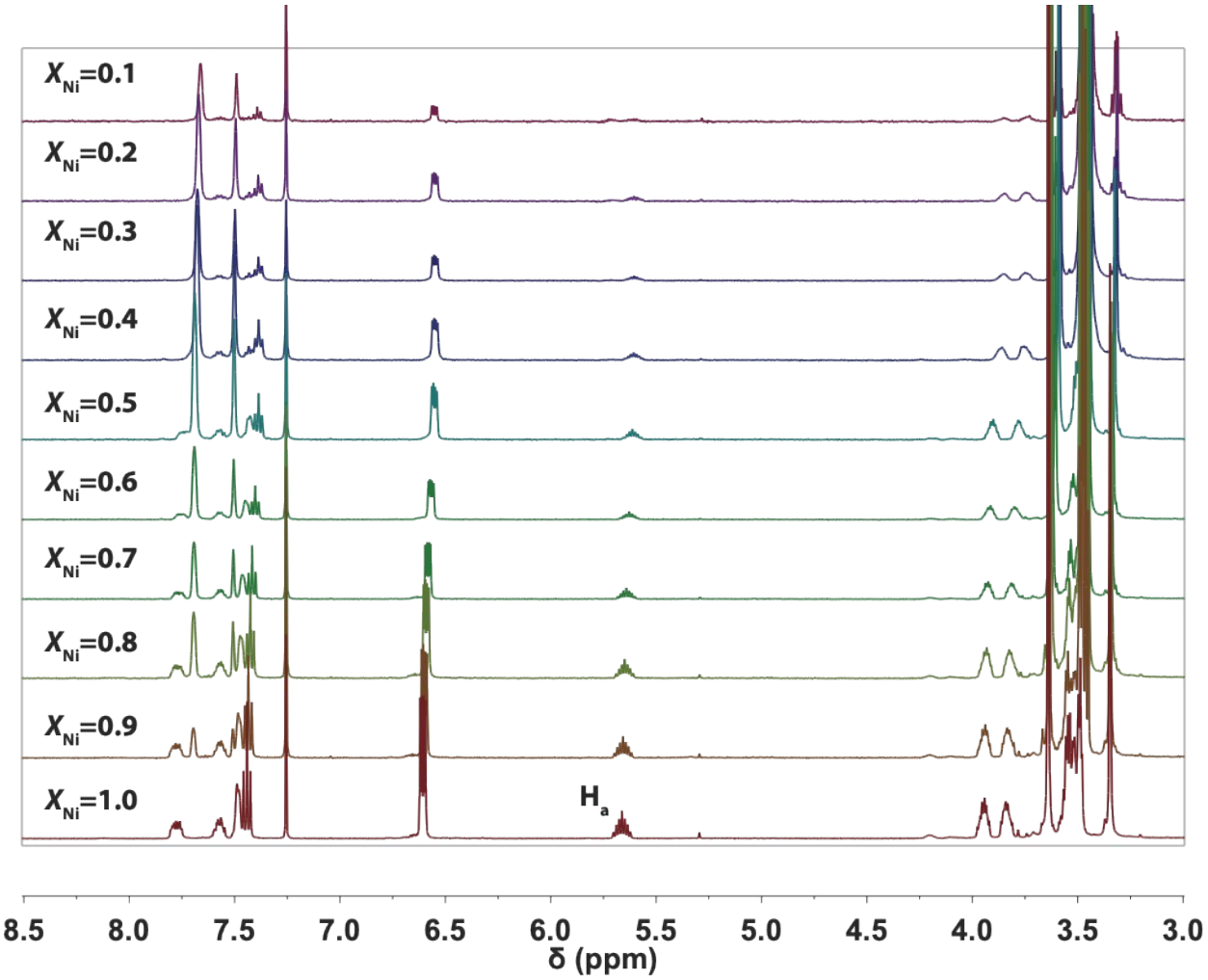

Figure S4. Job plot study: ^{1}H NMR spectra ($CDCl_3$, 500 MHz) of samples containing complex **4b** and $KBAr^F{}_4$ mixed in different ratios. The mole fraction of **4b** (χ_{Ni}) is defined as [**4b**]/([**4b**]+[K^+]). The peaks labeled as H_a was assigned to the hydrogen attached to the central carbon of the allyl group in **4b**.

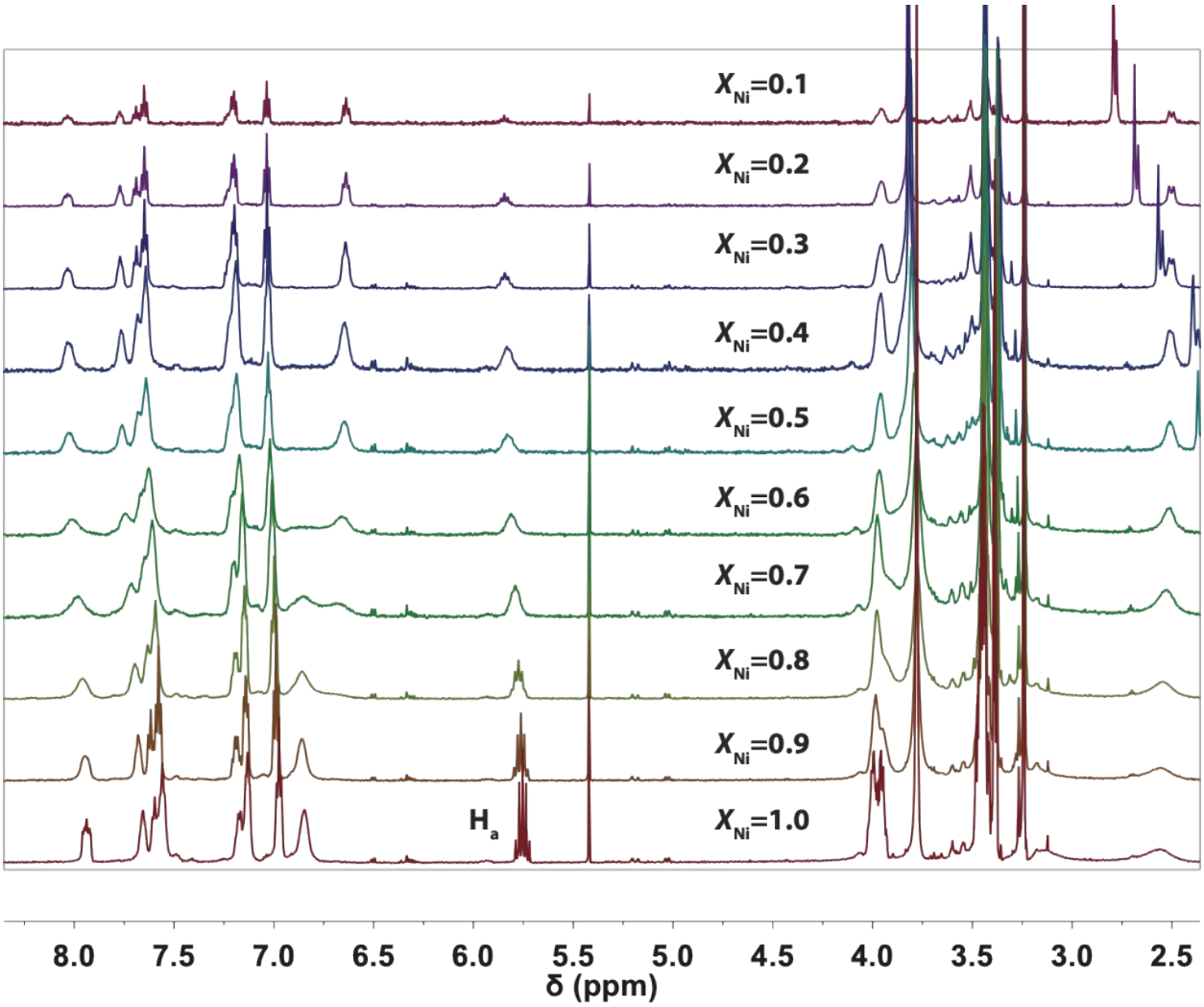

Figure S5. Job plot study: ^{1}H NMR spectra (CD_3CN, 500 MHz) of samples containing complex **4a** and $Zn(OTf)_2$ mixed in different ratios. The mole fraction of **4a** (χ_{Ni}) is defined as [**4a**]/([**4a**]+[Zn^{2+}]). The peaks labeled as H_a was assigned to the hydrogen attached to the central carbon of the allyl group in **4a**.

Table S1. NMR Job Plot Data for **4a** and $NaBAr^F{}_4$[a]

Ni (mL)	**Na^+** (mL)	**[Ni]/([Ni]+[Na^+])**	**δ** (ppm)[b]	**Δδ** (ppm)	**(Δδ)[Ni]/([Ni]+[Na^+])**
1	0	1	5.7223	0	0
0.9	0.1	0.9	5.7079	0.0144	0.01296
0.8	0.2	0.8	5.6918	0.0305	0.0244
0.7	0.3	0.7	5.6725	0.0498	0.03486
0.6	0.4	0.6	5.6471	0.0752	0.04512
0.5	0.5	0.5	5.6206	0.1017	0.05085
0.4	0.6	0.4	5.6077	0.1146	0.04584
0.3	0.7	0.3	5.5806	0.1417	0.04251
0.2	0.8	0.2	5.5788	0.1435	0.0287
0.1	0.9	0.1	5.5784	0.1439	0.01439
0	1	0	-	-	0

[a]Concentrations of stock solutions: [**4a**] = 6 mM in $CDCl_3$, [Na^+] = 6 mM in $CDCl_3/Et_2O$. [b]The peaks listed correspond to H_a in Figure S1.

Table S2. NMR Job Plot Data for **4b** and $NaBAr^F{}_4$[a]

Ni (mL)	**Na^+** (mL)	**[Ni]/([Ni]+[Na^+])**	**δ** (ppm)[b]	**Δδ** (ppm)	**(Δδ)[Ni]/([Ni]+[Na^+])**
1	0	1	5.6577	0	0
0.9	0.1	0.9	5.6464	0.0113	0.01017
0.8	0.2	0.8	5.6403	0.0174	0.01392
0.7	0.3	0.7	5.6314	0.0263	0.01841
0.6	0.4	0.6	5.6190	0.0387	0.02322
0.5	0.5	0.5	5.6072	0.0505	0.02525
0.4	0.6	0.4	5.6022	0.0555	0.0222
0.3	0.7	0.3	5.5938	0.0639	0.01917
0.2	0.8	0.2	5.5915	0.0662	0.01324
0.1	0.9	0.1	5.5895	0.0682	0.00682
0	1	0	-	-	0

[a]Concentrations of stock solutions: [**4b**] = 6 mM in $CDCl_3$, [Na^+] = 6 mM in $CDCl_3/Et_2O$. [b]The peaks listed correspond to H_a in Figure S2.

Table S3. NMR Job Plot Data for **4b** and $LiBAr^F{}_4$[a]

Ni (mL)	**Li^+** (mL)	**[Ni]/([Ni]+[Li^+])**	**δ** (ppm)[b]	**Δδ** (ppm)	**(Δδ)[Ni]/([Ni]+[Li^+])**
1	0	1	5.6672	0	0
0.9	0.1	0.9	5.6635	0.0037	0.00333
0.8	0.2	0.8	5.6569	0.0103	0.00824
0.7	0.3	0.7	5.6520	0.0152	0.01064
0.6	0.4	0.6	5.6389	0.0283	0.01698
0.5	0.5	0.5	5.6231	0.0441	0.02205
0.4	0.6	0.4	5.6162	0.051	0.0204
0.3	0.7	0.3	5.6165	0.0507	0.01521
0.2	0.8	0.2	5.6149	0.0523	0.01046
0.1	0.9	0.1	5.6121	0.0551	0.00551
0	1	0	-	-	0

[a]Concentrations of stock solutions: [**4b**] = 6 mM in $CDCl_3$, [Li^+] = 6 mM in $CDCl_3/Et_2O$. [b]The peaks listed correspond to H_a in Figure S3.

Table S4. NMR Job Plot Data for **4b** and $KBAr^F{}_4$[a]

Ni (mL)	**K^+** (mL)	**[Ni]/([Ni]+[K^+])**	**δ** (ppm)[b]	**Δδ** (ppm)	**(Δδ)[Ni]/([Ni]+[K^+])**
1	0	1	5.6672	0	0
0.9	0.1	0.9	5.6617	0.0055	0.00495
0.8	0.2	0.8	5.6543	0.0129	0.01032
0.7	0.3	0.7	5.6455	0.0217	0.01519
0.6	0.4	0.6	5.6329	0.0343	0.02058
0.5	0.5	0.5	5.6177	0.0495	0.02475
0.4	0.6	0.4	5.6104	0.0568	0.02272
0.3	0.7	0.3	5.6097	0.0507	0.01725
0.2	0.8	0.2	5.6089	0.0583	0.01166
0.1	0.9	0.1	5.5973	0.0699	0.00699
0	1	0	-	-	0

[a]Concentrations of stock solutions: [**4b**] = 6 mM in $CDCl_3$, [K^+] = 6 mM in $CDCl_3/Et_2O$. [b]The peaks listed correspond to H_a in Figure S4.

Table S5. NMR Job Plot Data for **4a**+ $Zn(OTf)_2$[a]

Ni (mL)	**Zn^{2+}** (mL)	**[Ni]/([Ni]+[Zn^{2+}])**	**δ** (ppm)[b]	**Δδ** (ppm)	**(Δδ)[Ni]/([Ni]+[Zn^{2+}])**
1	0	1	5.7516	0	0
0.9	0.1	0.9	5.7600	0.0084	0.00756
0.8	0.2	0.8	5.7718	0.0202	0.01616
0.7	0.3	0.7	5.7890	0.0374	0.02618
0.6	0.4	0.6	5.8072	0.0556	0.03336
0.5	0.5	0.5	5.8296	0.078	0.039
0.4	0.6	0.4	5.8315	0.0799	0.03196
0.3	0.7	0.3	5.8405	0.0889	0.02667
0.2	0.8	0.2	5.8429	0.0913	0.01826
0.1	0.9	0.1	5.8439	0.0923	0.00923
0	1	0	-	-	0

[a]Concentrations of stock solutions: [**4a**] = 6 mM in CD_3CN, [Zn^{2+}] = 6 mM in CD_3CN. [b]The peaks listed correspond to H_a in Figure S5.

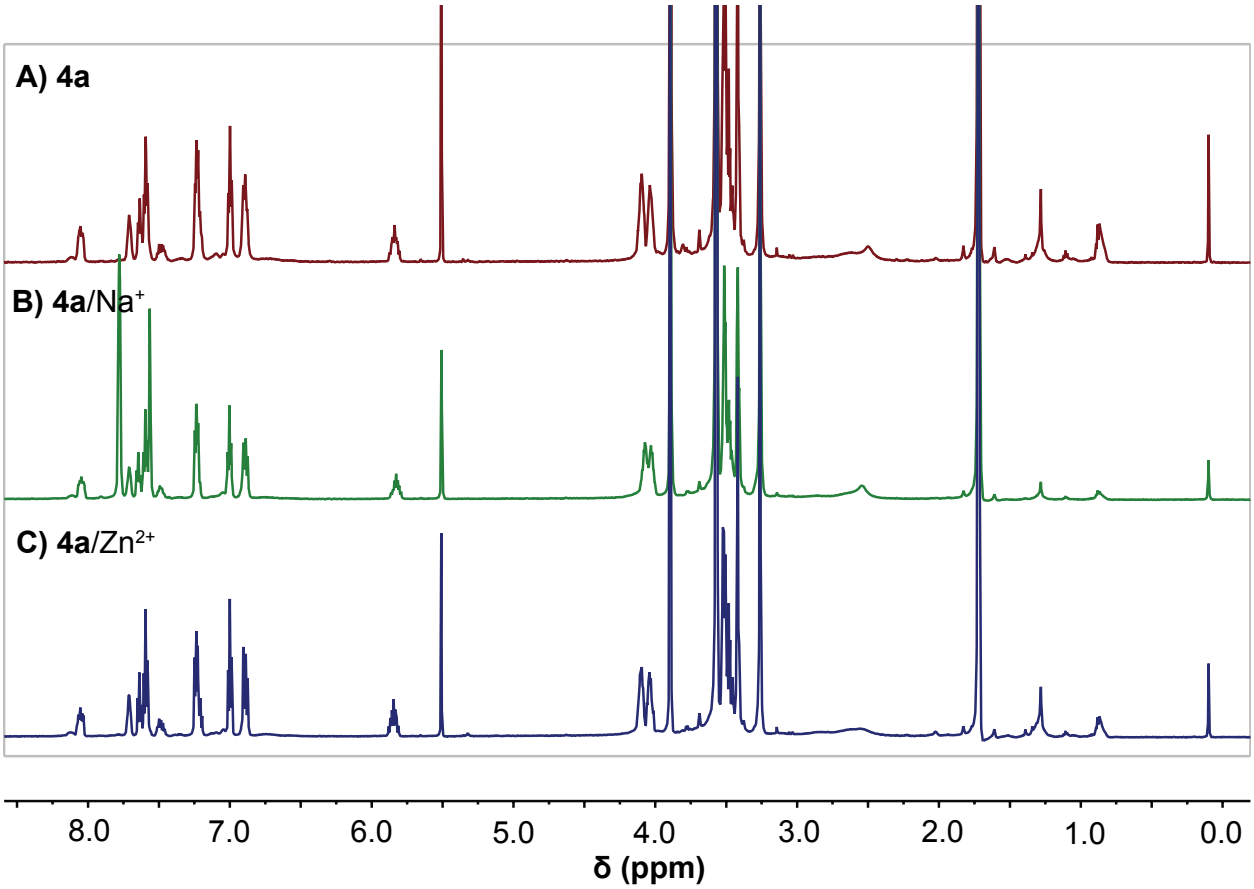

Figure S6. ^{1}H NMR spectra (THF-d_8, 600 MHz, RT) of A) complex **4a**, B) **4a** + $NaBAr^F{}_4$ (1:1), and C) **4a** + $Zn(OTf)_2$ (1:1). The amount of **4a** used in each sample was 5.3 μmol in 0.5 mL.

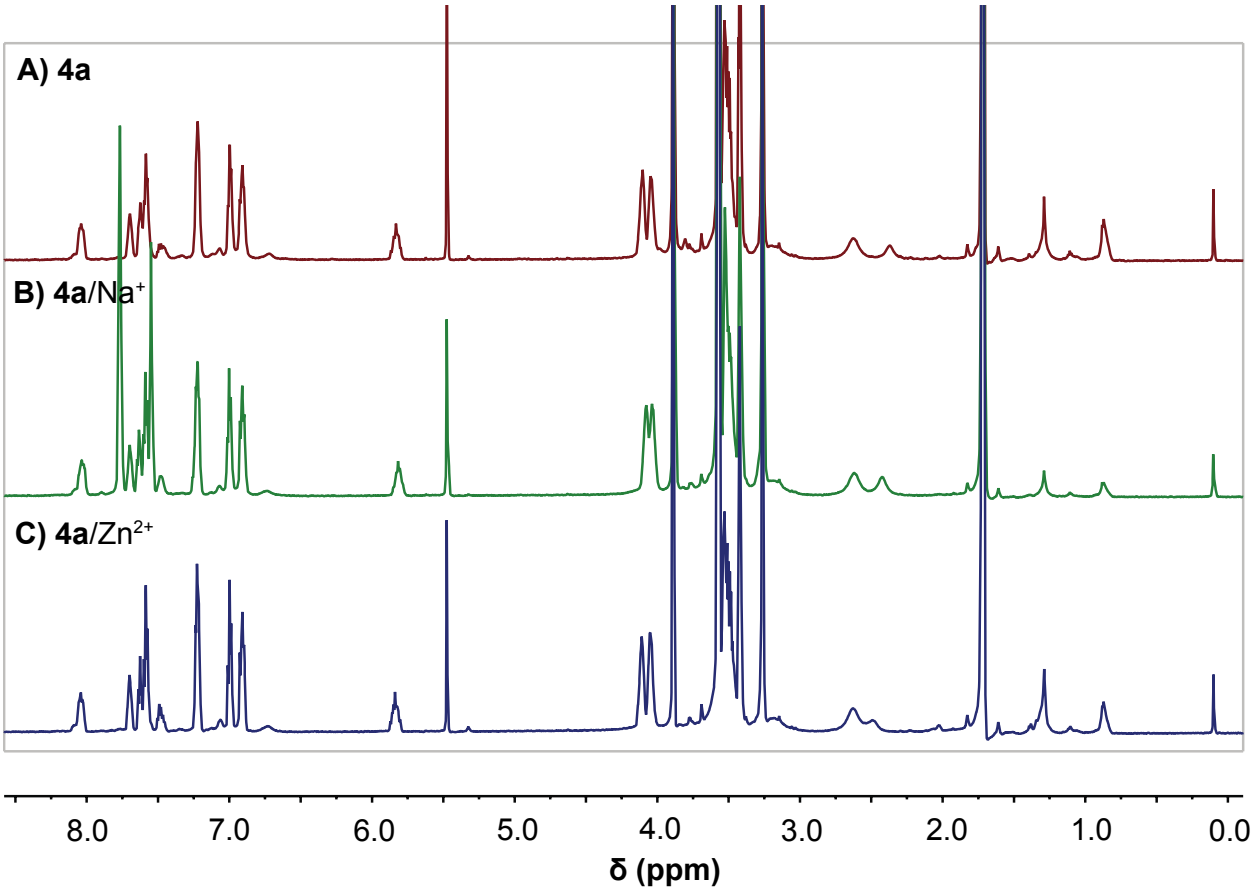

Figure S7. ^{1}H NMR spectra (THF-d_8, 600 MHz, 40 °C) of A) complex **4a**, B) **4a** + $NaBAr^F{}_4$ (1:1), and C) **4a** + $Zn(OTf)_2$ (1:1). The amount of **4a** used in each sample was 5.3 μmol in 0.5 mL.

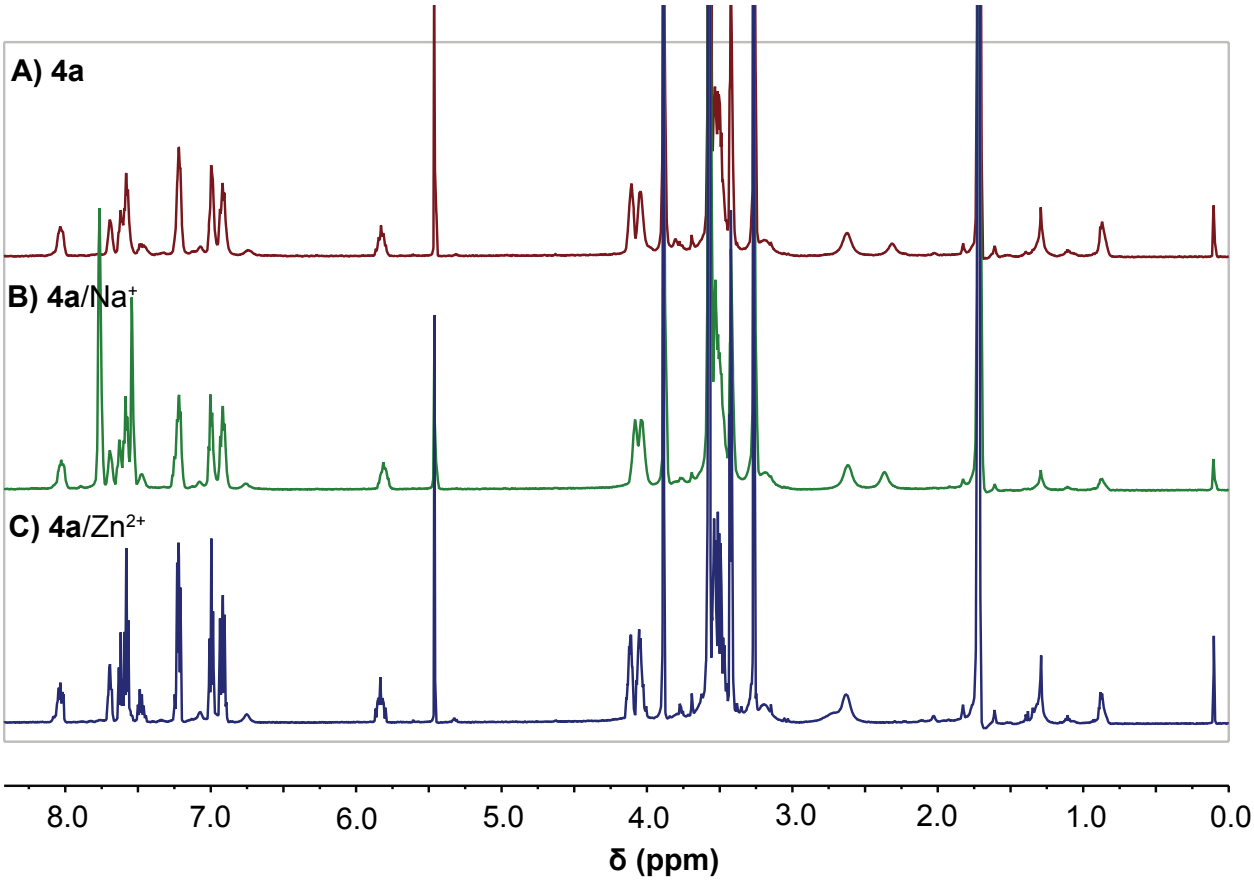

Figure S8. ^{1}H NMR spectra (THF-d_8, 600 MHz, 50 °C) of A) complex **4a**, B) **4a** + $NaBAr^{F}_{4}$ (1:1), and C) **4a** + $Zn(OTf)_2$ (1:1). The amount of **4a** used in each sample was 5.3 μmol in 0.5 mL.

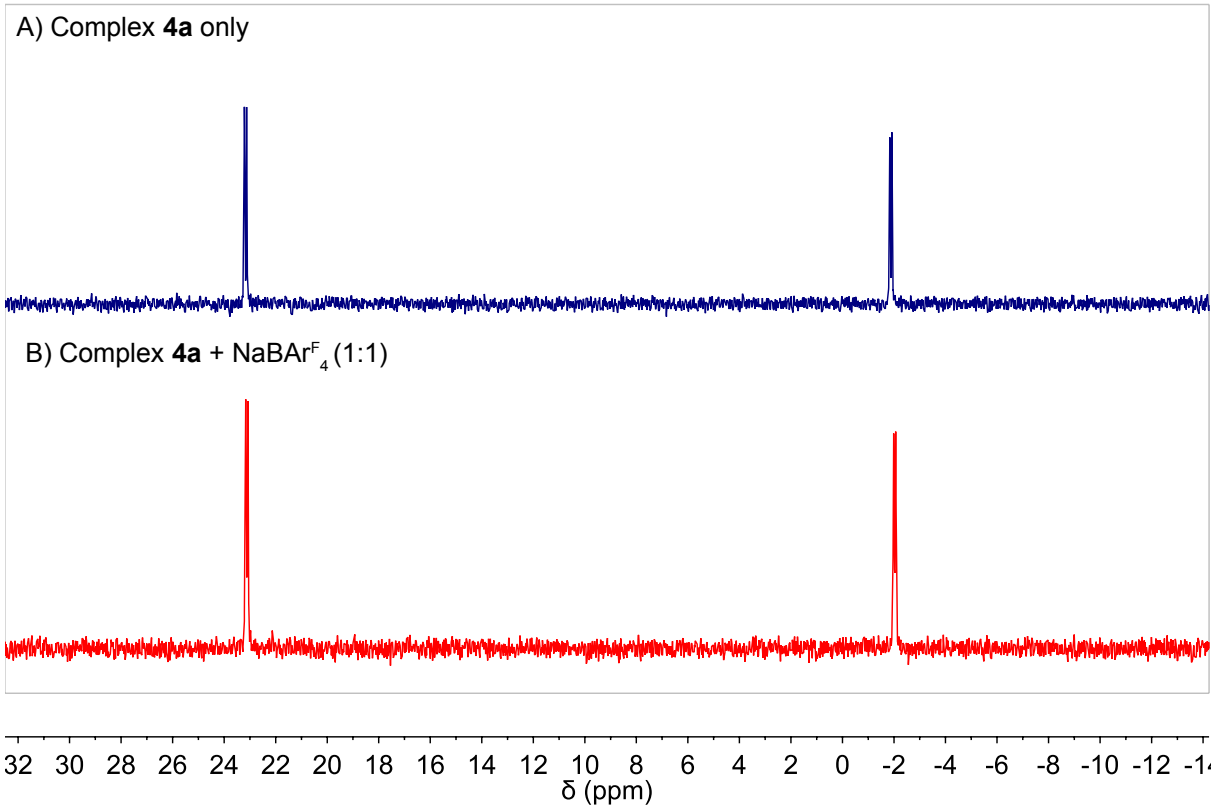

Figure S9. ^{31}P NMR ($CDCl_3$, 242 MHz) spectra of A) complex **4a** and B) complex **4a** + NaBAr$^F_4$ (1:1).

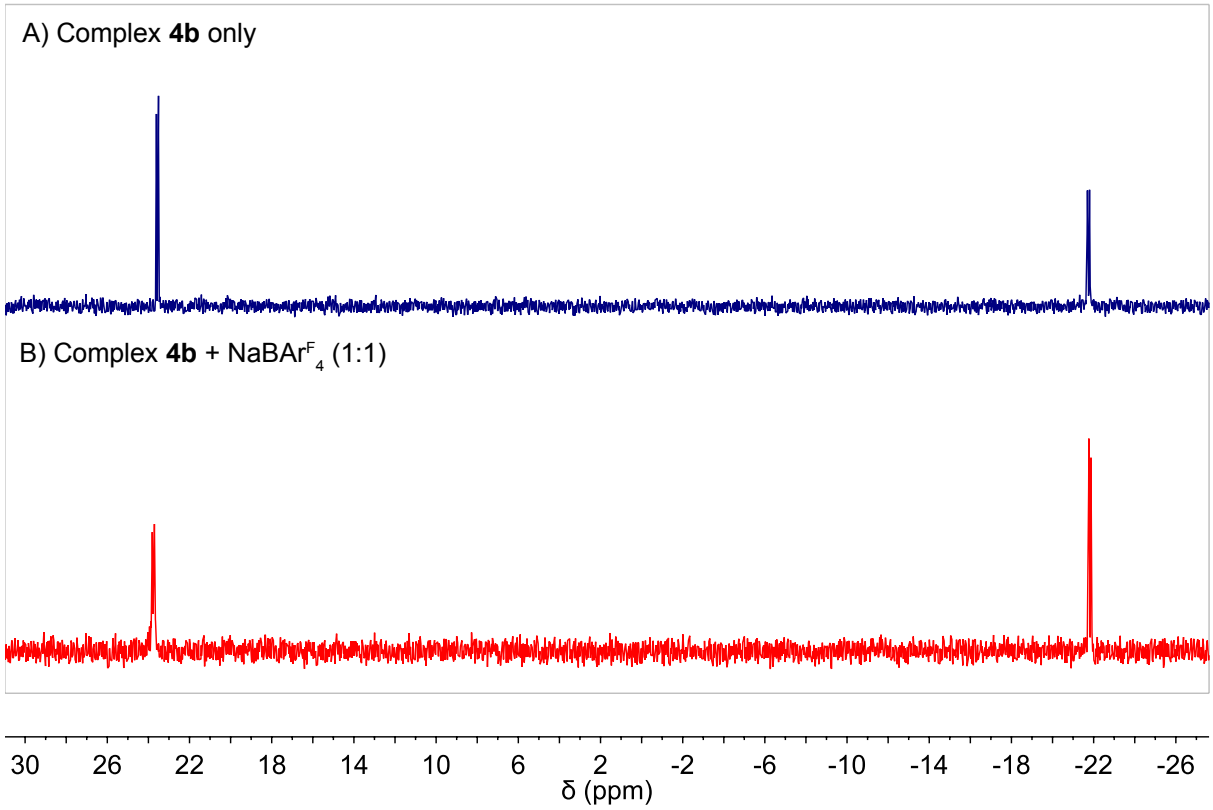

Figure S10. ^{31}P NMR ($CDCl_3$, 242 MHz) spectra of A) complex **4b** and B) complex **4b** + NaBAr$^F_4$ (1:1).

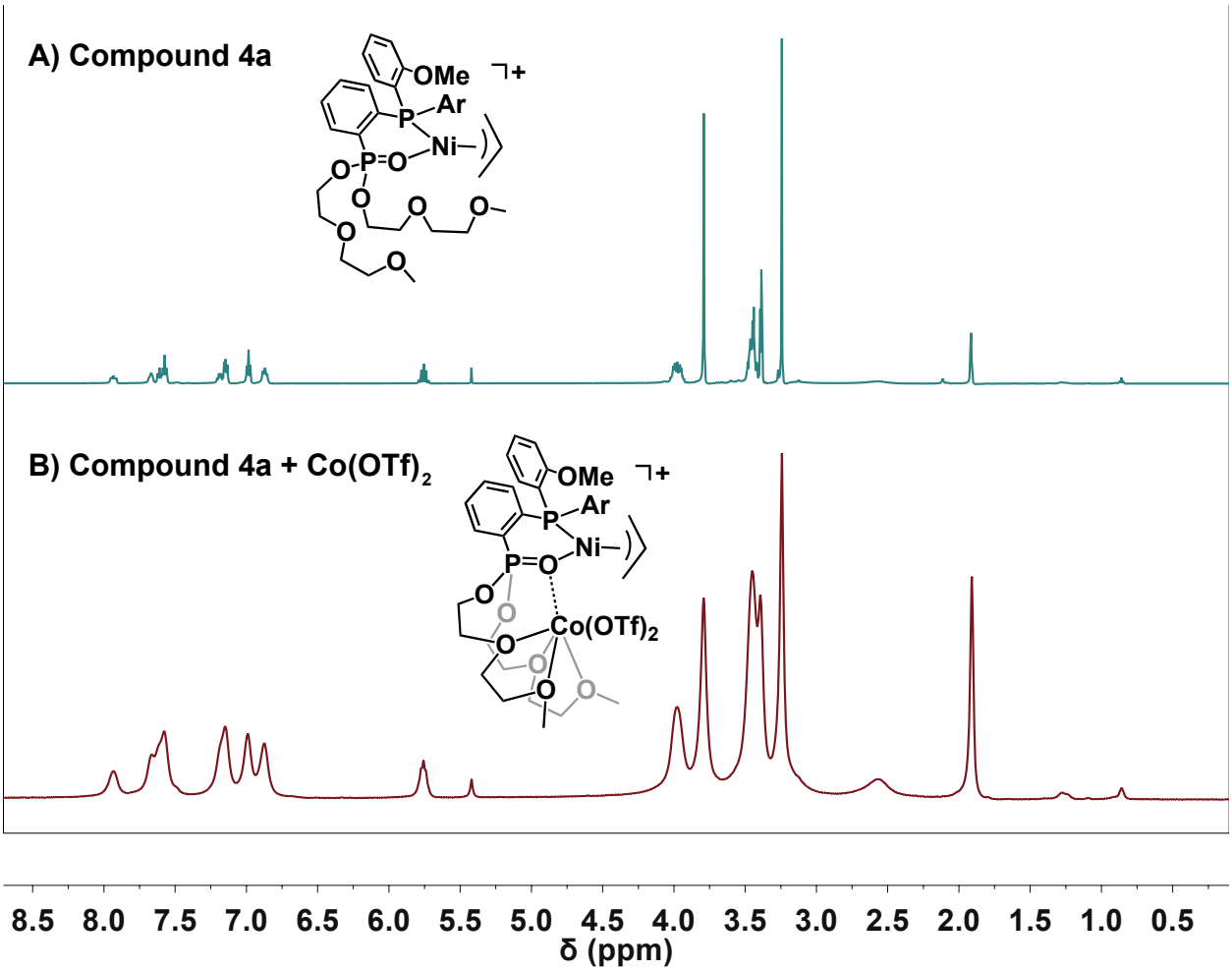

Figure S11. ^{1}H NMR spectra (CD_3CN, 600 MHz) of A) compound **4a** and B) compound **4a**/ $Co(OTf)_2$ (1:1). A proposed structure for the **4a**-Co complex is shown above. The peaks in spectrum B are broad due to the paramagnetism of cobalt(II) ions. The proposed structure for **4a**-Co is tentative.

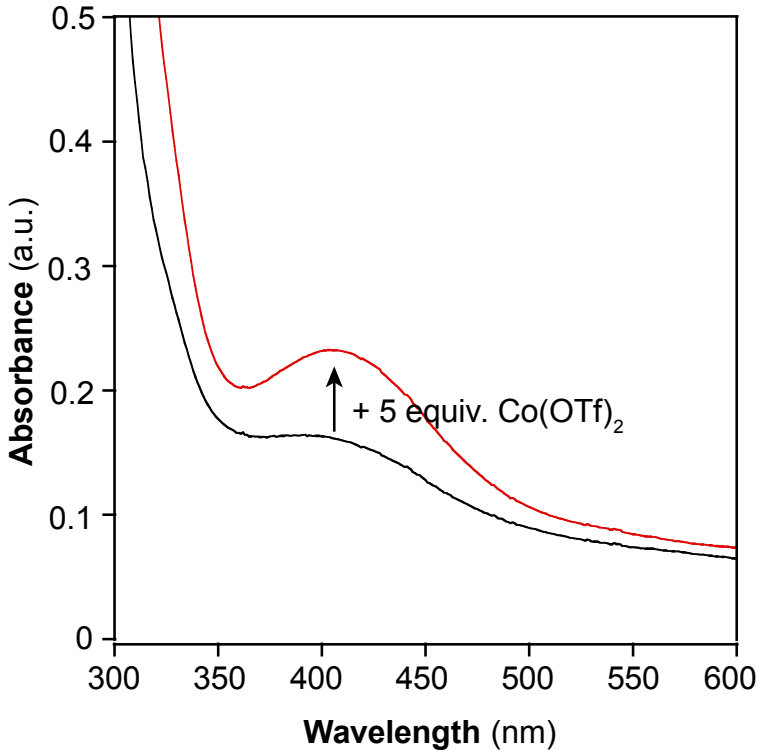

Figure S12. UV-vis absorption spectra of complex **4a** (100 μM) before (black trace) and after addition of 5 equiv. of $Co(OTf)_2$ (red trace) in THF.

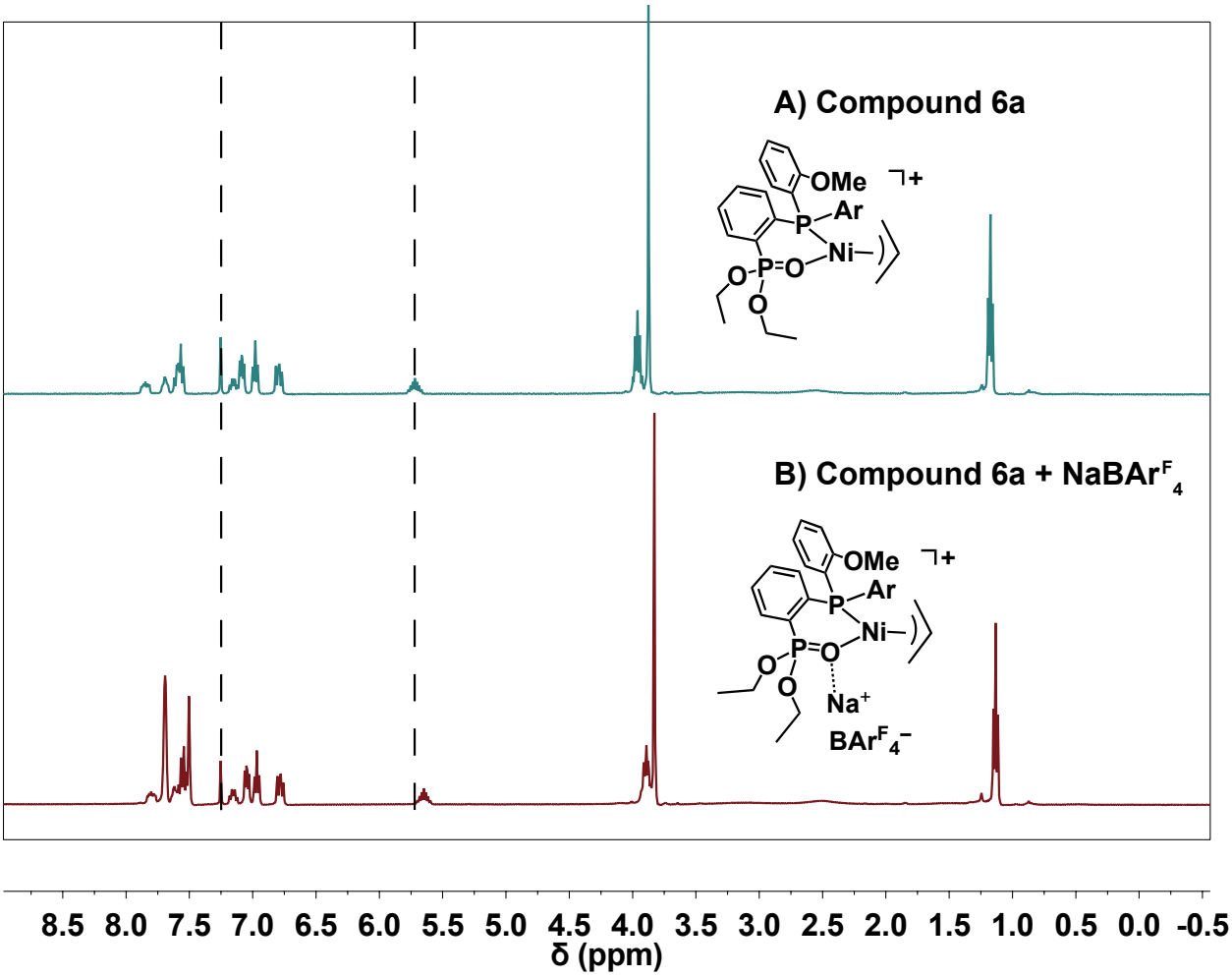

Figure S13. ^{1}H NMR spectra ($CDCl_3$, 500 MHz) of A) compound **6a** and B) compound **6a**/ $NaBAr^F_4$ (1:1). The precise structure of the **6a**-Na complex is uncertain, but a proposed structure is provided above. The dotted lines were added to aid in making spectral comparison.

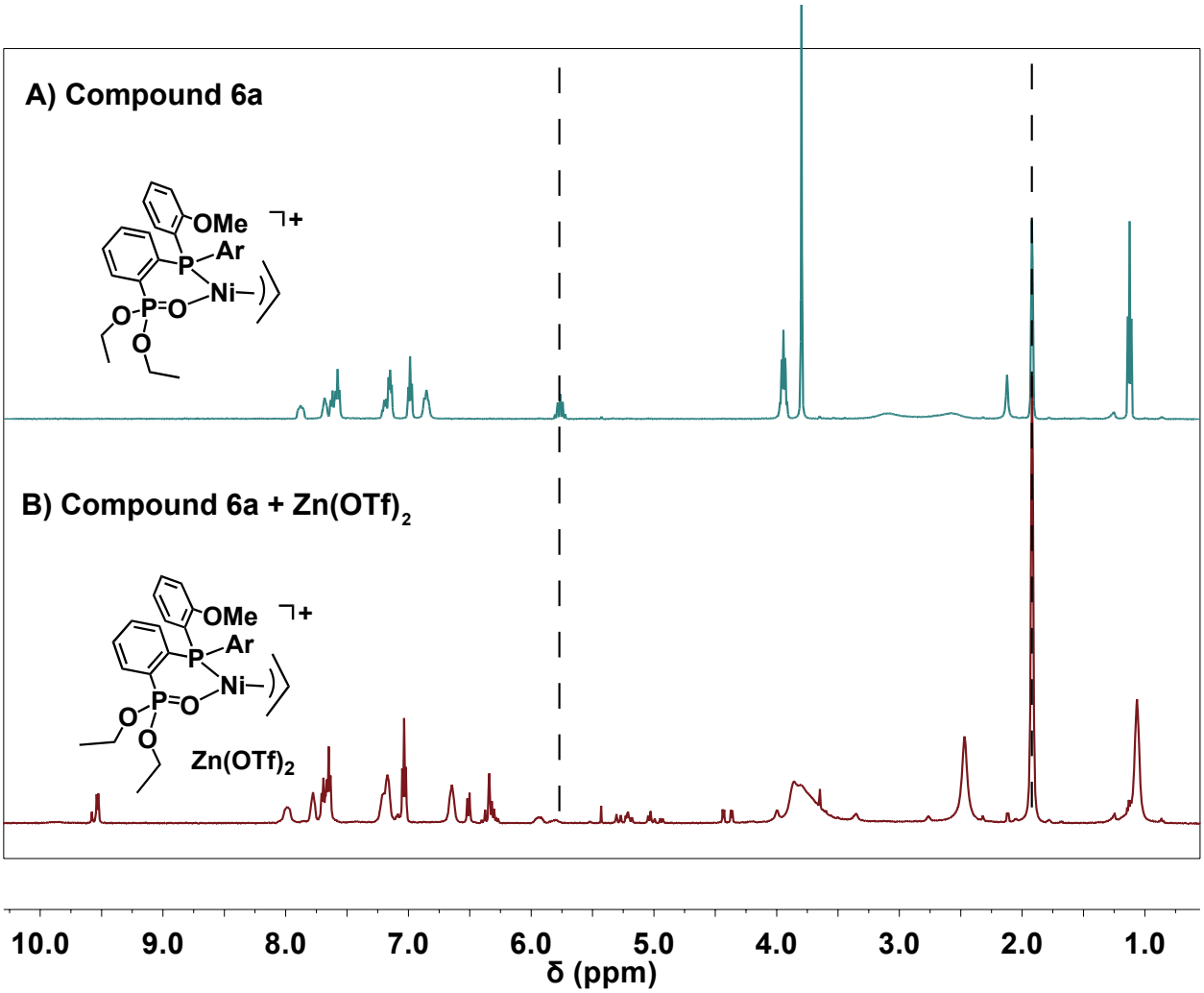

Figure S14. ^{1}H NMR spectra (CD_3CN, 500 MHz) of A) compound **6a** and B) compound **6a**/ $Zn(OTf)_2$ (1:1). The product(s) of the **6a**/$Zn(OTf)_2$ reaction is (are) uncertain. The dotted lines were added to aid in making spectral comparison.

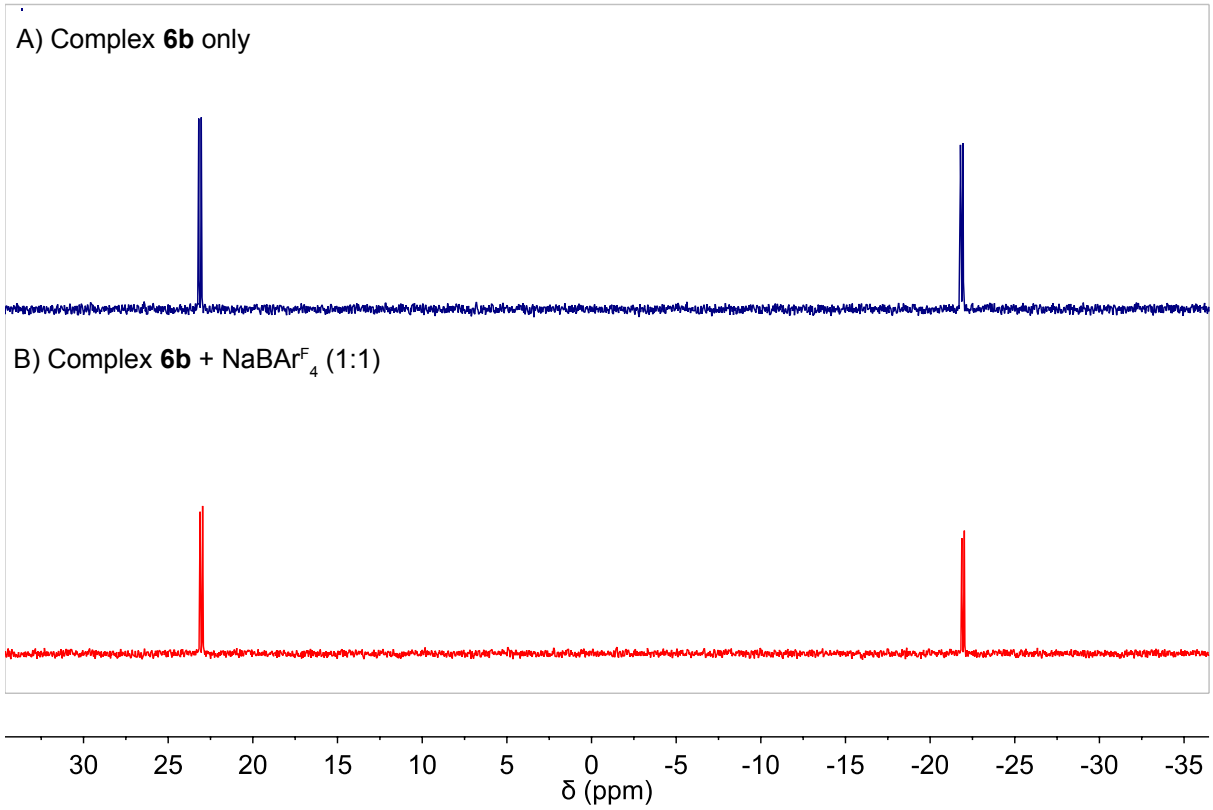

Figure S15. ^{31}P NMR ($CDCl_3$, 242 MHz) spectra of A) complex **6a** and B) complex **6a** + $NaBAr^F_4$ (1:1).

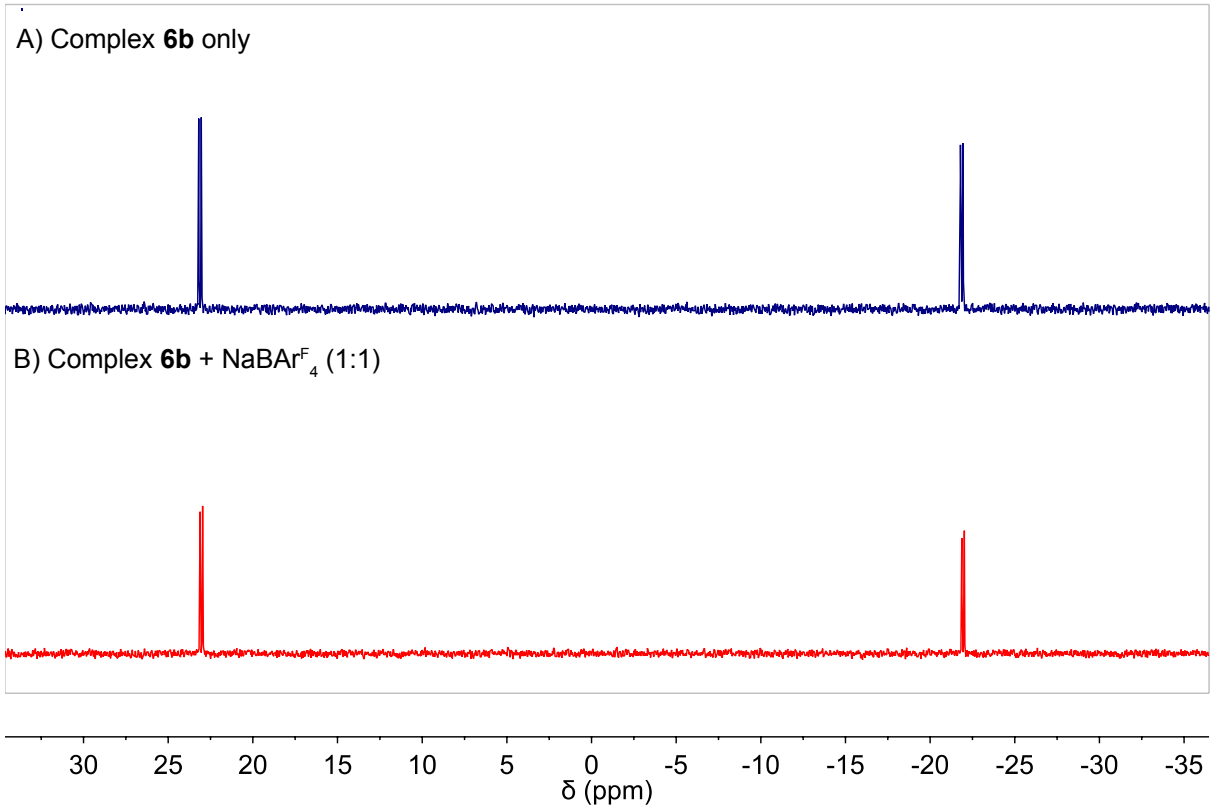

Figure S16. ^{31}P NMR ($CDCl_3$, 242 MHz) spectra of A) complex **6b** and B) complex **6b** + $NaBAr^F_4$ (1:1).

Table S6. Ethylene Homopolymerization by **4a**, **4b**, **6a**, and **6b** with Alkali Salts[a]

Entry	Complex	Salt	Polymer Yield (g)	Activity (10^5g/mol·h)	Branches[c] (/1000 C)	M_n[d] ($\times 10^3$)	M_w/M_n[d]
1	**4a**	Li^+	23.4	23.4	31	0.77	1.2
2	**4a**	K^+	28.9	28.9	28	1.12	1.2
3[b]	**4b**	Li^+	5.7	2.8	10	7.07	1.3
4[b]	**4b**	K^+	3.7	1.8	19	7.32	1.4
5	**6a**	Li^+	26.7	26.7	23	1.03	1.4
6	**6a**	K^+	25.4	25.4	22	0.73	1.7
7[b]	**6b**	Li^+	5.1	2.6	14	14.13	1.3
8[b]	**6b**	K^+	2.8	1.4	16	14.44	1.3

[a]Polymerization conditions: Ni catalyst (10 μmol), $MBAr^F{}_4$ (10 μmol), ethylene (200 psi), 2 mL DCM, 48 mL toluene, 1 h at 80 °C. [b]Polymerization conditions: Ni catalyst (20 μmol), $MBAr^F{}_4$ (20 μmol), ethylene (400 psi), 2 mL DCM, 2 mL DCM, 48 mL toluene, 1 h at 80 °C. [c]The total number of branches per 1000 carbons was determined by ^{1}H NMR spectroscopy. [d]Determined by GPC in trichlorobenzene at 150 °C.

Table S7. Ethylene Homopolymerization by **4a** with Different Metal Halides in THF

Entry	Salt (equiv.)	Polymer Yield (g)	Activity (10^5 g/mol·h)	Branches[b] (/1000 C)	M_n[c] ($\times 10^3$)	M_w/M_n[c]
1	$ZnCl_2$ (5)	16.8	16.8	30	1.03	1.1
2	$ZnBr_2$ (5)	1.7	1.7	22	0.81	2.6
3	ZnI_2 (5)	1.7	1.7	26	1.21	1.4
4	$Zn(OAc)_2$ (5)	1.3	1.3	22	0.64	1.5
5	$MgCl_2$ (5)	0	0	-	-	-
6	$AlCl_3$ (5)	0	0	-	-	-
7	$CaCl_2$ (5)	0.2	0.2	-	-	-
8	$CoCl_2$ (5)	1.4	1.4	22	1.52	2.1
9	$FeCl_3$ (5)	0	0	-	-	-
10	$CuCl_2$ (5)	0	0	-	-	-

[a]Polymerization conditions: Ni catalyst (10 μmol), metal salt (various equiv.), ethylene (200 psi), 50 mL THF, 1 h at 80 °C. [b]The total number of branches per 1000 carbons was determined by ^{1}H NMR spectroscopy. [c]Determined by GPC in trichlorobenzene at 150 °C.

Table S8. Ethylene Homopolymerization Data for **4a** and **6a** with Metal Triflate Salts in THF[a]

Entry	Complex	Salt	Polymer Yield (g)	Activity ($\times 10^5$ g/mol·h)	Branches[b] (/1000 C)	M_n[c] ($\times 10^3$)	M_w/M_n[c]
1	**4a**	none	2.5	2.5	21	0.70	1.1
2	**4a**	K^+	3.9	3.9	-	-	-
3	**4a**	Zn^{2+}	12.1	12.1	27	0.84	1.2
4[d]	**4a**	Zn^{2+}	10.2	10.2	-	-	-
5[e]	**4a**	Zn^{2+}	5.0	5.0	-	-	-
6	**4a**	Mg^{2+}	6.2	6.2	23	0.86	1.8
7	**4a**	Ca^{2+}	7.7	7.7	24	0.98	1.2
8	**4a**	La^{3+}	5.2	5.2	25	0.66	1.4
9	**4a**	Sc^{3+}	3.7	3.7	22	0.62	1.3
10	**4a**	Ga^{3+}	5.5	5.5	18	0.79	2.1
11	**4a**	Co^{2+}	26.6	26.6	18	0.91	1.8
12	**4a**	Cu^{2+}	0	0	-	-	-
13	**4a**	Al^{3+}	0.5	0.5	-	-	-
14	**4a**	Sn^{2+}	2.3	2.3	22	0.93	1.4
15	**4a**	Bi^{3+}	0.3	0.3	-	-	-
16	**6a**	none	2.5	2.5	19	0.90	1.2
17	**6a**	K^+	3.2	3.2	-	-	-
18	**6a**	Zn^{2+}	2.5	2.5	19	0.87	2.2
19	**6a**	Mg^{2+}	3.2	3.2	19	0.76	1.5
20	**6a**	Ca^{2+}	2.8	2.8	19	0.77	1.7
21	**6a**	La^{3+}	2.1	2.1	19	0.76	1.2
22	**6a**	Sc^{3+}	2.0	2.0	20	0.68	1.6
23	**6a**	Ga^{3+}	2.4	2.4	19	0.79	1.3
24	**6a**	Co^{2+}	1.9	1.9	22	0.99	2.3

[a]Polymerization conditions: Ni catalyst (10 μmol), $M(OTf)_n$ (10 μmol), ethylene (200 psi), 50 mL THF, 1 h at 80 °C. [b]The total number of branches per 1000 carbons was determined by ^{1}H NMR spectroscopy. [c]Determined by GPC in trichlorobenzene. [d]5 equiv. of $Zn(OTf)_2$ used instead of 1 equiv. [e]Polymerization conditions: Ni catalyst (10 μmol), $M(OTf)_n$ (10 μmol), ethylene (200 psi), 48 mL Toluene and 2 mL CH_2Cl_2, 1 h at 80 °C.

Table S9. Comparison of Ni/Pd Catalysts for Ethylene and Polar Ether Olefins

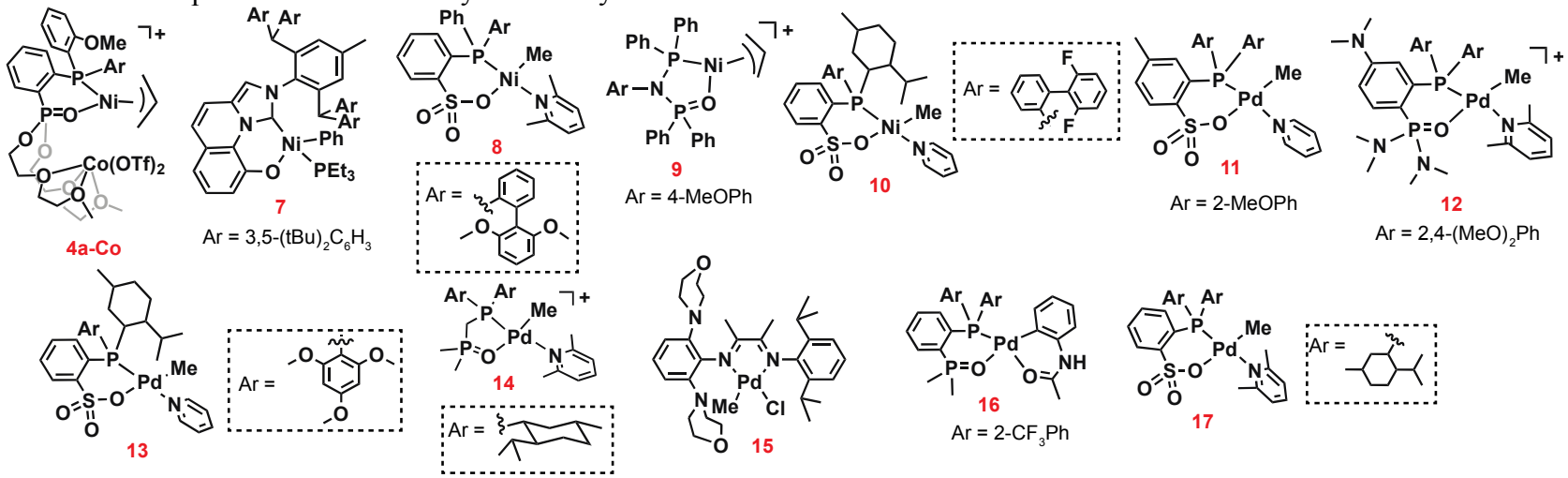

Complex (μmol)	Comonomer (conc.)[a]	C_2H_4 (psi)	Temp. (°C)	Time (h)	Activity (kg PE/mol·h)	TON (×10³ mol C_2H_4/ mol Ni)	*Inc.* (mol %)	M_n	M_w/M_n	Reference (Compound name in original reference)
4a-Co (40)	PVE (1.0 M)	400	80	2	34.2	2.4	0.2	1290	1.3	This work
4a-Co (40)	ABE (0.5 M)	400	80	2	1.9	0.1	0.2	3350	2.4	This work
7 (10)	AEE (1.8 M)	435	60	15	2.1	1.1	0.4	10000	2.1	Nozaki (**7c**)[4]
8 (20)	ABE (1.0 M)	118	80	1	10.0	0.3	1.6	19600	1.8	Chen (**1**)[5]
9 (20)	BVE (1.0 M)	118	80	6	1.7	0.4	2.0	8000	2.0	Chen (**Ni4**)[6]
10 (20)	ABE (1.0 M)	294	50	2	2.0	0.1	0.6	15886	3.5	Jian (**4**)[2]
11 (5)	BVE (2.4 M)	20	80	19	1.0	0.7	6.9	3100	-	Jordan (**1**)[1]
12 (15)	BVE (1.0 M)	435	90	48	1.0	1.8	0.5	12353	1.7	Carrow (**3i**)[7]
13 (20)	ABE (0.3 M)	294	90	1	116	4.1	0.1	45263	1.9	Jian (**4**)[8]
14 (10)	BVE (6.3 M)	435	100	15	2.5	1.3	1.6	9000	1.9	Nozaki (**3f**)[9]
15 (20)	AEE (1.0M)	118	RT	3	5.0	0.5	1.6	4600	1.5	Chen(**NO-iPr-Pd⁺**)[10]
16 (10)	BVE (2.6 M)	435	80	20	9.8	7.0	0.1	11000	3.8	Nozaki (**2f**)[11]
17 (10)	BVE (3.9 M)	435	80	3	54.0	5.8	1.1	15000	4.1	Nozaki (**1f**)[12]

[a]Comonomer abbreviations: PVE = propyl vinyl ether, AEE = allyl ethyl ether, ABE = allyl butyl ether, BVE = butyl vinyl ether.

Table S10. Comparison of Polymerization Activity and the Cation Properties of NiM Complexes

Metal (M)	**Charge**	**Crystal Ionic Radius**[a] (pm)	**Lewis Acidity**[b]	**Activity of NiM Complex**[c] (10^5 g/mol·h)
K	+1	152	0.126	3.9
Mg	+2	86	0.33	6.2
Ca	+2	114	0.30	7.7
Co[d]	+2	88.5	0.42	26.6
Cu	+2	87	0.42	0
Zn	+2	88	0.50	12.1
Sn	+2	-	0.36	2.3
Sc	+3	88.5	0.50	3.7
Al	+3	67.5	0.73	0.5
Ga	+3	76	0.75	5.5
Bi	+3	117	0.50	0.3
La	+3	117	-	5.2

[a]Data obtained from Shannon (*Acta Cryst*., 1976)[13] for metal cations with coordination number of 6. [b]Data obtained from Brown (*Acta Cryst*., 1988)[14] for metal cations with divalent anions. [c]Polymerization data from Table S9. [d]High spin configuration.

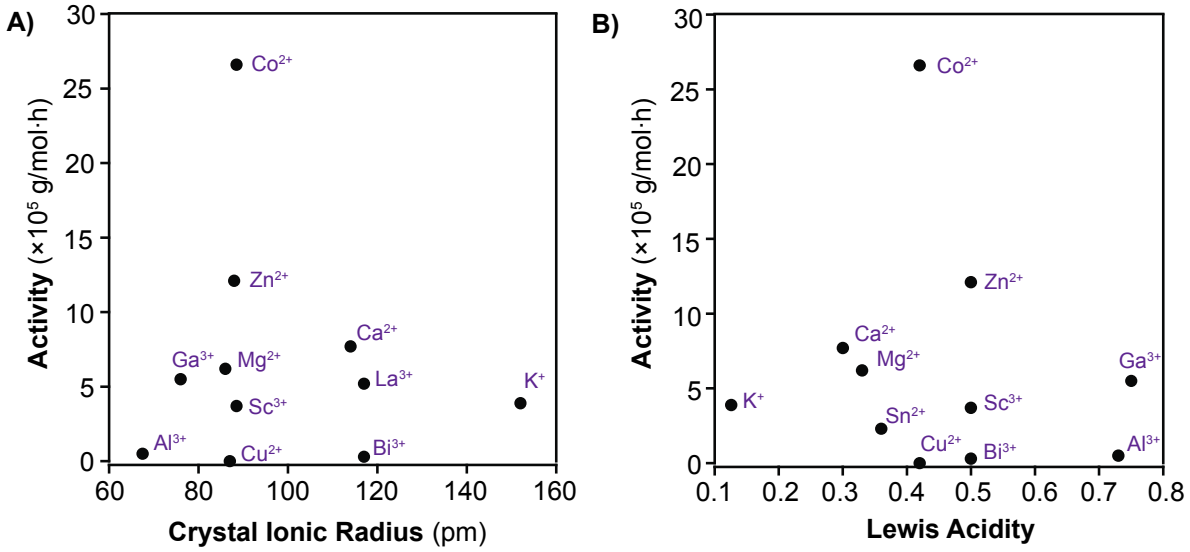

Figure S17. Graphical representation of the data in Table S10 examining the possible correlation between catalyst polymerization activity and either the crystal ionic radius (A) or Lewis acidity (B) of the secondary metal cation.

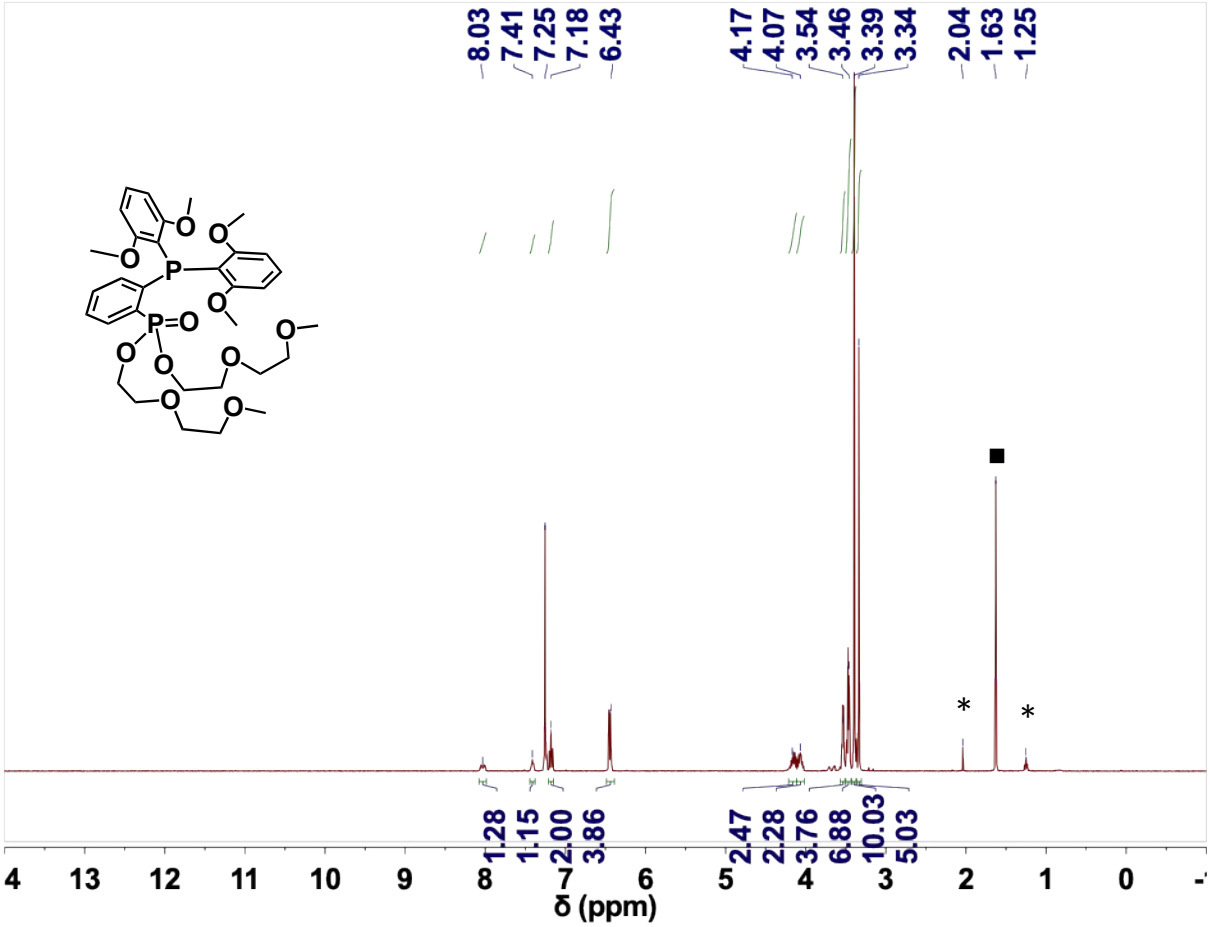

Figure S18. ^{1}H NMR spectrum ($CDCl_3$, 400 MHz) of **3b**. The peaks at 1.27, 2.04 marked with an asterisk (*) come from trace ethyl acetate, whereas the peak at 1.6 marked with a square (■) comes from trace water.

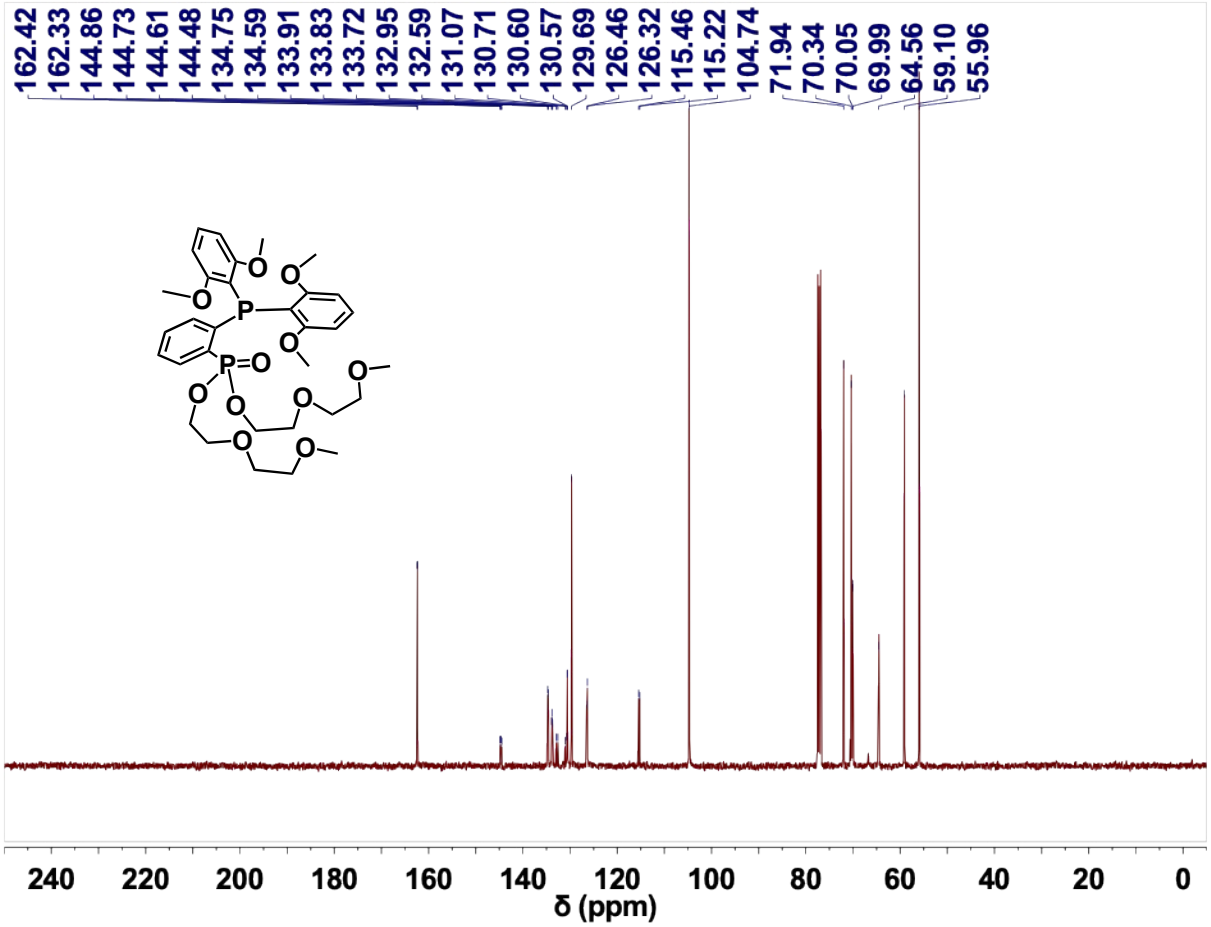

Figure S19. ^{13}C NMR spectrum ($CDCl_3$, 100 MHz) of **3b**.

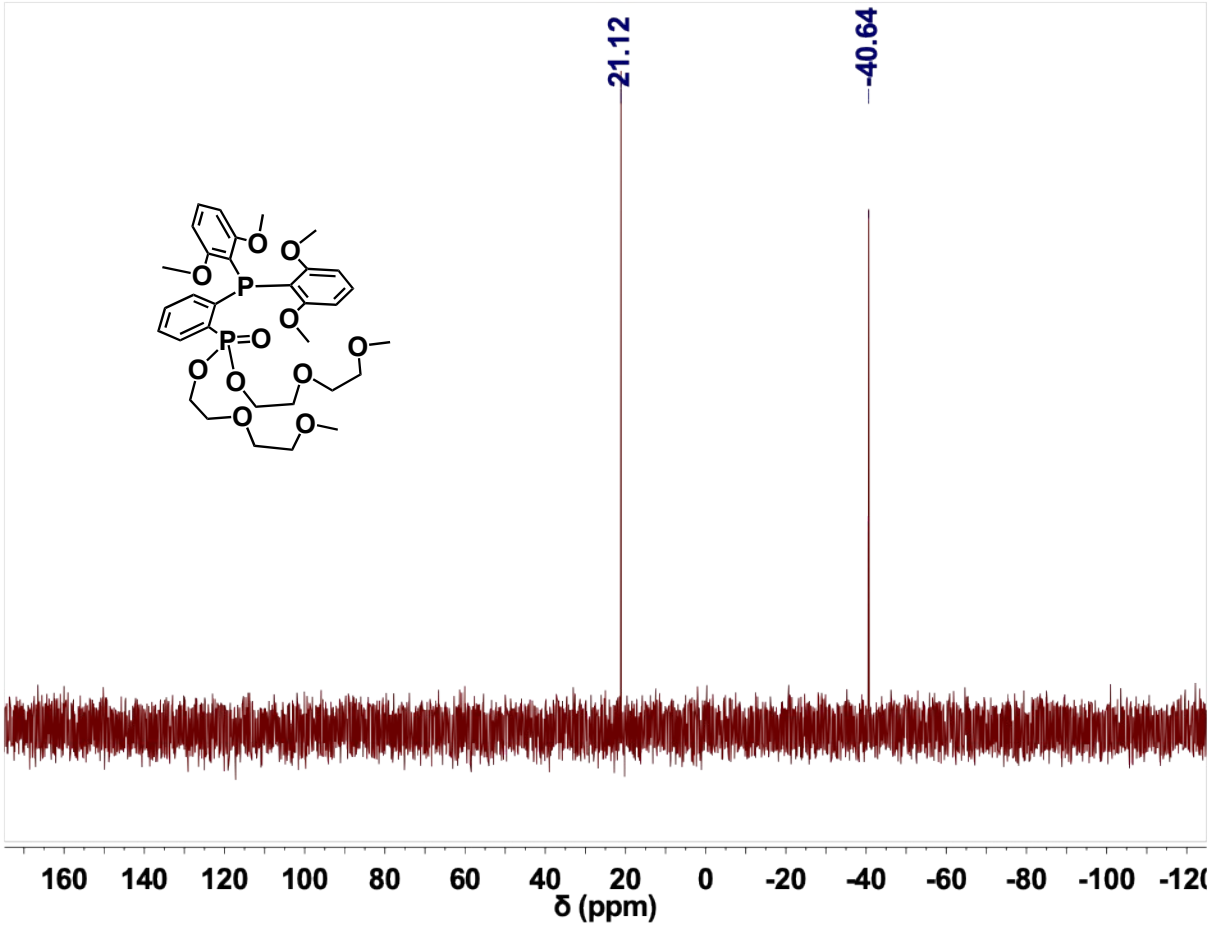

Figure S20. ^{31}P NMR spectrum ($CDCl_3$, 162 MHz) of **3b**.

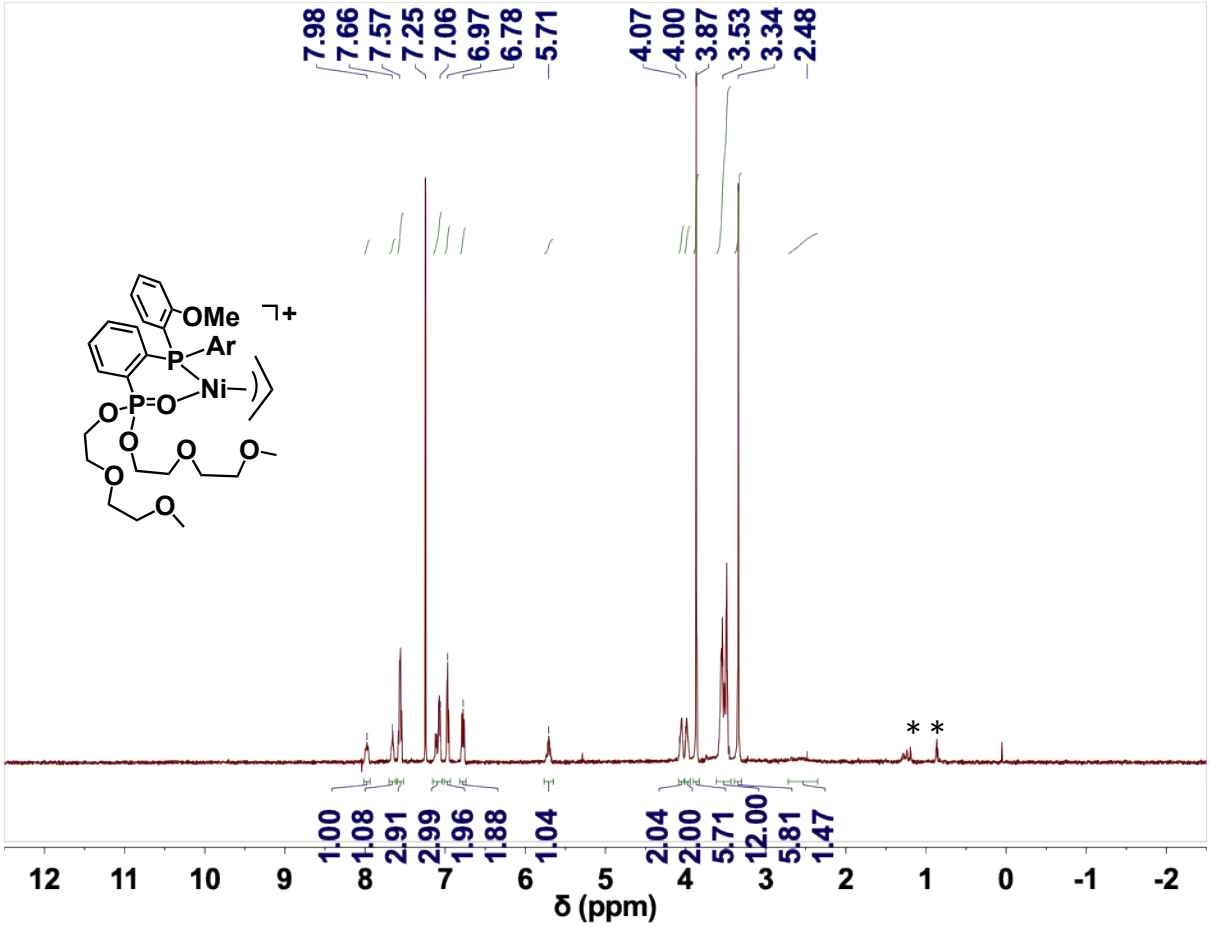

Figure S21. ^{1}H NMR spectrum ($CDCl_3$, 400 MHz) of **4a**. The peaks at 0.86 and 1.29 ppm marked with a square (*) come from trace pentane.

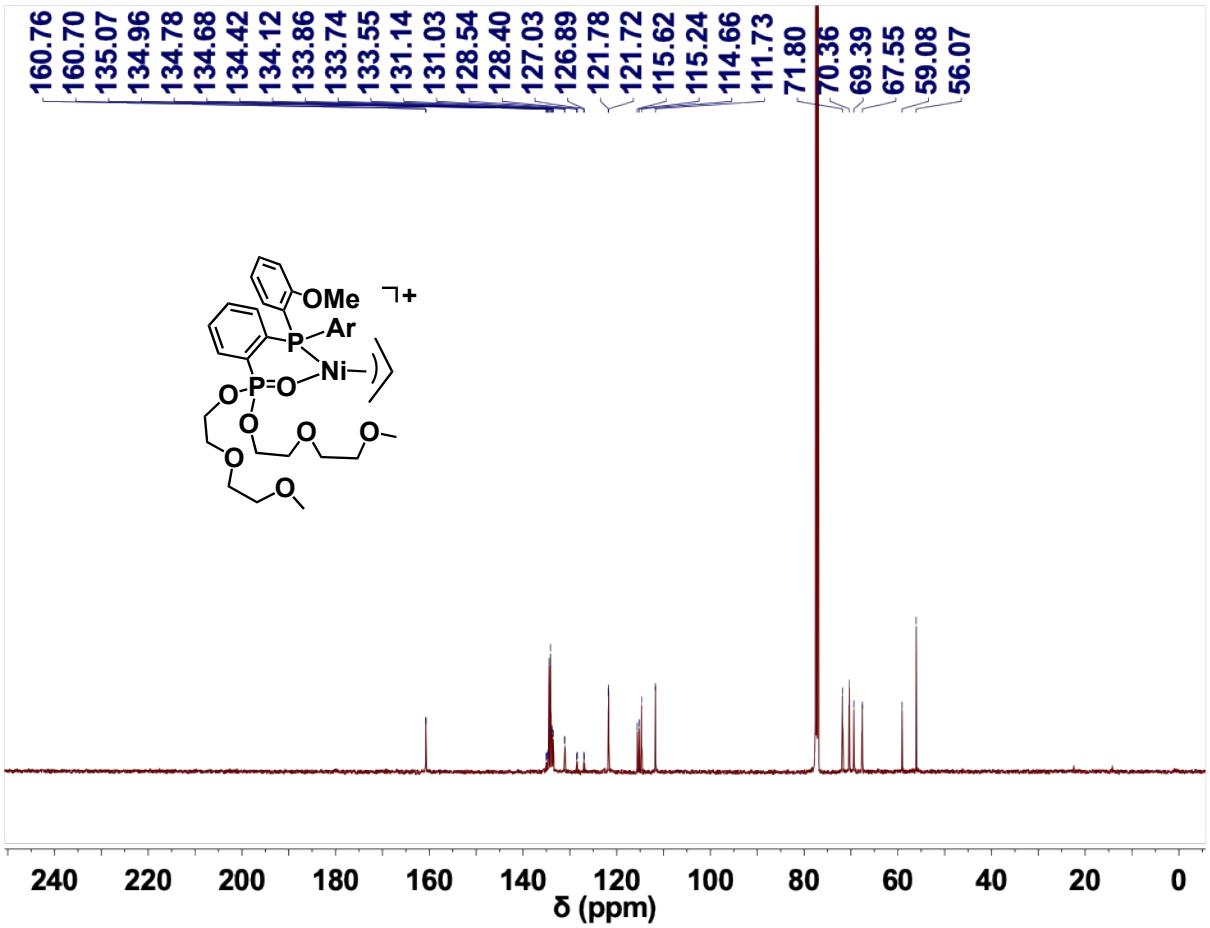

Figure S22. ^{13}C NMR spectrum ($CDCl_3$, 125 MHz) of **4a**.

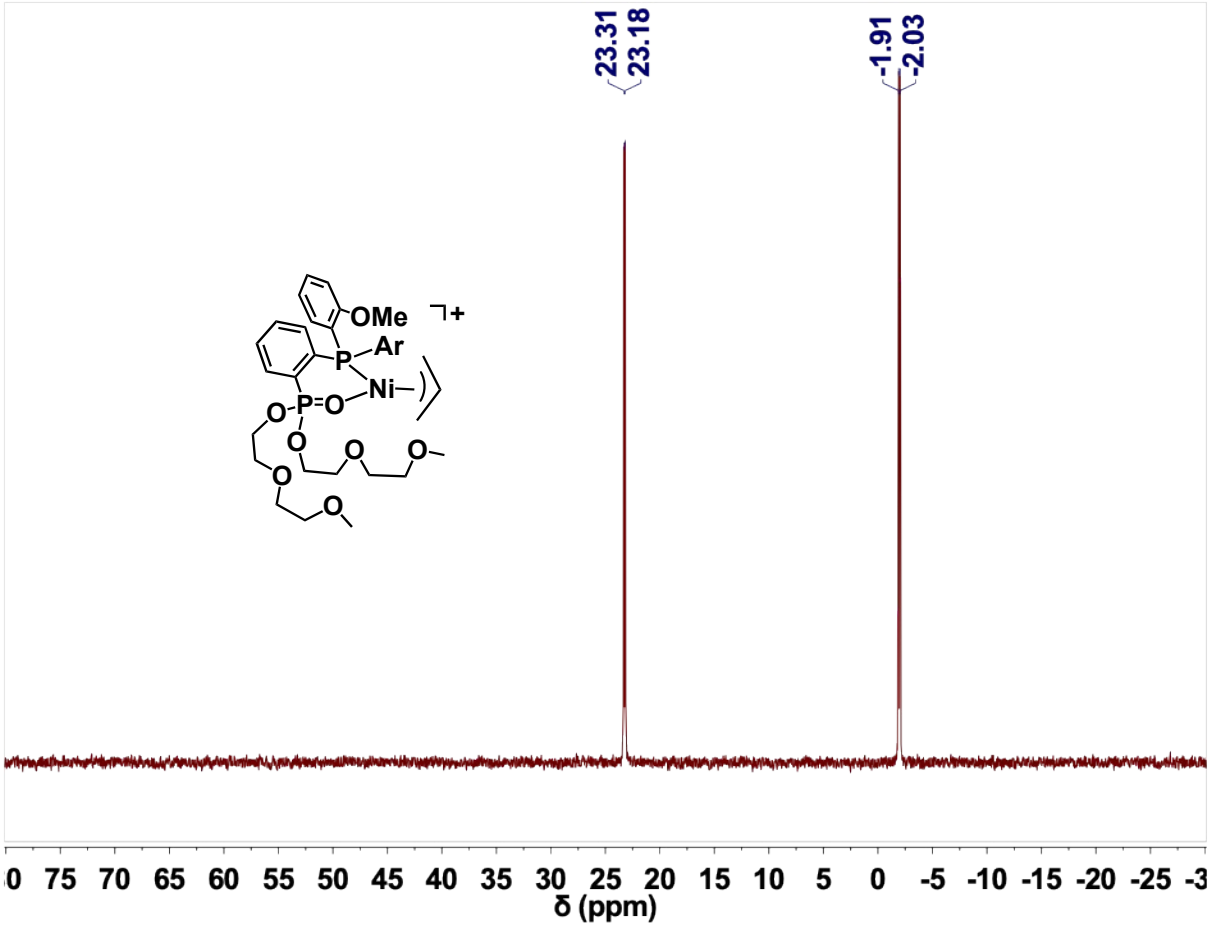

Figure S23. ^{31}P NMR spectrum ($CDCl_3$, 162 MHz) of **4a**.

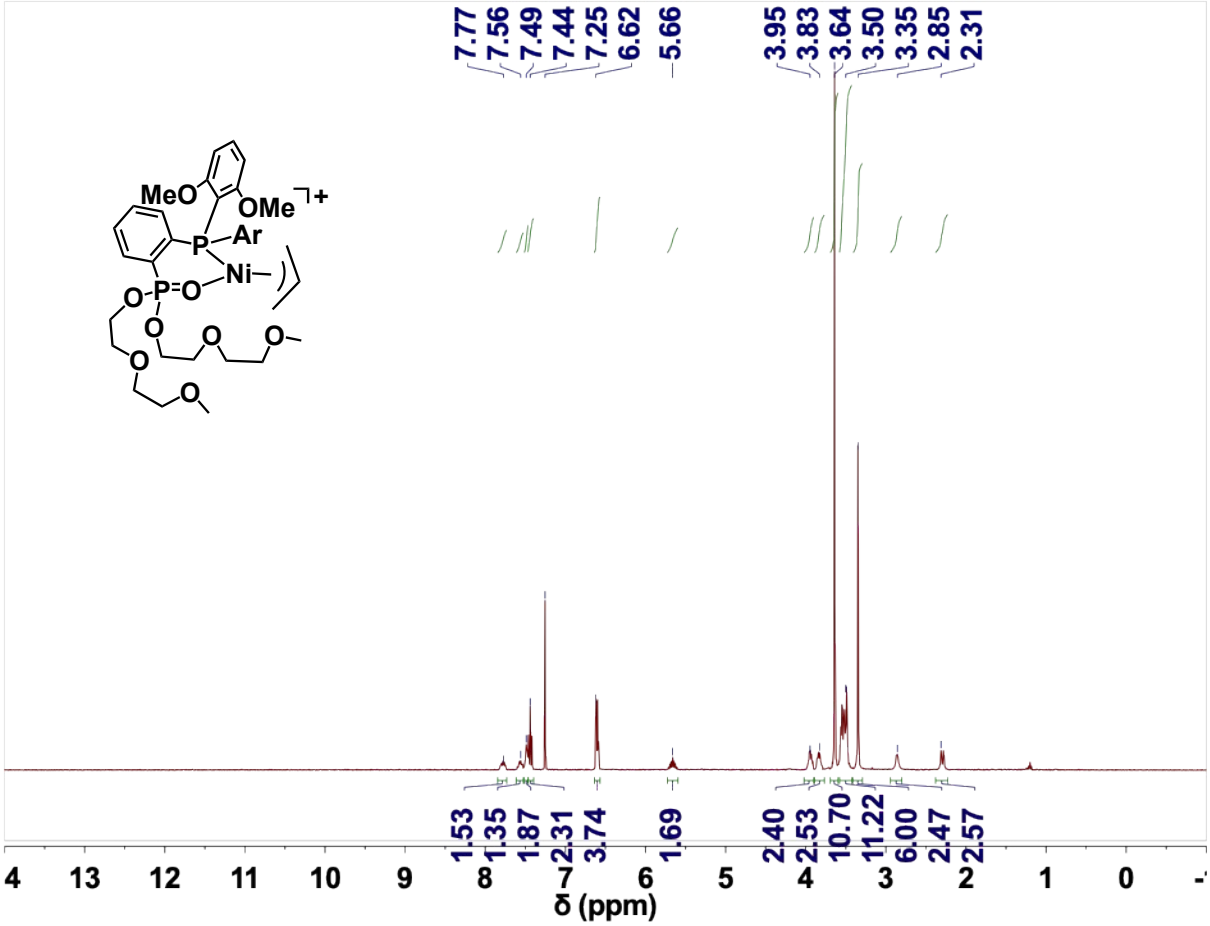

Figure S24. ^{1}H NMR spectrum ($CDCl_3$, 400 MHz) of **4b**.

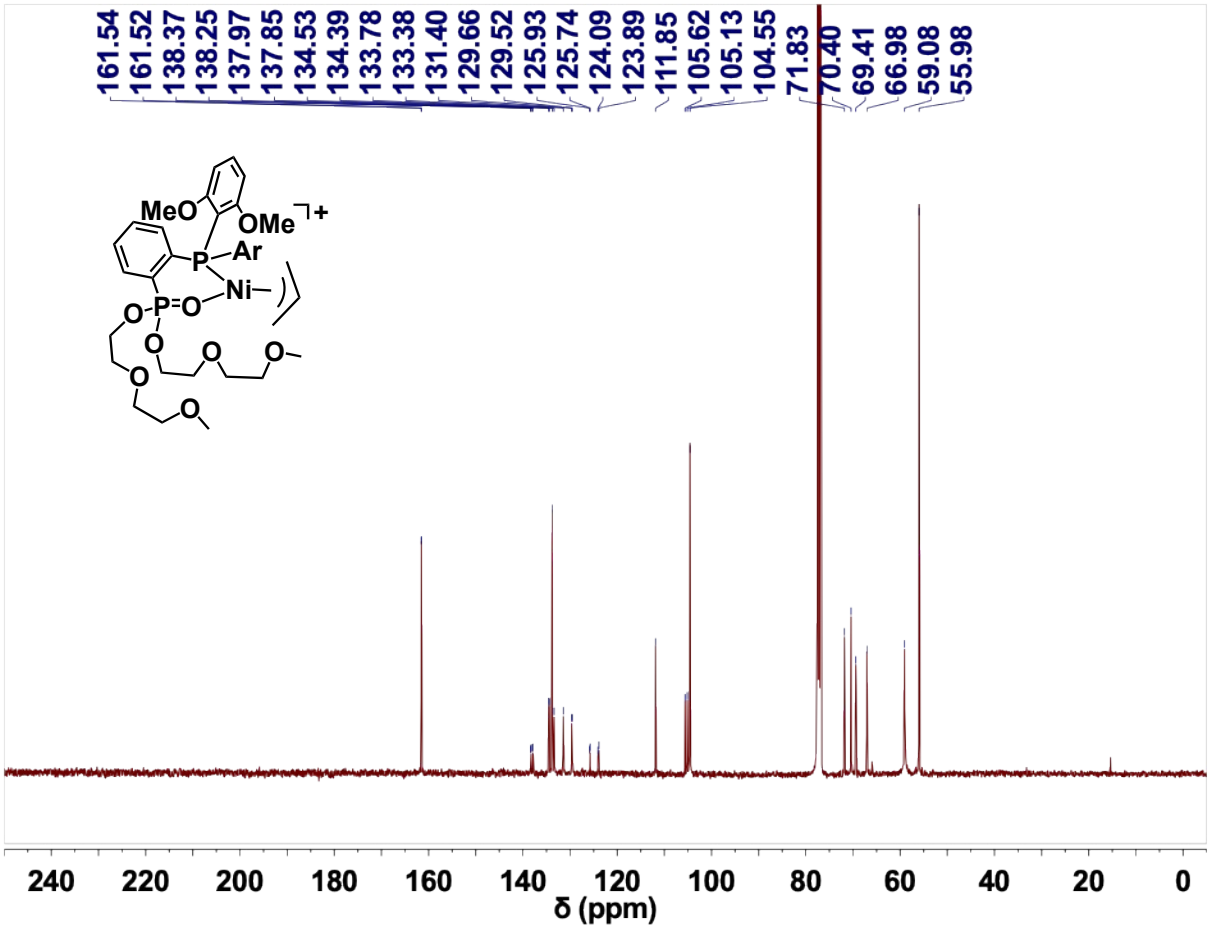

Figure S25. ^{13}C NMR spectrum ($CDCl_3$, 125 MHz) of **4b**.

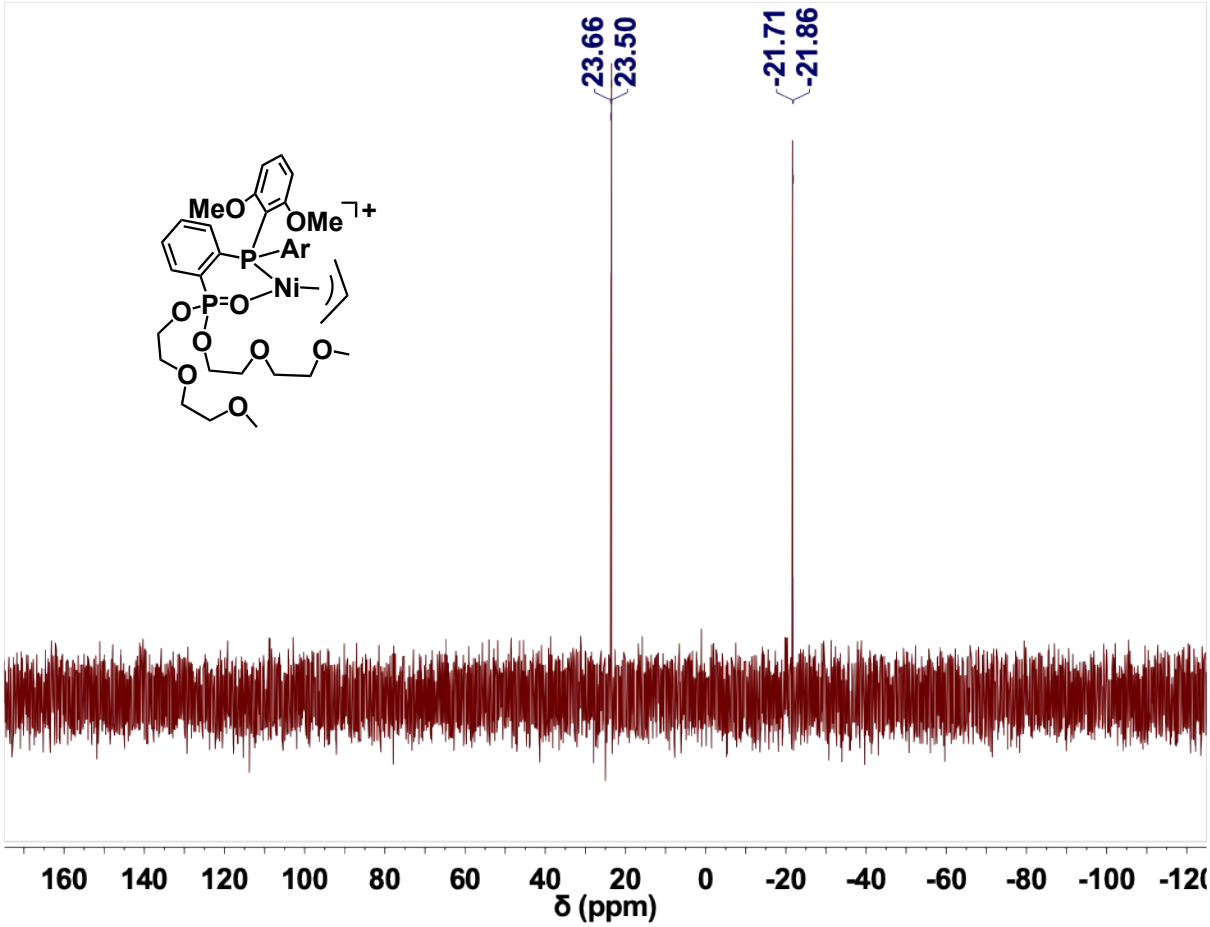

Figure S26. ^{31}P NMR spectrum ($CDCl_3$, 162 MHz) of **4b**.

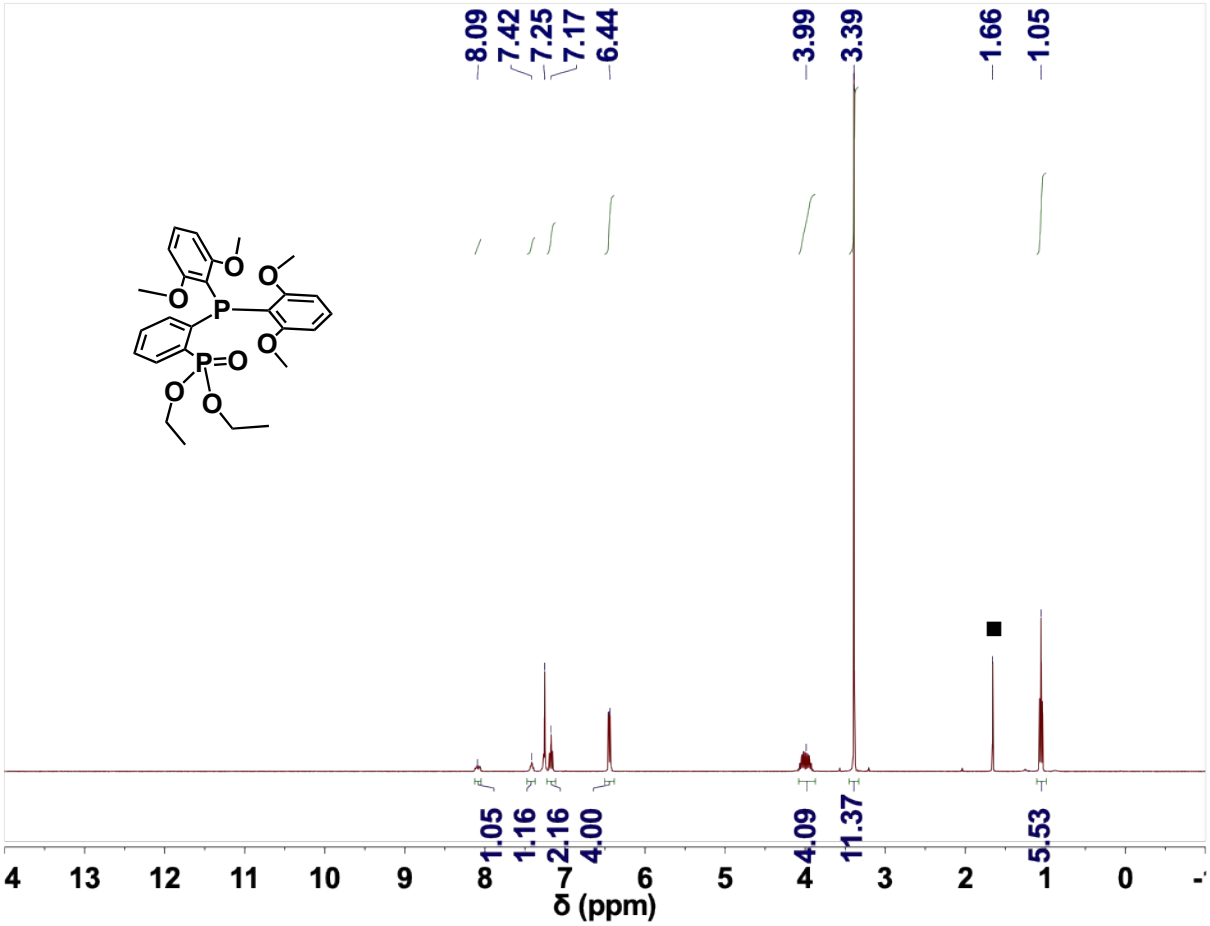

Figure S27. ^{1}H NMR spectrum ($CDCl_3$, 400 MHz) of **5b**. The peak at 1.66 ppm marked with an asterisk (■) comes from trace water.

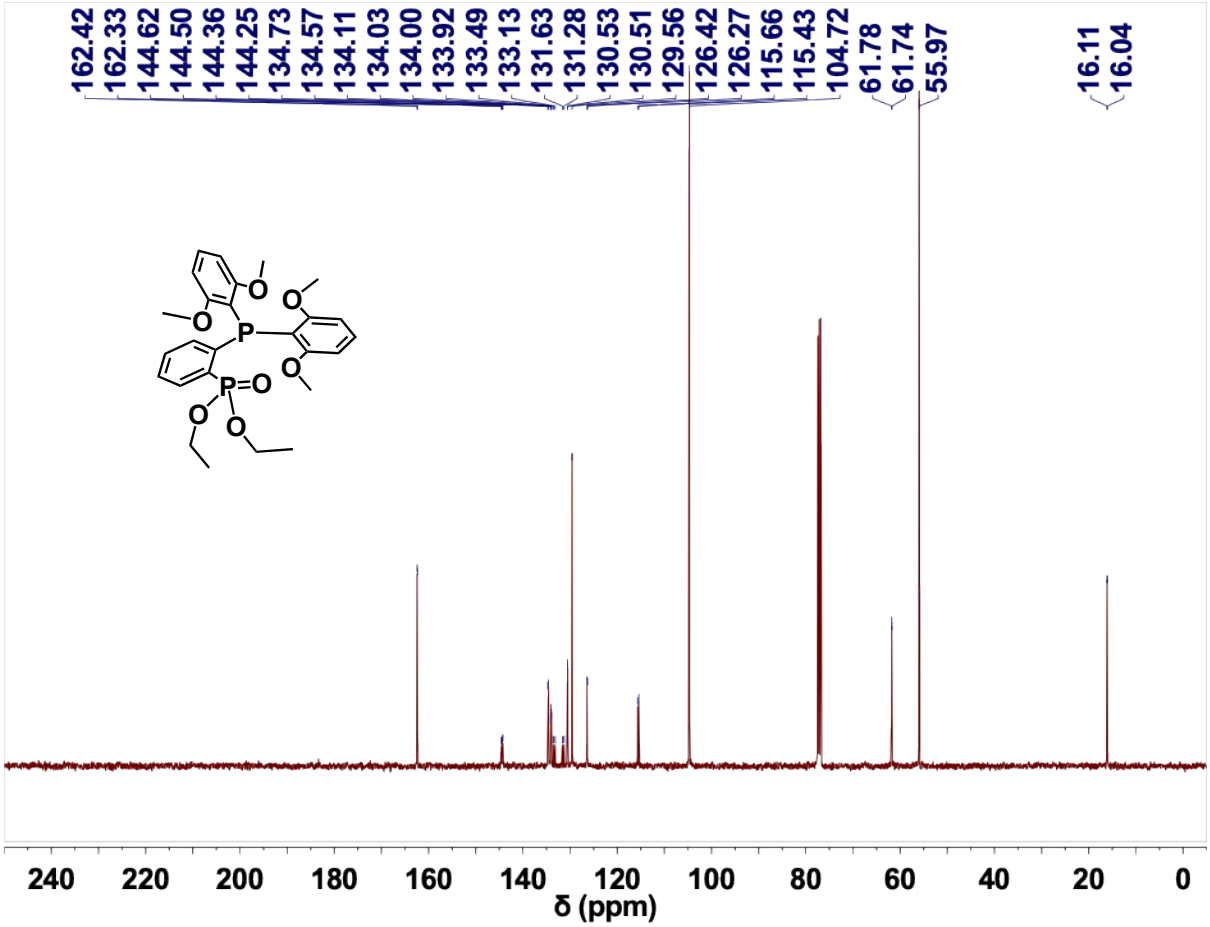

Figure S28. ^{13}C NMR spectrum ($CDCl_3$, 100 MHz) of **5b**.

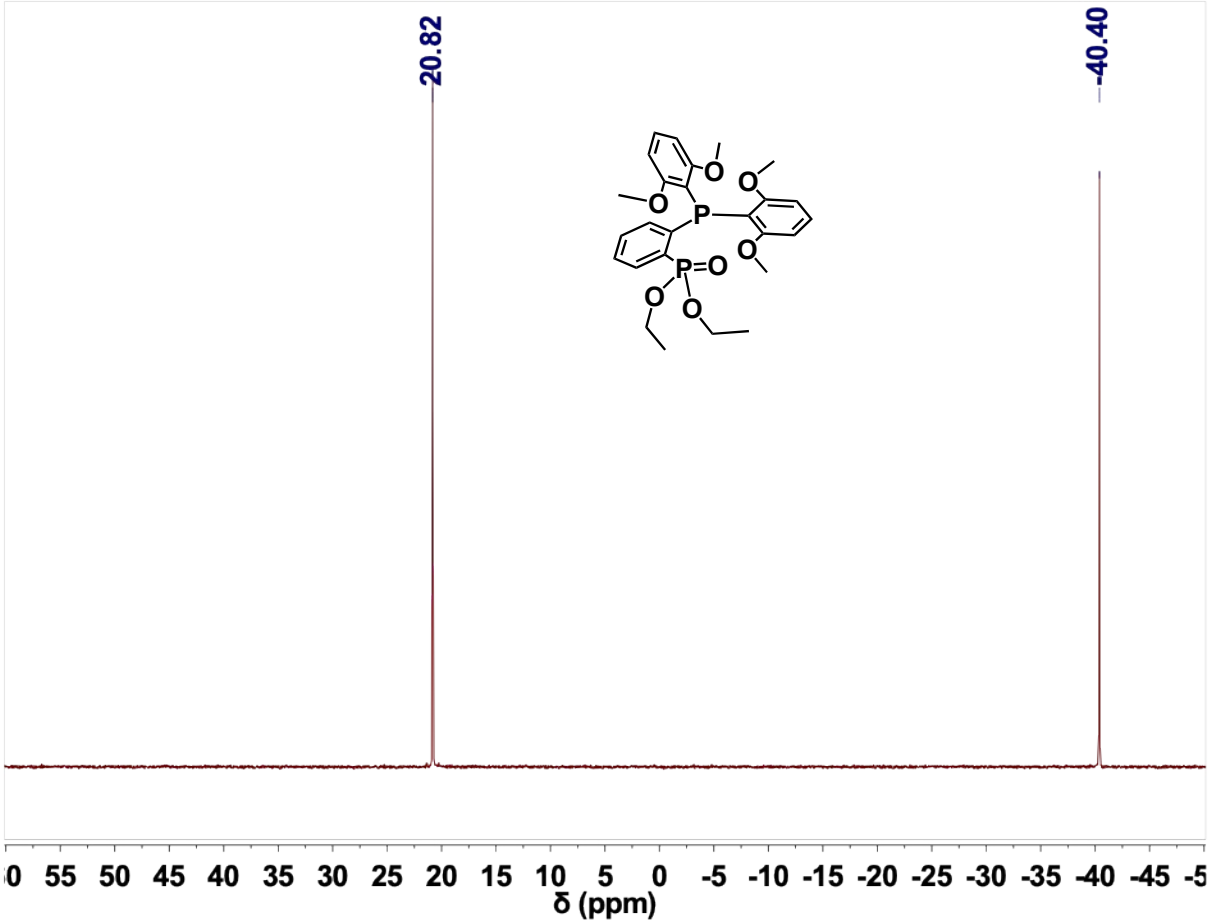

Figure S29. ^{31}P NMR spectrum ($CDCl_3$, 162 MHz) of **5b**.

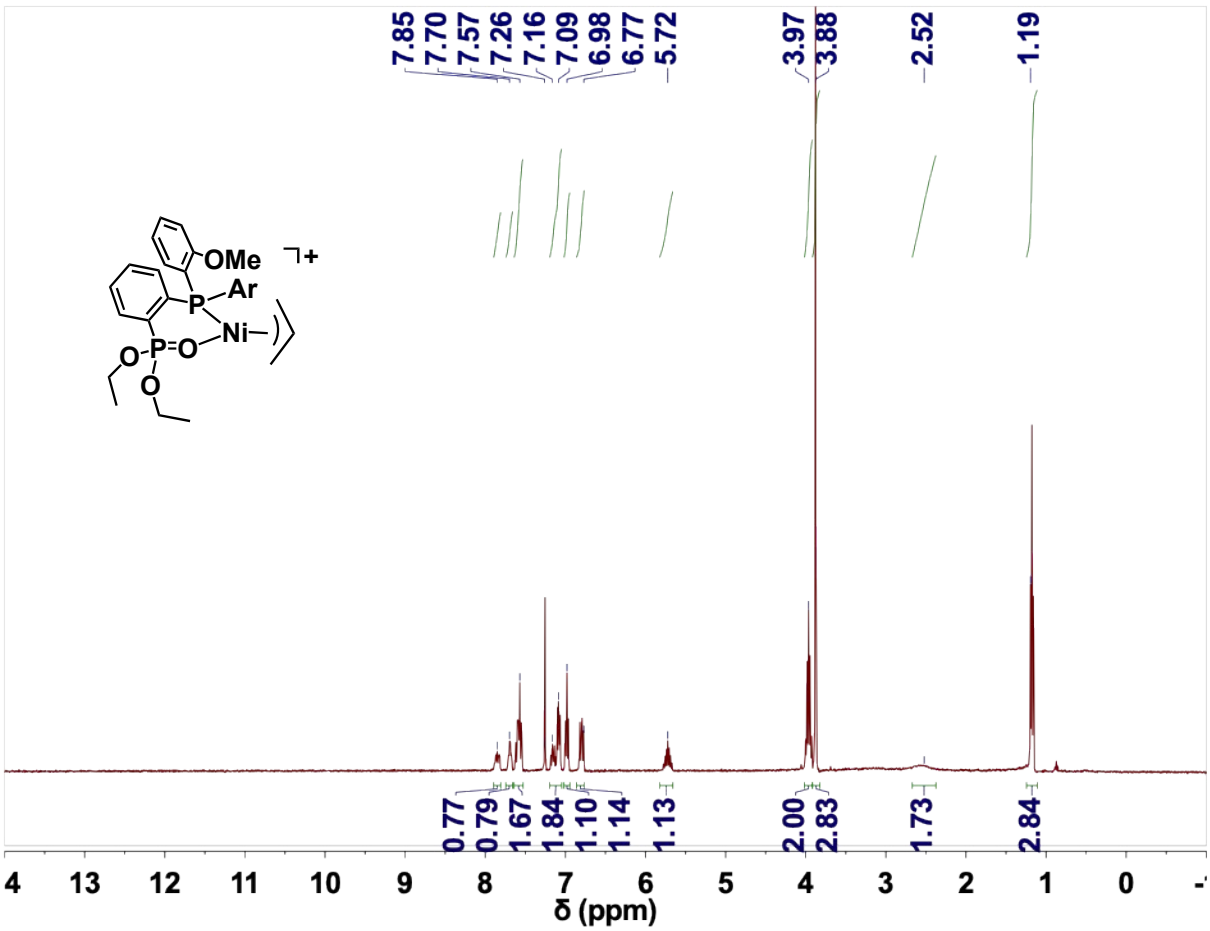

Figure S30. ^{1}H NMR spectrum ($CDCl_3$, 400 MHz) of **6a**.

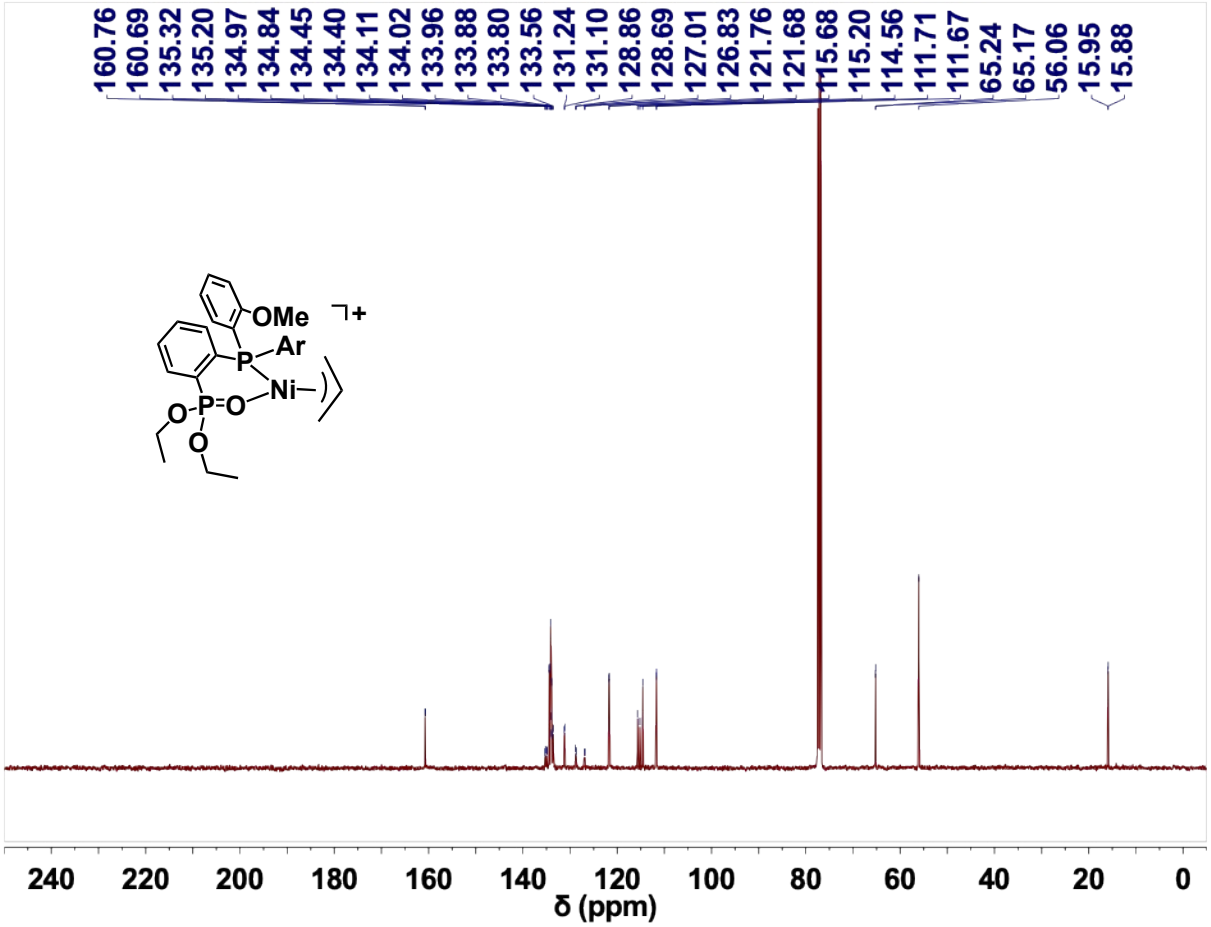

Figure S31. ^{13}C NMR spectrum ($CDCl_3$, 100 MHz) of **6a**.

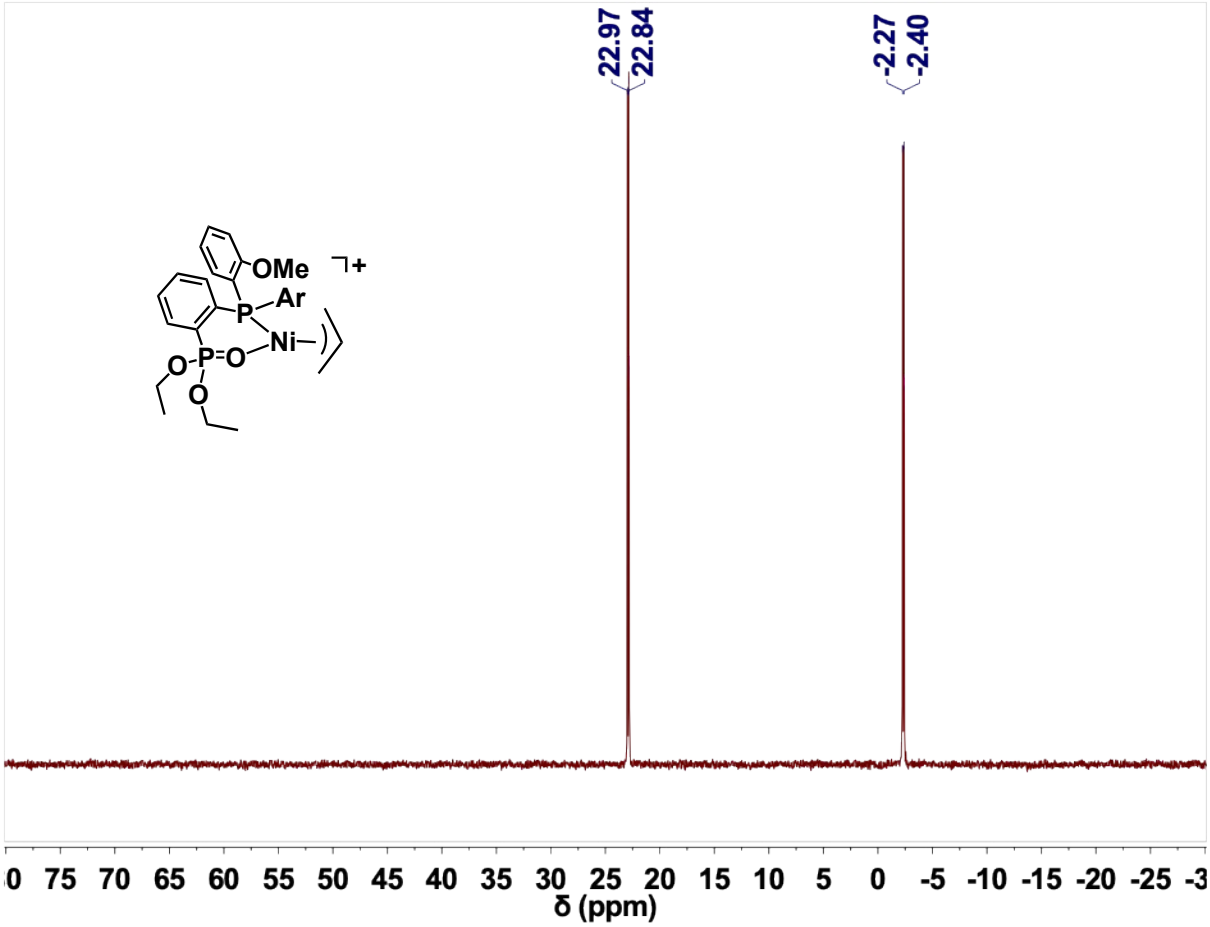

Figure S32. ^{31}P NMR spectrum ($CDCl_3$, 162 MHz) of **6a**.

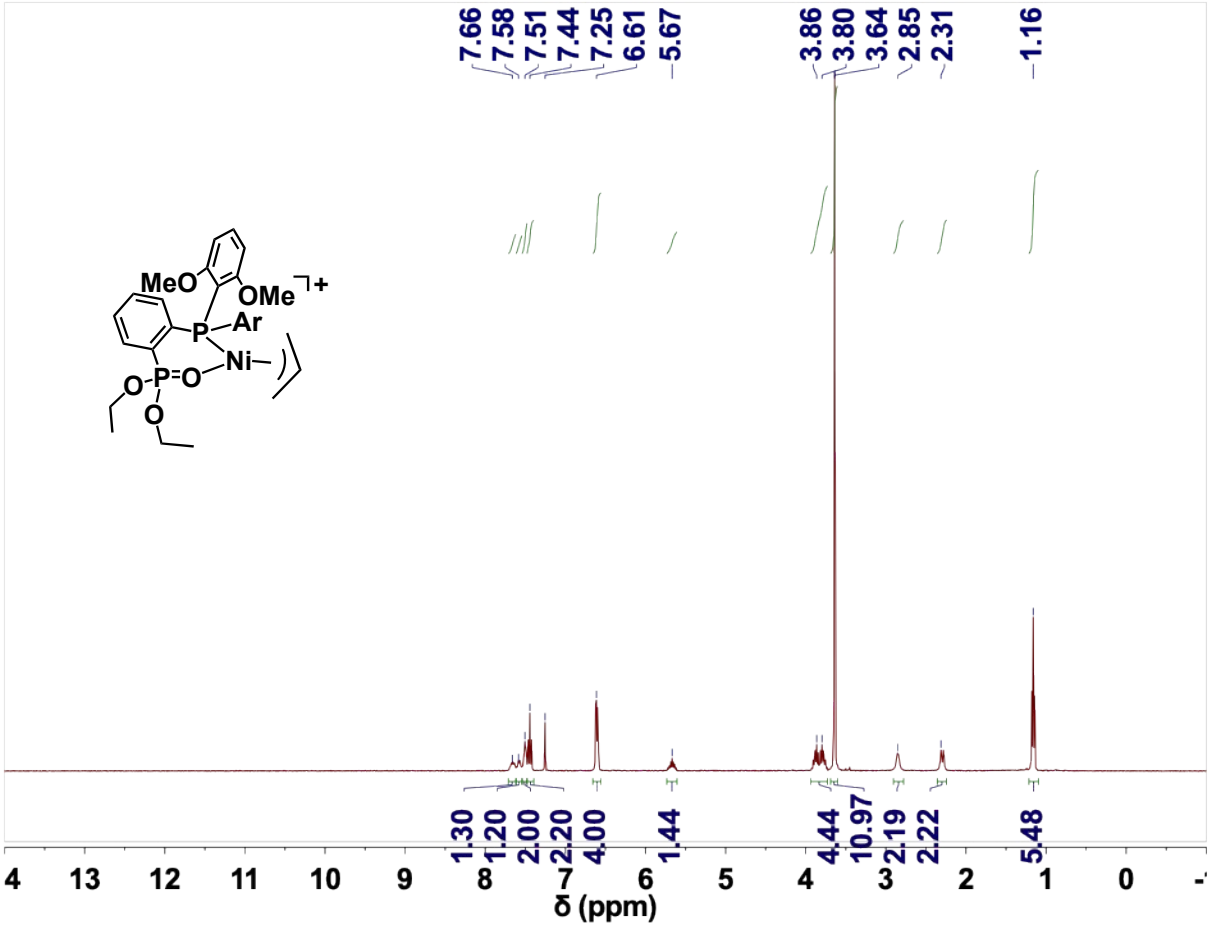

Figure S33. ^{1}H NMR spectrum ($CDCl_3$, 400 MHz) of **6b**.

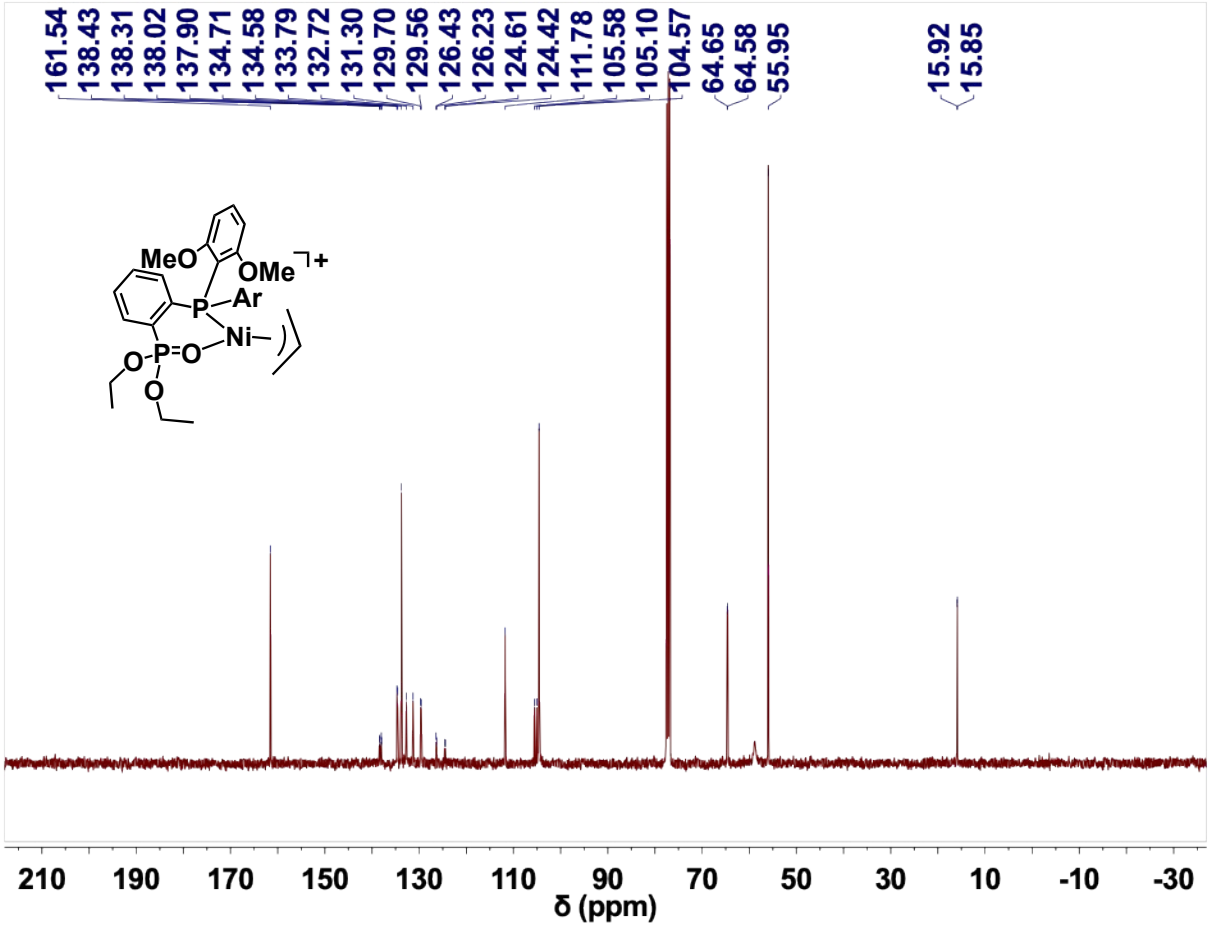

Figure S34. ^{13}C NMR spectrum ($CDCl_3$, 100 MHz) of **6b**.

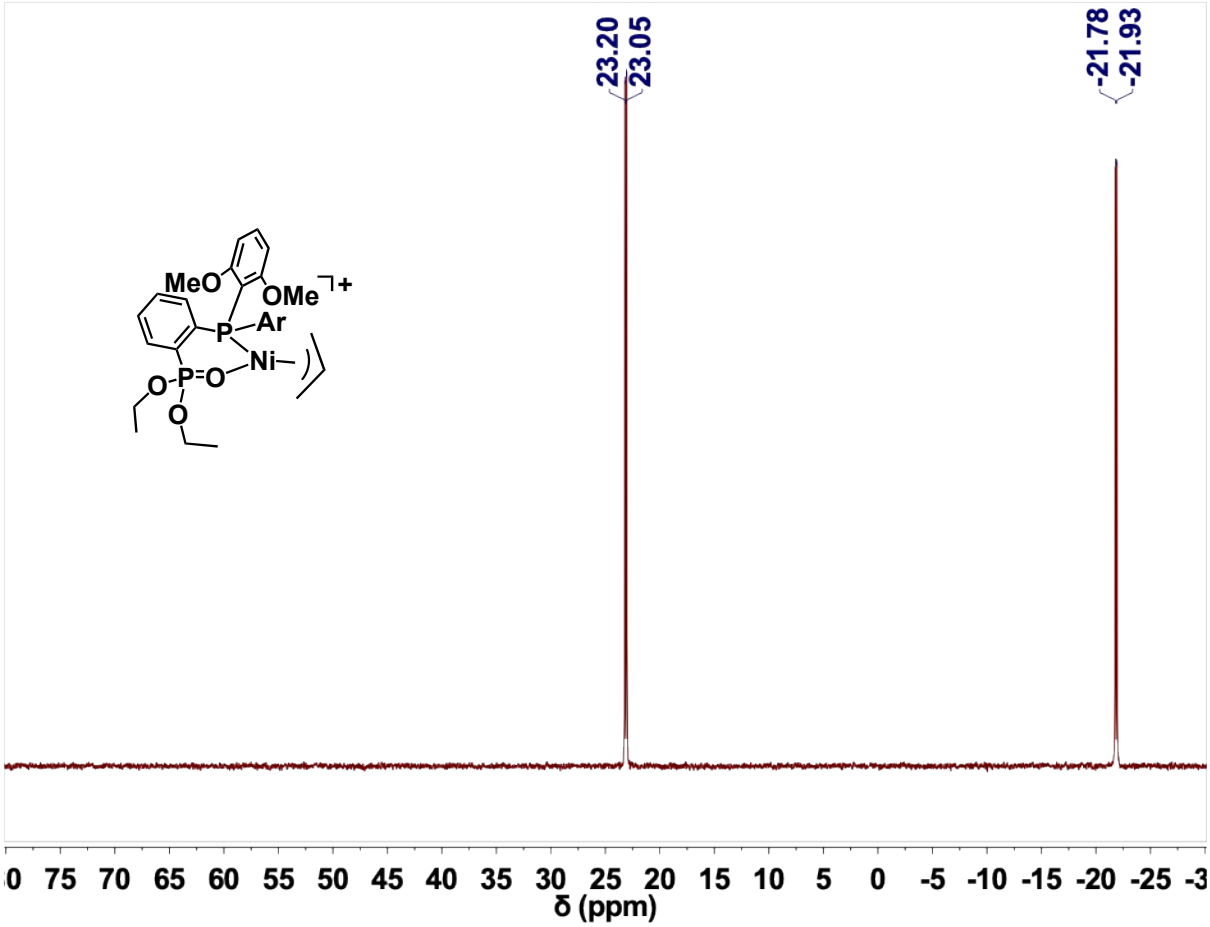

Figure S35. ^{31}P NMR spectrum ($CDCl_3$, 162 MHz) of **6b**.

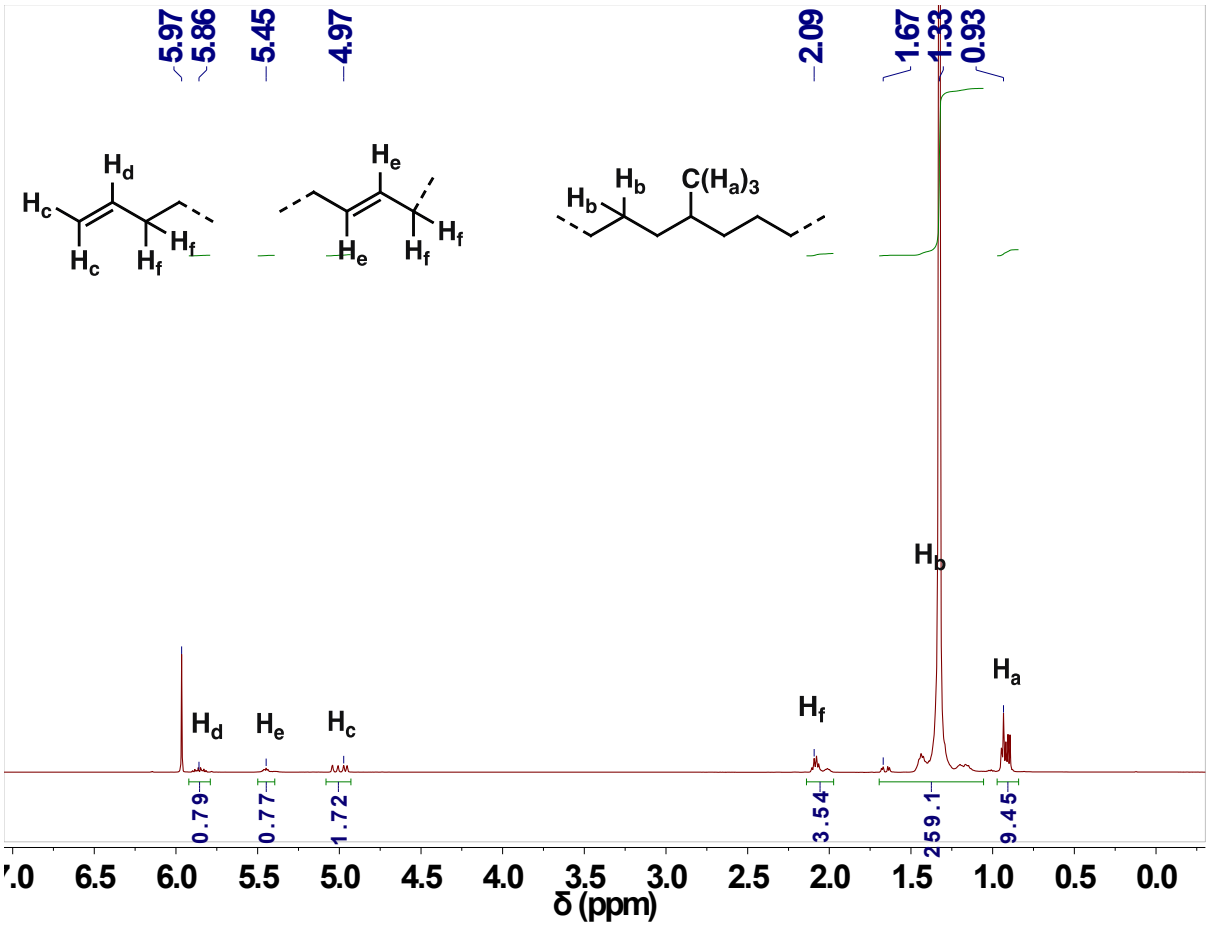

Figure S36. ^{1}H NMR spectrum ($C_2D_2Cl_4$, 500 MHz, 120 °C) of polyethylene produced by **4a** in DCM/toluene (1:24) (Table 1, entry 1).

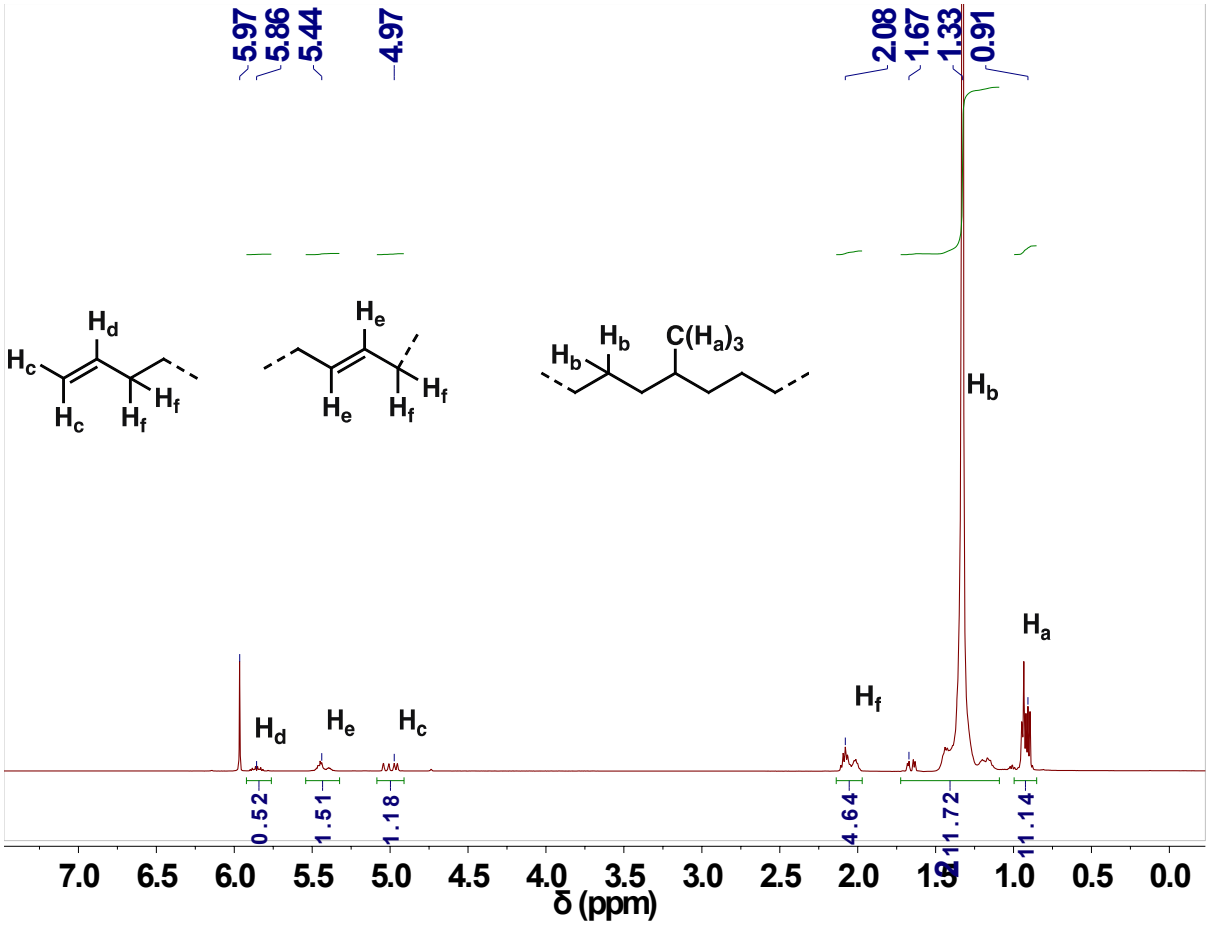

Figure S37. ^{1}H NMR spectrum ($C_2D_2Cl_4$, 500 MHz, 120 °C) of polyethylene produced by **4a**-Na in DCM/toluene (1:24) (Table 1, entry 2).

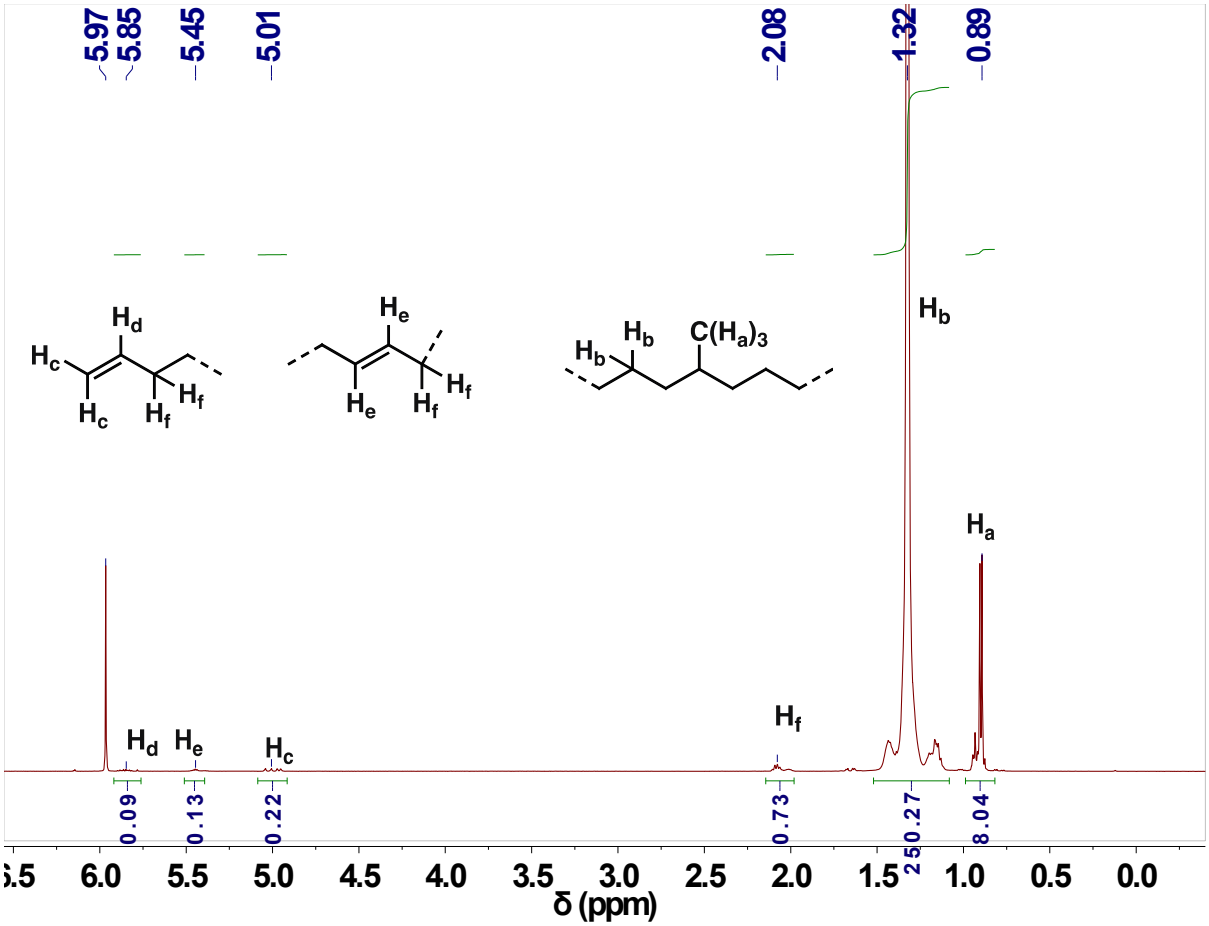

Figure S38. ^{1}H NMR spectrum ($C_2D_2Cl_4$, 500 MHz, 120 °C) of polyethylene produced by **4b** in DCM/toluene (1:24) (Table 1, entry 3).

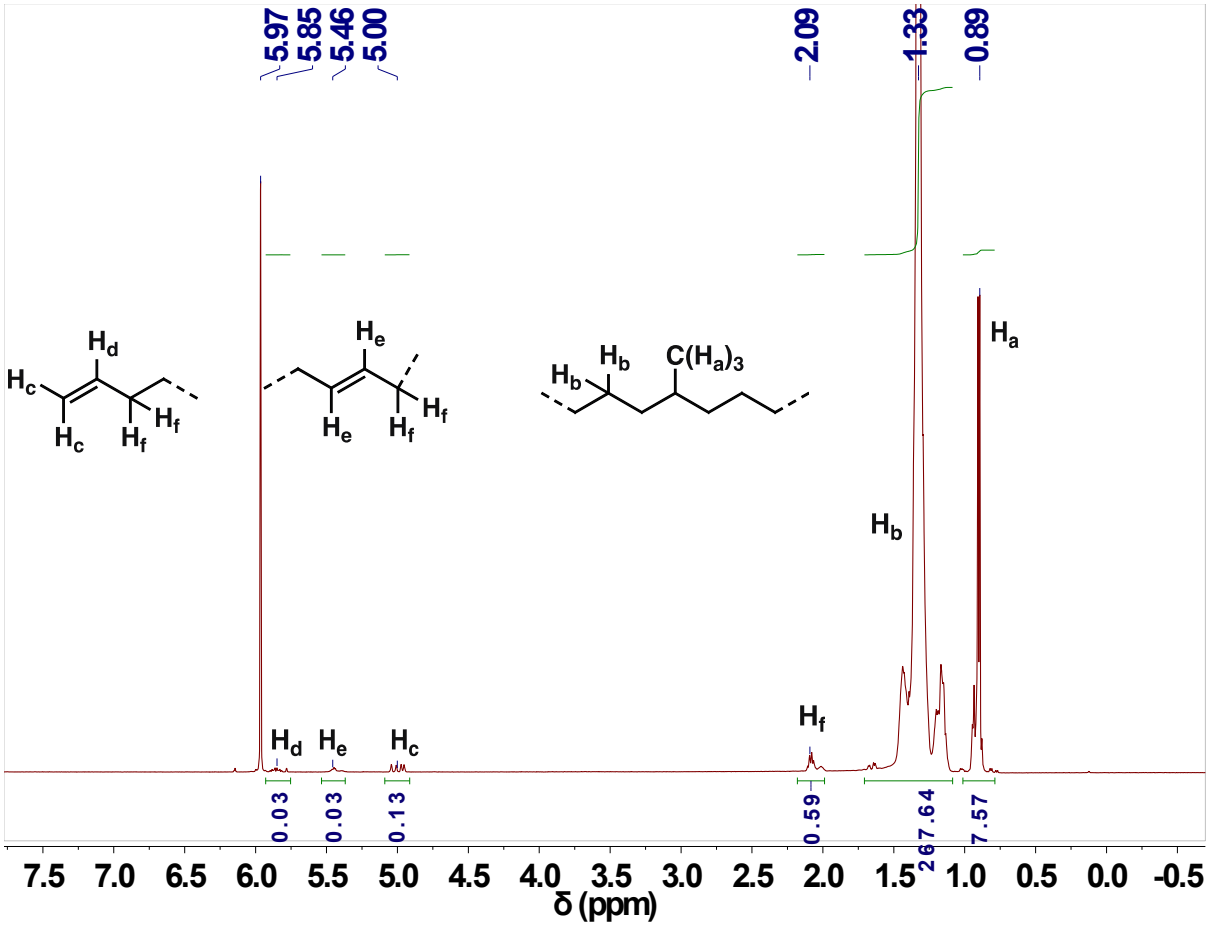

Figure S39. ^{1}H NMR spectrum ($C_2D_2Cl_4$, 500 MHz, 120 °C) of polyethylene produced by **4b**-Na in DCM/toluene (Table 1, entry 4).

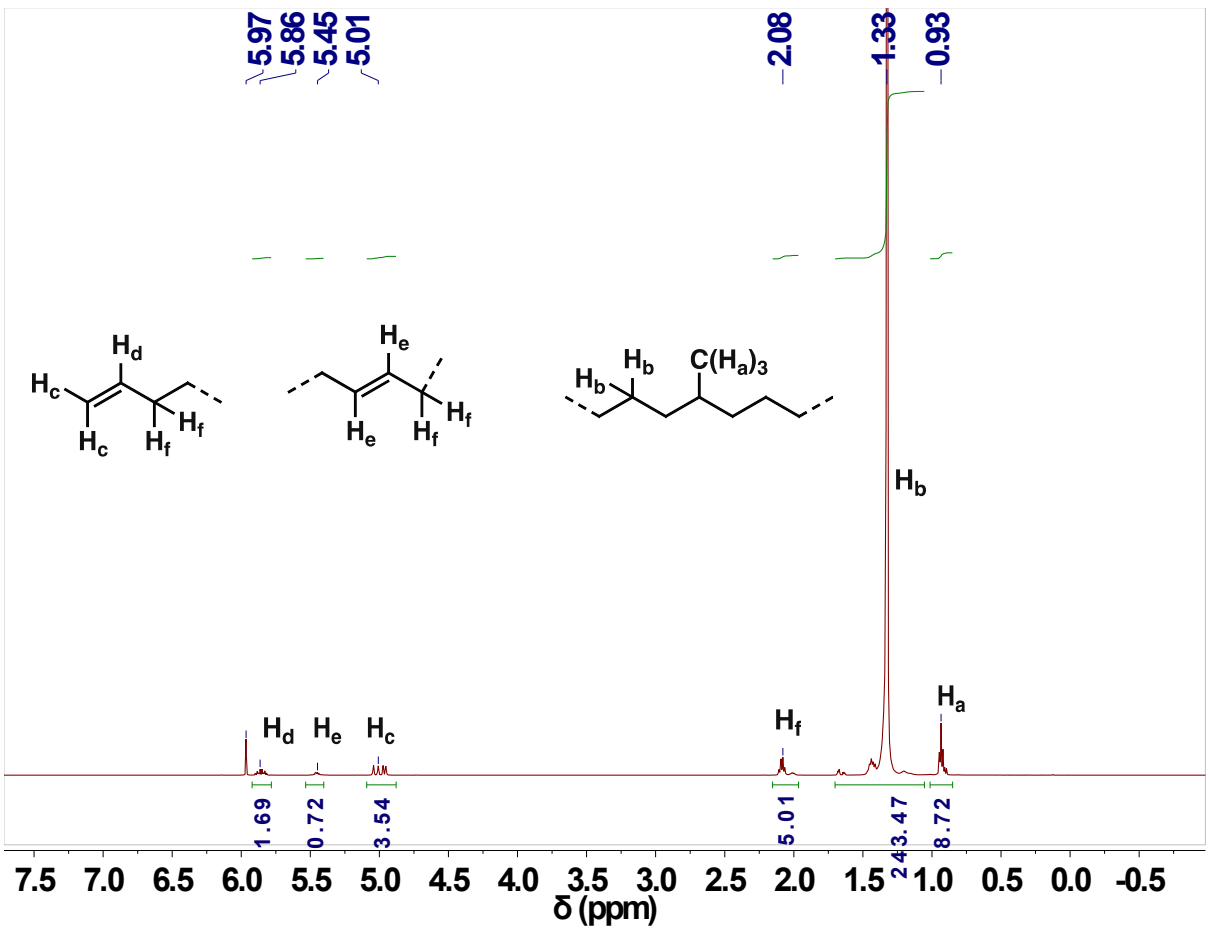

Figure S40. ^{1}H NMR spectrum ($C_2D_2Cl_4$, 500 MHz, 120 °C) of polyethylene produced by **4a** in THF (Table 2, entry 4).

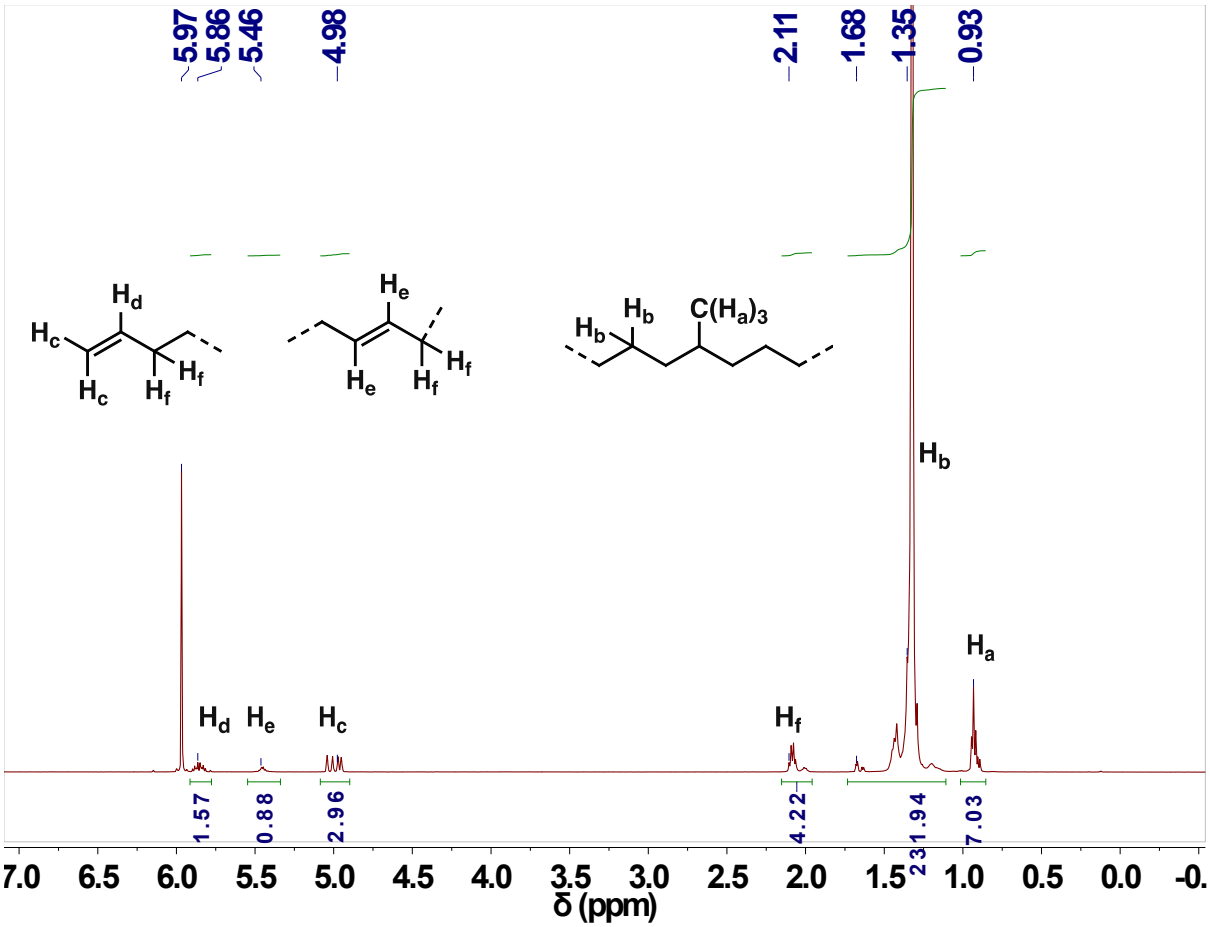

Figure S41. ^{1}H NMR spectrum ($C_2D_2Cl_4$, 500 MHz, 120 °C) of polyethylene produced by **4a**-Co in THF (Table S8, entry 10).

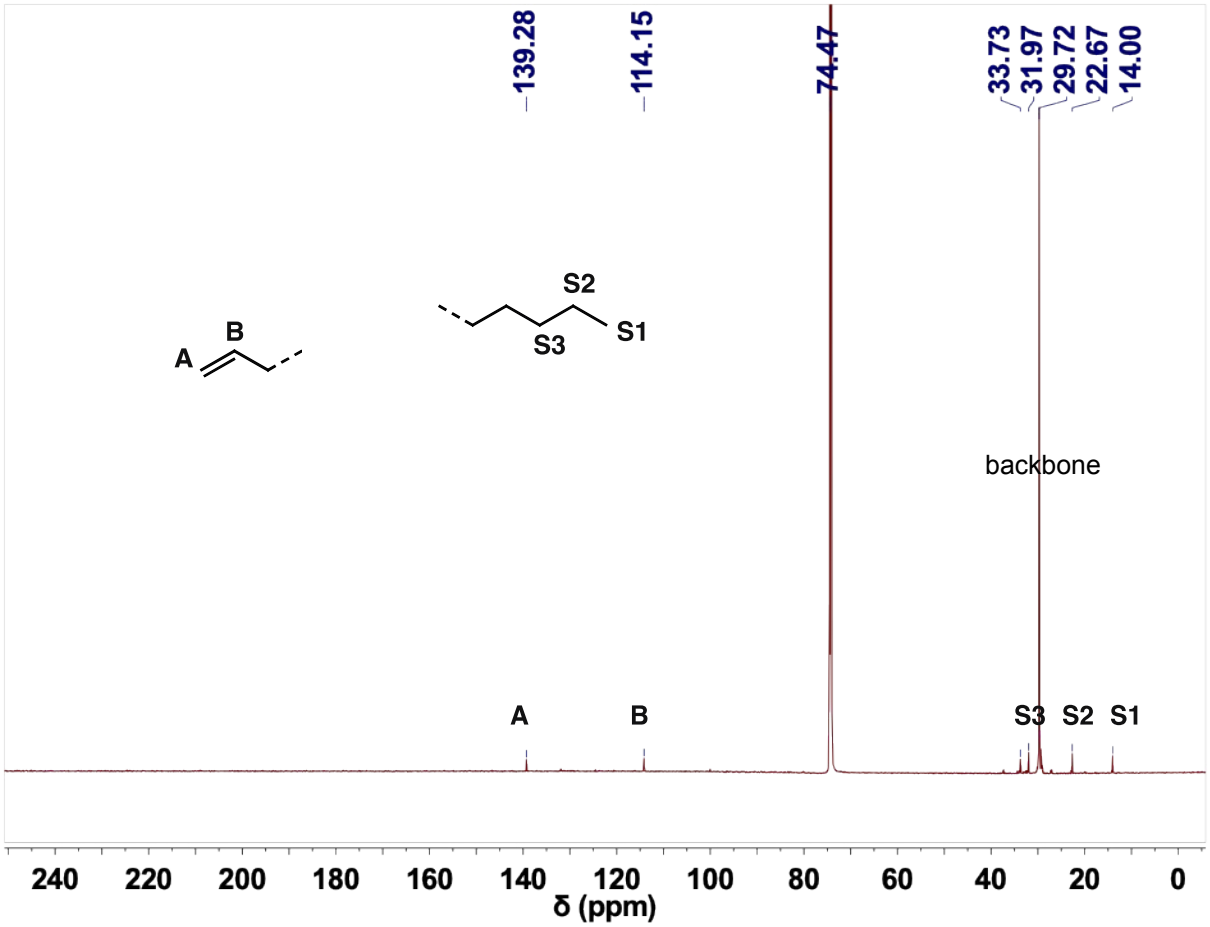

Figure S42. ^{13}C NMR spectrum ($C_2D_2Cl_4$, 150 MHz, 120 °C) of polyethylene produced by **4a**-Co in THF (Table S8, entry 10).

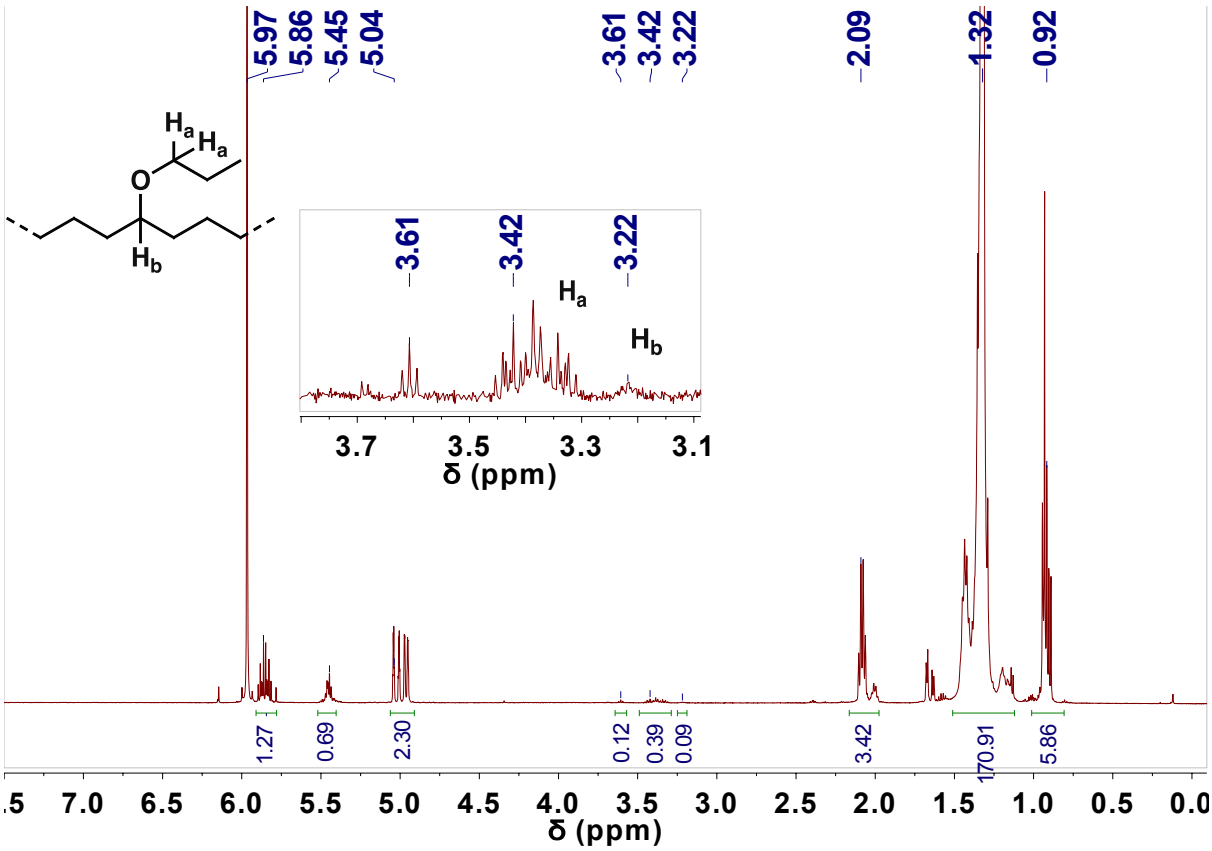

Figure S43. ^{1}H NMR spectrum ($C_2D_2Cl_4$, 500 MHz, 120 °C) of ethylene/PVE copolymer produced by **4a** in THF (Table 3, entry 1).

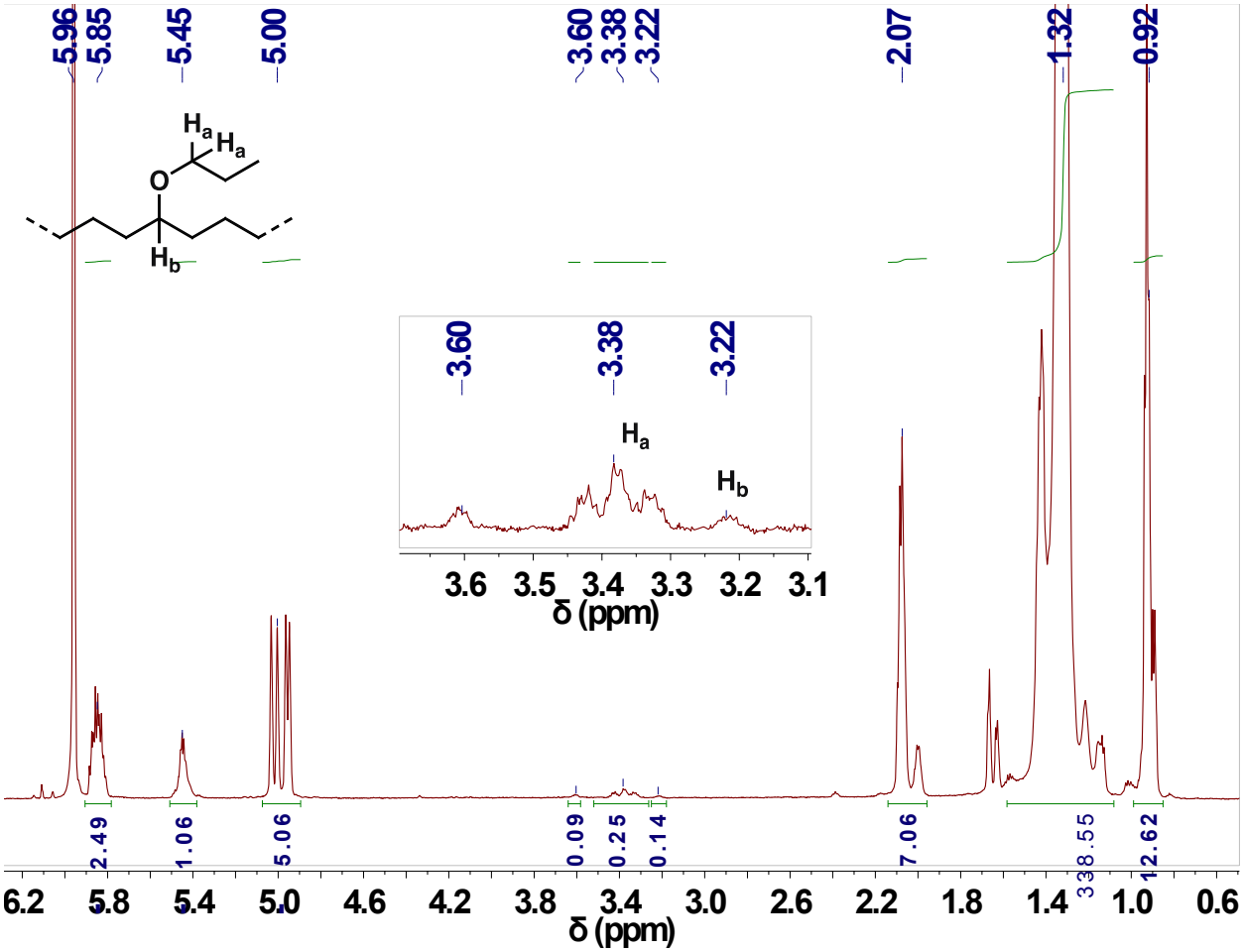

Figure S44. ^{1}H NMR spectrum ($C_2D_2Cl_4$, 500 MHz, 120 °C) of ethylene/PVE copolymer produced by **4a**-Co in THF (Table 3, entry 2).

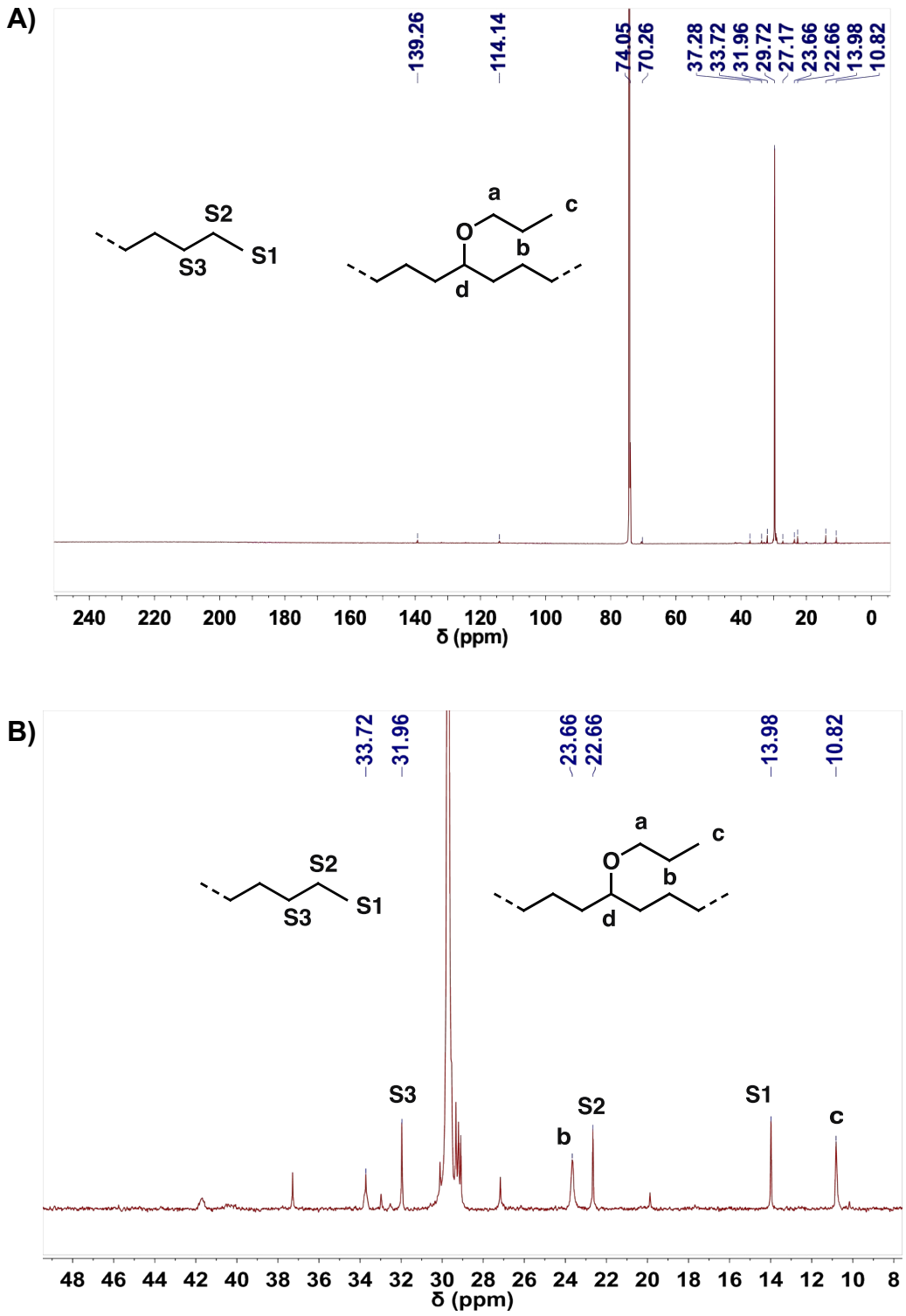

Figure S45. ^{13}C NMR spectrum ($C_2D_2Cl_4$, 150 MHz, 120 °C) of ethylene/propyl vinyl ether copolymer produced by **4a**-Co in THF (Table 3, entry 2). The full spectrum is shown in A and the expanded view from 0-50 ppm is shown in B.

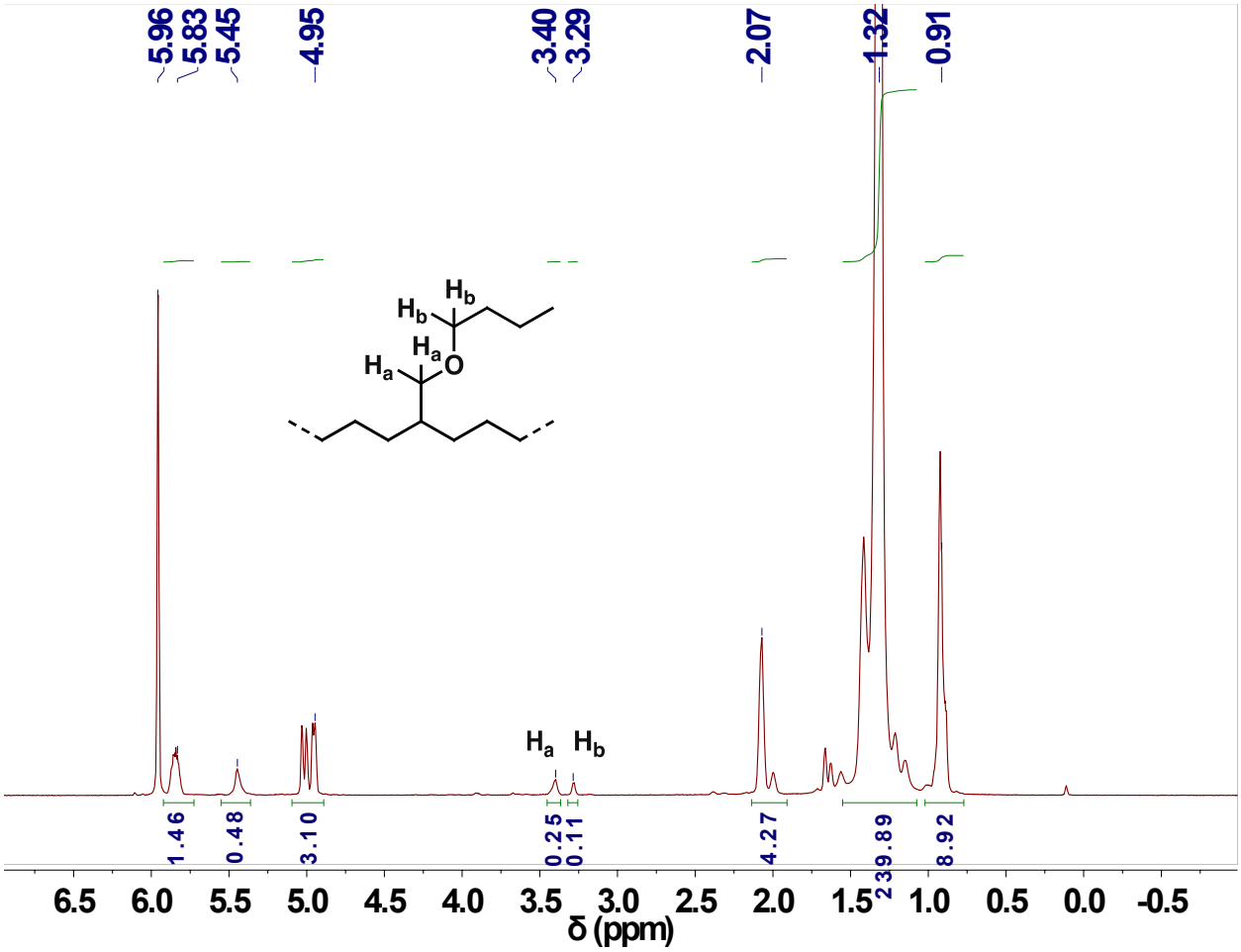

Figure S46. ^{1}H NMR spectrum ($C_2D_2Cl_4$, 600 MHz, 120 °C) of ethylene/allyl butyl ether copolymer produced by **4a**-Co in THF (Table 3, entry 9).

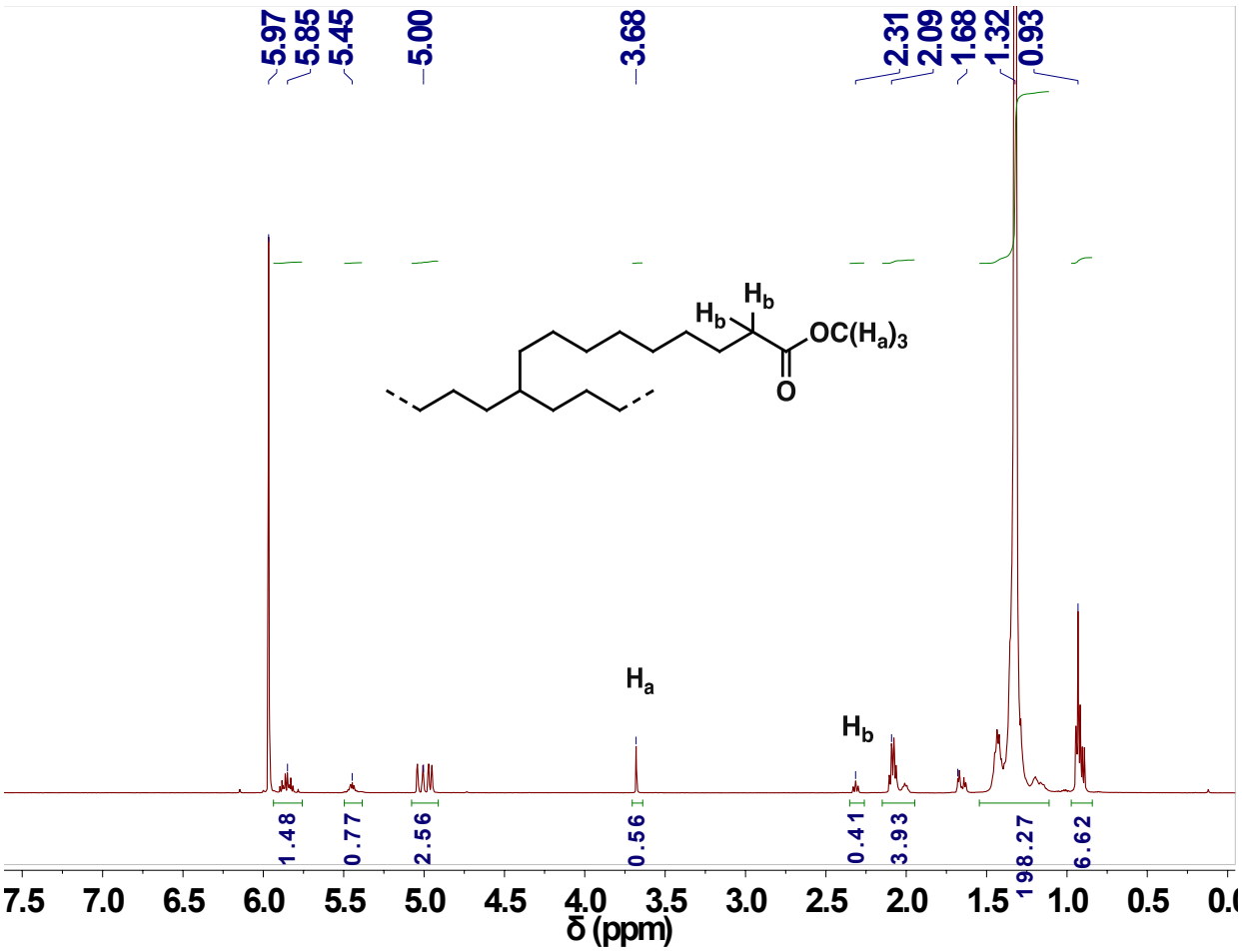

Figure S47. ^{1}H NMR spectrum ($C_2D_2Cl_4$, 500 MHz, 120 °C) of ethylene/methyl-10-Undecenoate copolymer produced by **4a** in THF (Table 3, entry 11).

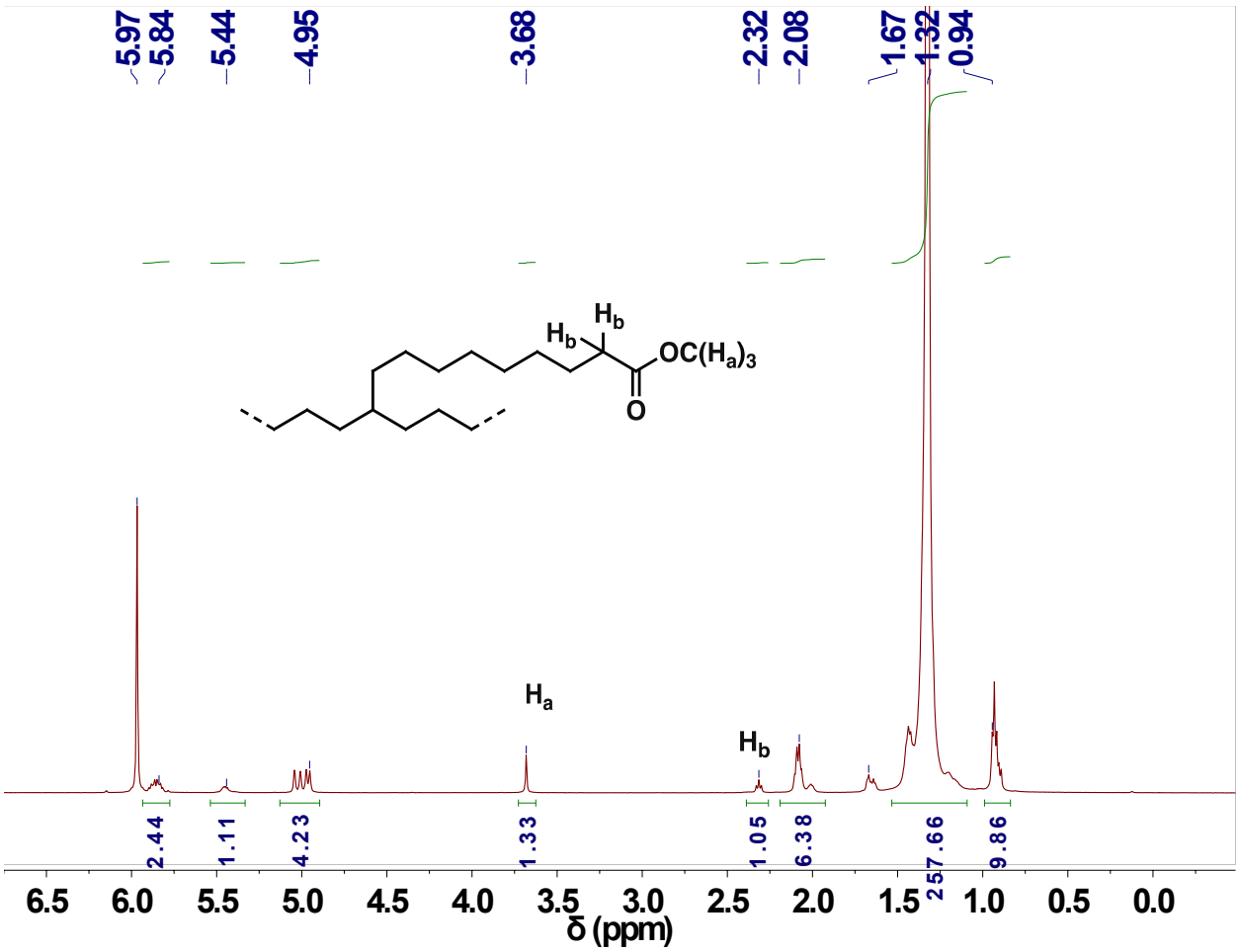

Figure S48. ^{1}H NMR spectrum ($C_2D_2Cl_4$, 500 MHz, 120 °C) of ethylene/methyl-10-Undecenoate copolymer produced by **4a**-Co in THF (Table 3, entry 12).

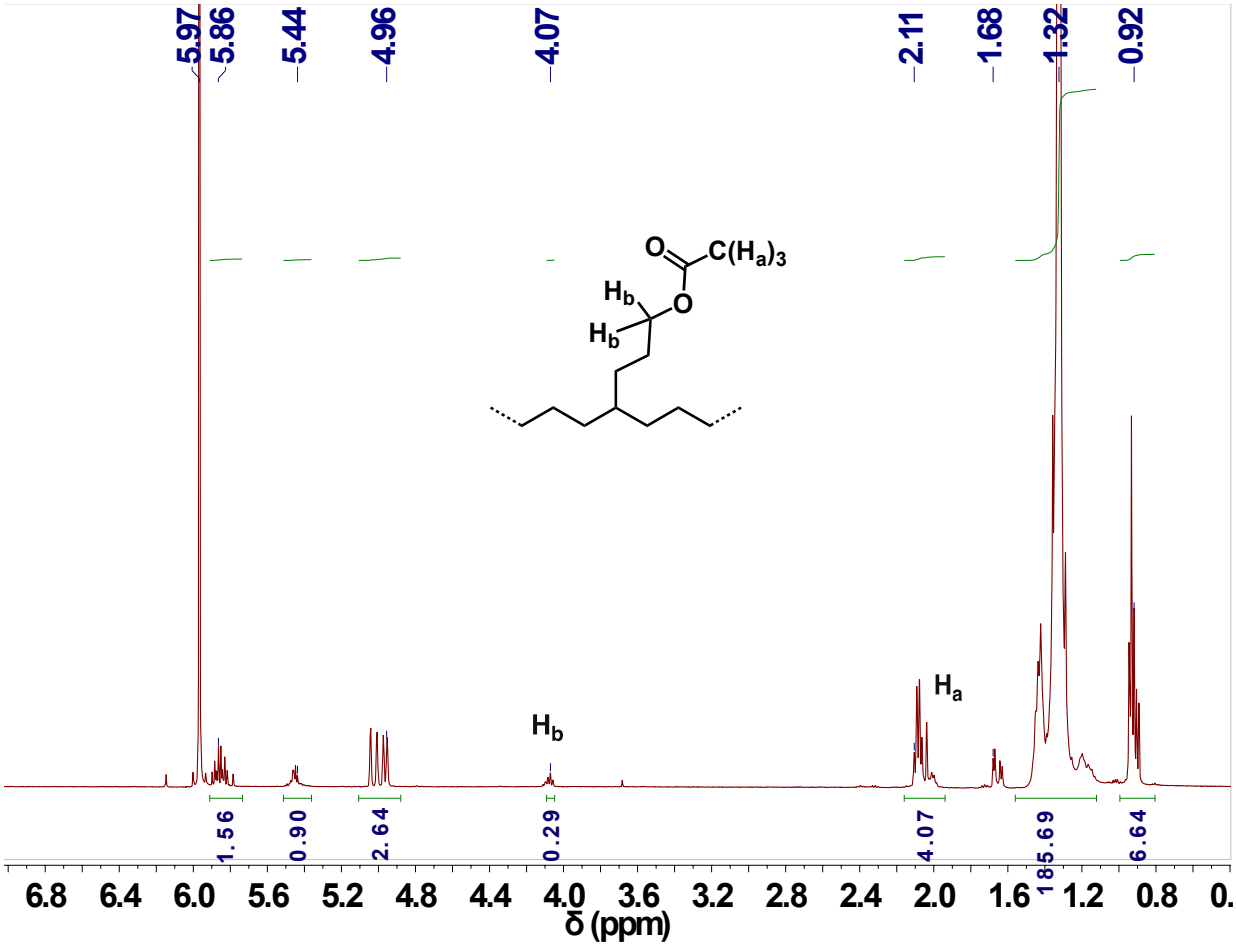

Figure S49. ^{1}H NMR spectrum ($C_2D_2Cl_4$, 500 MHz, 120 °C) of ethylene/5-acetoxy-1-pentene copolymer produced by **4a** in THF (Table 3, entry 14).

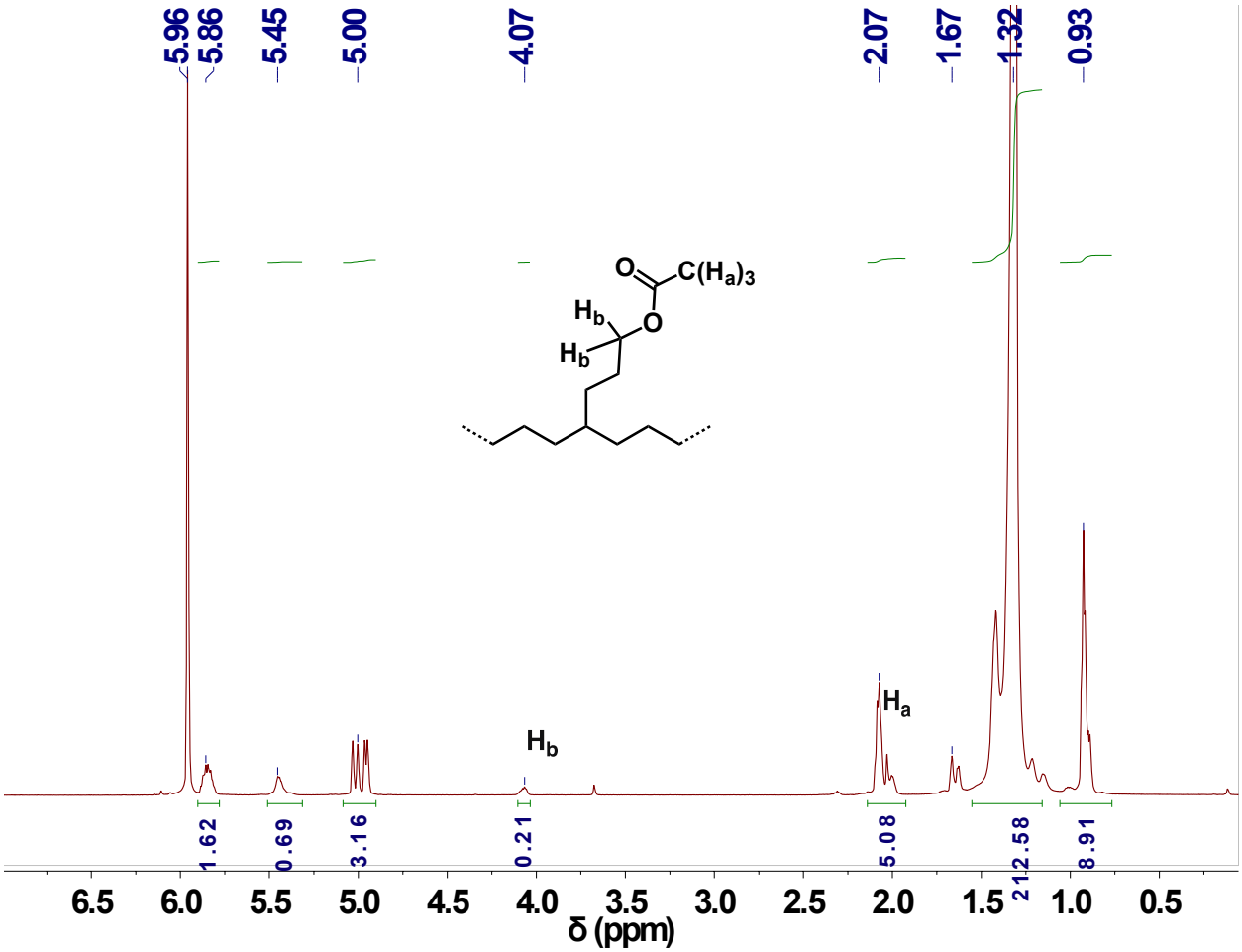

Figure S50. ^{1}H NMR spectrum ($C_2D_2Cl_4$, 500 MHz, 120 °C) of ethylene/5-acetoxy-1-pentene copolymer produced by **4a**-Co (Table 3, entry 15).

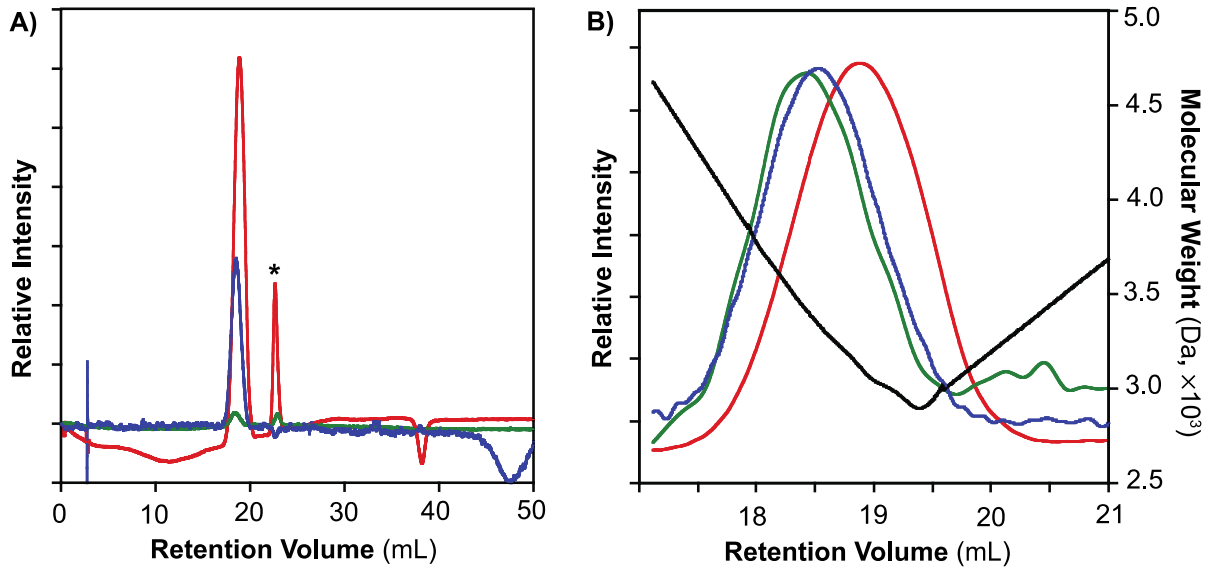

Figure S51. A) GPC chromatograms of the polyethylene obtained in ethylene polymerization using **4a** (Table 1, entry 1). B) Normalized chromatograms showing the peaks corresponding to the polyethylene product and the molecular weight range (black line). The data were acquired using a triple detector system: red = refractive index, green = right angle light scattering, blue = viscometer. The peak at ~21 mL retention volume marked with an asterisk (*) is derived from a contaminant in the GPC column, not the sample itself.

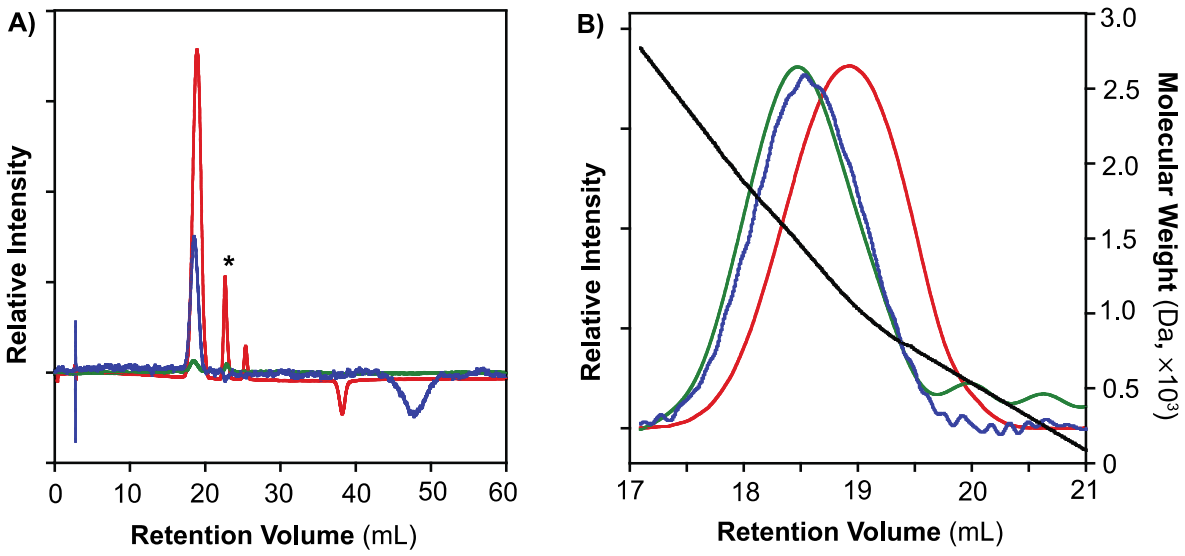

Figure S52. A) GPC chromatograms of the polyethylene obtained in ethylene polymerization using **4a**/NaBAr$^F{}_4$ (Table 1, entry 2). B) Normalized chromatograms showing the peaks corresponding to the polyethylene product and the molecular weight range (black line). The data were acquired using a triple detector system: red = refractive index, green = right angle light scattering, blue = viscometer. The peak at ~21 mL retention volume marked with an asterisk (*) is derived from a contaminant in the GPC column, not the sample itself.

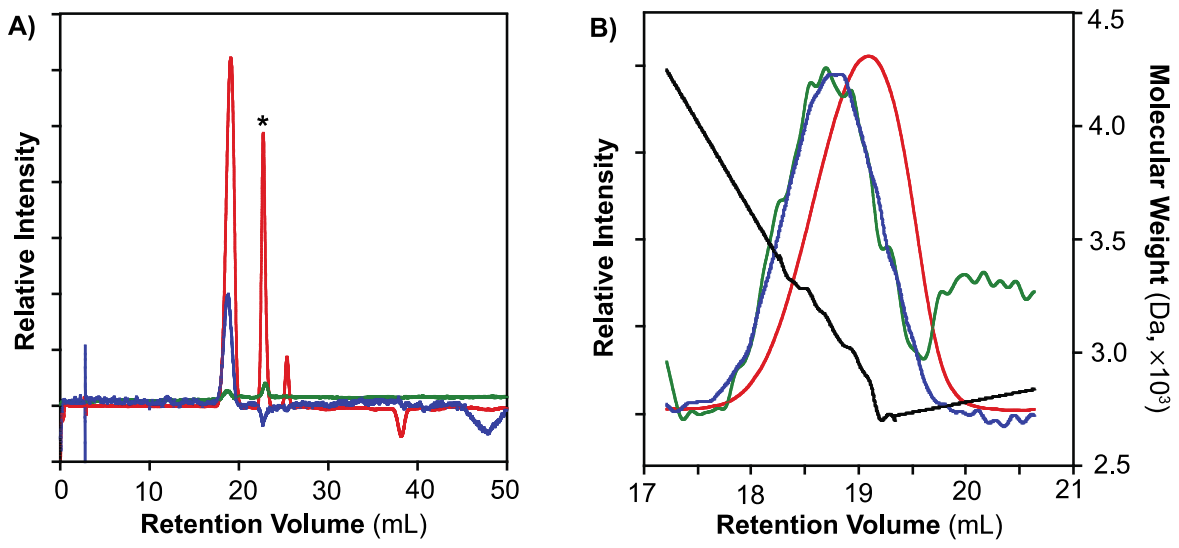

Figure S53. A) GPC chromatograms of the polyethylene obtained in ethylene and PVE copolymerization using **4a**/Co(OTf)$_2$ (Table 4, entry 2). B) Normalized chromatograms showing the peaks corresponding to the polyethylene product and the molecular weight range (black line). The data were acquired using a triple detector system: red = refractive index, green = right angle light scattering, blue = viscometer. The peak at ~21 mL retention volume marked with an asterisk (*) is derived from a contaminant in the GPC column, not the sample itself.

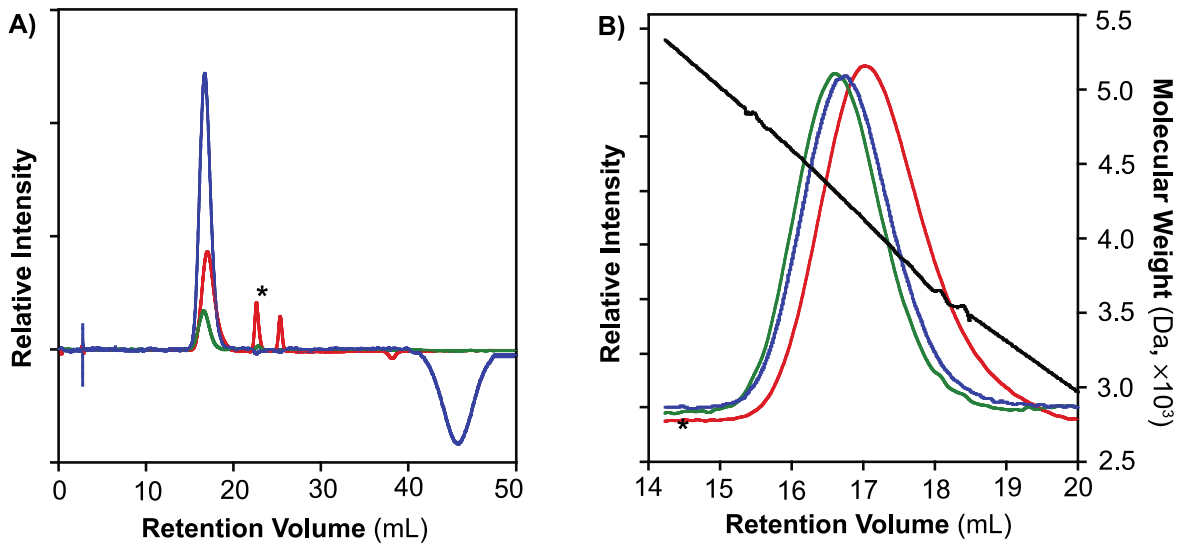

Figure S54. A) GPC chromatograms of the polyethylene obtained in ethylene homopolymerization using **4b**/NaBAr$^{F}_{4}$ (Table 1, entry 4). B) Normalized chromatograms showing the peaks corresponding to the polyethylene product and the molecular weight range (black line). The data were acquired using a triple detector system: red = refractive index, green = right angle light scattering, blue = viscometer. The peak at ~21 mL retention volume marked with an asterisk (*) is derived from a contaminant in the GPC column, not the sample itself.

X-RAY DATA COLLECTION AND REFINEMENT

Crystals suitable for X-ray diffraction analysis were picked out of the crystallization vials and mounted onto Mitogen loops using Paratone oil and then frozen under a nitrogen stream at -100 °C during data collection. The crystals were collected at a 6.0 cm detector distance. The structures were solved by direct methods using the program SHELXT and refined by SHELXLE. Hydrogen atoms connected to carbon were placed at idealized positions using standard riding models and refined isotropically. All non-hydrogen atoms were refined anisoptriocally.

Single crystals of **4a**-Na were obtained via slow diffusion of pentane into a solution of the complex and $NaSbF_6$ (1:1) in a mixture of THF and diethyl ether. The unit cell contains a severely disordered solvent molecule, which was modeled with partial occupancy by pentane and THF. The structures of disordered solvents were refined using a fragment database provided by SHELXLE.

Single crystals of **4b**-Na were obtained via slow diffusion of pentane into a solution of the complex and $NaSbF_6$ (1:1) in a mixture of THF and diethyl ether. The nickel center (Ni1) and coordinating phosphine (P1) and phosphine oxide (P2-O1) atoms were refined with positional disorder with (78% and 22%). The structure also contains two SbF_6^- anions, one coordinated and the other is not. The free anion was found to be disordered over two different positions with occupancies of ~47% and 53%. Additional residual electron density was found near the 47% occupied SbF_6^- anion, suggesting that it is further disordered (Alert A in checkcif report). However, stable refinement of a third SbF_6^- component could not be achieved. Because this SbF_6^- anion is a spectator ion, failure to completely model its disorder does not affect the Ni complex of interest.

Single crystals of **6a** were obtained via slow diffusion of pentane into a solution of the complex in dichloromethane. No solvent molecules were found in the crystal lattice.

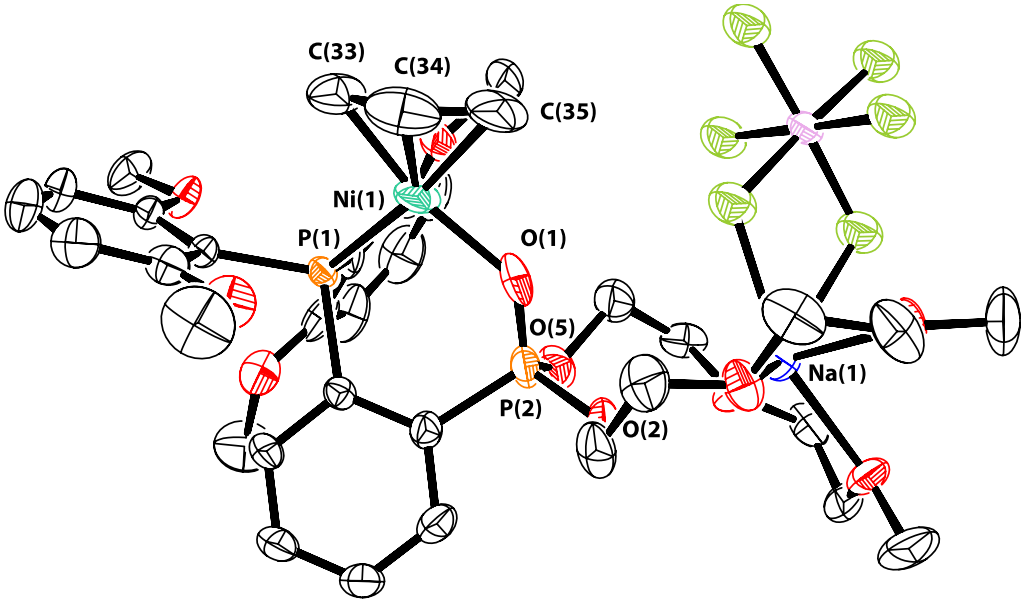

Figure S55. X-ray structure of complex **4b**-Na (ORTEP view, displacement ellipsoids drawn at 50% probability level.) Hydrogen atoms and free SbF_{6-} were omitted for clarity. The minor disordered nickel component is not depicted. Atom colors: green = nickel, orange = phosphine, red = oxygen, blue = sodium, black = carbon, light green = fluorine, magenta = antimony.

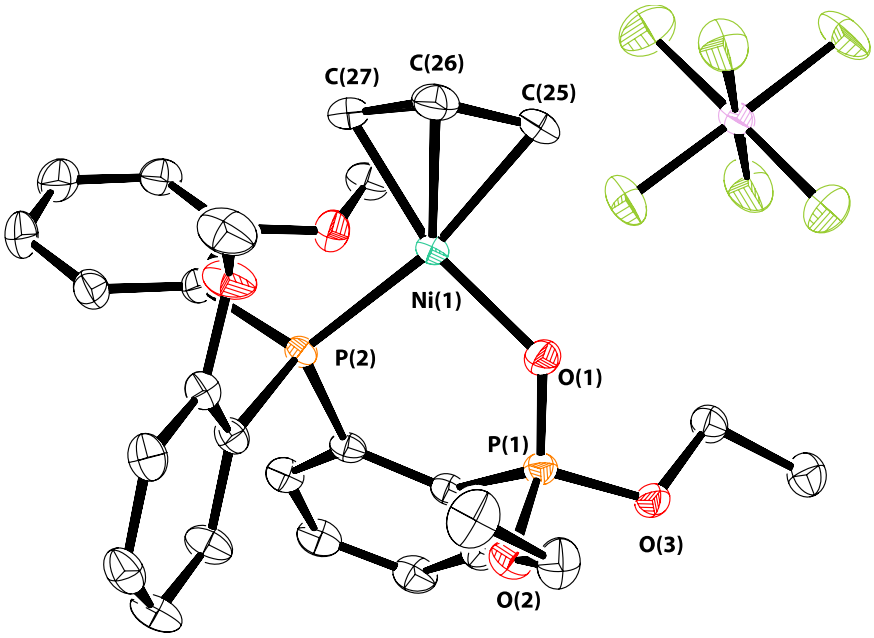

Figure S56. X-ray structure of complex **6a** (ORTEP view, displacement ellipsoids drawn at 50% probability level.) Hydrogen atoms were omitted for clarity. Atom colors: green = nickel, orange = phosphine, red = oxygen, black = carbon, light green = fluorine, magenta = antimony.

Table S11. Crystal Data and Structure Refinement

	4a-Na	**4b**-Na	**6a**
Empirical Formula	$NiNaC_{33}H_{43}O_9P_2(SbF_6)_2 \cdot (THF)_{0.53}(pentane)_{0.47}$	$NiNaC_{35}H_{49}O_{11}P_2(SbF_6)_2$	$NiC_{27}H_{33}O_5P_2(SbF_6)$
Formula Weight	1272.95	1256.85	793.93
Temperature (°C)	-100	-150	-150
Wavelength (Å)	0.71073	0.71073	0.71073
Crystal System	Triclinic	Monoclinic	Monoclinic
Space Group	P-1	C2/c	P2(1)/c
Unit Cell Dimensions			
a (Å)	10.2493(17)	40.567(3)	8.7204(4)
b (Å)	15.708(3)	9.3711(7)	14.0336(6)
c (Å)	17.072(3)	29.875(2)	25.4624(11)
α (°)	97.691(2)	90	90
β (°)	105.207(2)	121.9500(10)	90.9730(10)
γ (°)	108.910(2)	90	90
Volume ($Å^3$)	2436.0(7)	9636.7(12)	3115.6(2)
Z, Calculated Density (Mg/m^3)	2, 1.735	8, 1.733	4, 1.693
Absorption Coefficient (mm^{-1})	1.653	1.673	1.645
F(000)	1270	4976	1592
Theta Range for Data Collection (°)	1.273 to 28.555	1.183 to 27.509	2.160 to 27.522
Limiting Indices	$-13 \le h \le 13$ $-21 \le k \le 20$ $-21 \le l \le 22$	$-51 \le h \le 33$ $-11 \le k \le 12$ $-26 \le l \le 38$	$-10 \le h \le 11$ $-18 \le k \le 13$ $-32 \le l \le 32$
Reflections Collected/ Unique	14506 / 10664 [R(int) = 0.0142]	28627 / 10926 [R(int) = 0.0226]	18488 / 7187 [R(int) = 0.0086]
Max. and Min. Transmission	0.7457 and 0.6557	0.7456 and 0.6891	0.7456 and 0.7009
Data/ Restraints/ Parameters	10664 / 440 / 612	10926 / 486 / 582	7071 / 0 / 383
Goodness of Fit on F^2	1.034	1.030	1.030
Final R Indices	R_1= 0.0731	R_1= 0.0567	R_1= 0.0197
[I > 2σ(I)]	wR_2 = 0.2113	wR_2 = 0.1547	wR_2 = 0.0501
R Indices (All Data)*	R_1 = 0.0887 wR_2 = 0.2261	R_1 = 0.0741 wR_2 = 0.1723	R_1 = 0.0213 wR_2 = 0.0511
Largest Diff. Peak and Hole (e $Å^{-3}$)	1.607 and -2.004	4.891 and -1.325	0.786 and -0.579

*$R_1 = \Sigma\, ||F_o|-|F_o||/\Sigma|F_o|$; $wR_2 = [\Sigma[w(F_o^2 - F_c^2)^2]/\Sigma[w(F_o^2)_2]]^{1/2}$; $GOF = [\Sigma[w(F_o^2 - F_c^2)_2]/(n-p)]^{1/2}$, where *n* is the number of reflections and *p* is the total number of parameters refined

References

(1) Luo, S.; Vela, J.; Lief, G. R.; Jordan, R. F. Copolymerization of Ethylene and Alkyl Vinyl Ethers by a (Phosphine- sulfonate)PdMe Catalyst. *J. Am. Chem. Soc.* **2007**, *129*, 8946-8947.

(2) Xia, J.; Zhang, Y.; Zhang, J.; Jian, Z. High-Performance Neutral Phosphine-Sulfonate Nickel(II) Catalysts for Efficient Ethylene Polymerization and Copolymerization with Polar Monomers. *Organometallics* **2019**, *38*, 1118-1126.

(3) Hong, C.; Sui, X.; Li, Z.; Pang, W.; Chen, M. Phosphine Phosphonic Amide Nickel Catalyzed Ethylene Polymerization and Copolymerization with Polar Monomers. *Dalton Trans.* **2018**, *47*, 8264-8267.

(4) Tao, W.-j.; Nakano, R.; Ito, S.; Nozaki, K. Copolymerization of Ethylene and Polar Monomers by Using Ni/IzQO Catalysts. *Angew. Chem., Int. Ed. Engl.* **2016**, *55*, 2835-2839.

(5) Chen, M.; Chen, C. Rational Design of High-Performance Phosphine Sulfonate Nickel Catalysts for Ethylene Polymerization and Copolymerization with Polar Monomers. *ACS Catal.* **2017**, *7*, 1308-1312.

(6) Chen, M.; Chen, C. A Versatile Ligand Platform for Palladium- and Nickel-Catalyzed Ethylene Copolymerization with Polar Monomers. *Angew. Chem., Int. Ed. Engl.* **2018**, *57*, 3094-3098.

(7) Zhang, W.; Waddell, P. M.; Tiedemann, M. A.; Padilla, C. E.; Mei, J.; Chen, L.; Carrow, B. P. Electron-Rich Metal Cations Enable Synthesis of High Molecular Weight, Linear Functional Polyethylenes. *J. Am. Chem. Soc.* **2018**, *140*, 8841-8850.

(8) Xia, J.; Zhang, Y.; Hu, X.; Ma, X.; Cui, L.; Zhang, J.; Jian, Z. Sterically Very Bulky Aliphatic/Aromatic Phosphine-Sulfonate Palladium Catalysts for Ethylene Polymerization and Copolymerization with Polar Monomers. *Polym. Chem.* **2019**, *10*, 546-554.

(9) Mitsushige, Y.; Yasuda, H.; Carrow, B. P.; Ito, S.; Kobayashi, M.; Tayano, T.; Watanabe, Y.; Okuno, Y.; Hayashi, S.; Kuroda, J.; Okumura, Y.; Nozaki, K. Methylene-Bridged Bisphosphine Monoxide Ligands for Palladium-Catalyzed Copolymerization of Ethylene and Polar Monomers. *ACS Macro Lett.* **2018**, *7*, 305-311.

(10) Li, M.; Wang, X.; Luo, Y.; Chen, C. A Second-Coordination-Sphere Strategy to Modulate Nickel- and Palladium-Catalyzed Olefin Polymerization and Copolymerization. *Angew. Chem., Int. Ed. Engl.* **2017**, *56*, 11604-11609.

(11) Mitsushige, Y.; Carrow, B. P.; Ito, S.; Nozaki, K. Ligand-Controlled Insertion Regioselectivity Accelerates Copolymerisation of Ethylene with Methyl Acrylate by Cationic Bisphosphine Monoxide–Palladium Catalysts. *Chem. Sci.* **2016**, *7*, 737-744.

(12) Ota, Y.; Ito, S.; Kuroda, J.-i.; Okumura, Y.; Nozaki, K. Quantification of the Steric Influence of Alkylphosphine–Sulfonate Ligands on Polymerization, Leading to High-Molecular-Weight Copolymers of Ethylene and Polar Monomers. *J. Am. Chem. Soc.* **2014**, *136*, 11898-11901.

(13) Shannon, R. Revised effective ionic radii and systematic studies of interatomic distances in halides and chalcogenides. *Acta Cryst. A* **1976**, *32*, 751-767.

(14) Brown, I. What factors determine cation coordination numbers? *Acta Cryst. B* **1988**, *44*, 545-553.